Assessing potential impacts of Solar Power Plants on hydrology: evapotranspiration and local scale effects on runoff

Ph.D. Dissertation

Tagele Mossie Aschale

University of Catania

DICAR - Department of Civil Engineering and Architecture

***A thesis submitted for the degree of Doctor of Philosophy in* Evaluation and Mitigation of Urban and Territorial Risks**

XXXVI Cycle

Assessing potential impacts of Solar Power Plants on hydrology: evapotranspiration and local scale effects on runoff

Tagele Mossie Aschale

Supervisor: Prof. Eng. Antonino CANCELLIERE

Co-supervisors: Prof. Eng. David Johnny PERES, Eng Aurora Gullotta, Eng. Guido Sciuto

Ph.D. coordinator: Prof. Eng. Antonino CANCELLIERE

Catania, Italy

November, 2023

Table of Contents

Contents Page

List of tables

List of figures

Acknowledgements

I would like to express my deepest gratitude and appreciation to everyone who has supported me throughout this incredible journey of completing my doctoral thesis.

First and foremost, I am profoundly grateful to my supervisor, Prof. Eng. Antonino Cancelliere, Prof. Eng David J. Peres, & Eng. Aurora Gullotta and Eng. Guido Sciuto for their unwavering guidance, expertise, and encouragement. Their mentorship has been invaluable, pushing me to explore new frontiers and challenge my intellectual boundaries. I am indebted to their patience, insightful feedback, and constant support, which have undoubtedly shaped the outcome of this research.

I extend my heartfelt appreciation to my colleagues at DICAR, University of Catania whose stimulating discussions and collaborations have played a pivotal role in shaping my ideas. Their intellectual contributions and camaraderie have made this academic journey all the more rewarding.

I would like to acknowledge the financial support provided by Ambiens Srl. Their investment in my research has allowed me to dedicate my time and resources to this project, and I am sincerely grateful for their belief in the importance of my work.

I acknowledge with deep gratitude the unwavering support and love of my family throughout the completion of this thesis. Their encouragement and understanding have been a constant source of motivation, making this achievement possible.
Last but not least, I would like to express my heartfelt gratitude to all the participants who generously shared their time, knowledge, and experiences, making this research possible. Their invaluable contributions have enriched the findings and significance of this study.

To all those mentioned above and to countless others who have played a part, no matter how big or small, in shaping this thesis, I extend my deepest gratitude. Your support and encouragement have made this achievement possible, and I am truly humbled and honoured to have had you by my side.

Thank you.

Abstract

The thesis aims to investigate three crucial aspects related to water resources and the newly emerging impact of solar parks on the local hydrology: evapotranspiration trends, evapotranspiration estimation model performance, and the impact of solar parks on local climatology, runoff, evapotranspiration, and soil moisture. Firstly, it analyzes the historical evapotranspiration trend over a specific period, examining the performance of evapotranspiration estimation models useful the analysis solar park's impact. By analyzing historical data and climatic factors, the research aims to identify any significant trends or patterns in evapotranspiration rates, providing valuable insights into potential impacts on water availability and regional climate conditions, and providing baseline information about the possibility of impacts of solar parks on the future local hydroclimate.

Characterizing hydroclimatic parameters changes and trends has a paramount importance for a better understanding of climate change related phenomena and for developing mitigation measures. Evapotranspiration is one of the most essential components of the hydrological cycle, having impacts on water resource management issues, agricultural practices, irrigation scheduling, and climate change adaptation measures. Accurate estimation of evapotranspiration from indirect methods based on temperature and other meteorological variables is beneficial in terms of spatial coverage, time, filed experiment cost savings. Moreover, analyzing the spatiotemporal trend of evapotranspiration and identifying the most influential climatological factors for its sensitivity plays a vital role for water resource management and the understanding the newly emerging large scale solar energy infrastructure impact on hydroclimatology. Large-scale solar farms are experiencing significant growth in different parts of the world, including Sicily, due to their potential for reducing greenhouse gas emissions for climate change mititgation. However, these infrastructures will have synergies and dilemmas concerning the hydroclimate of the ecosystem.

Considering the potential impacts of solar parks on evapotranspiration, the study aims to evaluate the performance of reference evapotranspiration (ETo) estimation methods properly applied for monitoring future large-scale solar farms. It will

examine the trend of evapotranspiration in different areas of Sicily, which is valuable as a baseline for future monitoring of the potential impacts of large-scale solar parks.

Given the aforementioned challenges, this study aims to evaluate the performance of different evapotranspiration estimation methods, examine the trend of reference evapotranspiration (ETo), identify the most influential climatological elements, analyze the spatio-temporal trend of potential evapotranspiration (PET) from multiple meteorological stations, and finally address the response of photovoltaic panels in terms of runoff using EPA SWMM simulation software.The meteorological data obtained from the Agrometeorological Information Service of Sicily (SIAS, http://www.sias.regione.sicilia.it/) were used to compute the reference evapotranspiration (ETo) and potential evapotranspiration (PET) using the FAO Penman-Monteith method (FAO PM method). This method is considered the best standard for evapotranspiration estimation by the Food and Agricultural Organization (FAO) and the American Society of Civil Engineers (ASCE). The performance of temperature-based and radiation-based evapotranspiration estimation methods was evaluated using different performance metrics to monitor the impacts of solar parks on hydrology.

The Hargreaves and Samani (HS), Baier and Robertson (BR), Priestley and Taylor (PT), Makkink (MKK), Turc (TUR), Thornthwaite (THN), Blaney and Criddle (BG), Ritchie (RT), and Jensen and Haise (JH) methods were evaluated using several performance metrics. The results showed that the PT method had the best performance with a Nash-Sutcliffe efficiency (NSE) of 0.91. The HS method performed the second best estimation method (NSE = 0.51) but significantly worse than PT.

To analyze the spatio-temporal trend of different climatological elements, ETo and PET were analyzed using the Mann-Kendall test with serial autocorrelation removal by Trend-free pre-whitening (TFPW). The Sen's slope was also used to examine the magnitude of the trend of monthly, seasonal, and annual meteorological variables, ETo, and PET. The sensitivity of ETo was analyzed using the sensitivity coefficient and contribution rate algorithms. The results showed that climatological elements

exhibited different trends seasonally and monthly, whereas ETo showed a monthly increasing trend only in November in Piazza Armerina. Specific humidity and wind speed were identified as the most climatological elements highly sensitive to and contributing to ETo in Piazza Armerina.

At multiple spatiotemporal scales, PET exhibited different trends in different meteorological stations across Sicily. August was the most detected month for an increasing trend of PET in multiple meteorological stations in Sicily. Moreover, five meteorological stations consistently detected an annual increasing trend, which could be essential for climate change mitigation and adaptation measures in the region.

The assessment of potential impacts on surface runoff of renewable energy related installation is crucial for a safe development of such projects. In the final part of the work, the response of ground-mounted photovoltaic panels in terms of runoff generation was analyzed using EPA SWMM software. The study simulated the EPA SWMM considering different factors that influenced runoff formation. These factors included different sizes of installation, soil types, input hyetographs, and varying surface roughness to compare the runoff peak flow and runoff volume between a reference catchment and a solar park. The results showed that there were no practical changes in runoff in the short term after installation. However, in the long term, modifications in soil cover may lead to a potential increase in runoff. For instance, peak flow increments from the solar park of up to 21% and 35% were obtained for roughness coefficient reductions of 10% and 20%, respectively. This information is crucial for future solar park infrastructure planning by Ambiens S.r.l. (the PhD funding source) and other solar energy companies in the region. Further experimental research is needed to understand the impact of solar parks on local hydroclimate under different scenarios. Long-term analysis of spatio-temporal trend of evapotranspiration would also be helpful in considering climate mitigation measures and solar energy projects.

Keywords: Evapotranspiration, solar parks, spatiotemporal trend, hydroclimate, FAO PM method, Mann Kendall, Sen's Slope, EPA SWMM, runoff

Chapter 1

Introduction

1.1 Overview

Currently, there is an increasing demand for renewable energy, showing high promise in reducing the concentration of greenhouse gases in the atmosphere (Armstrong et al., 2016; Armstrong et al., 2014; Cagle et al., 2020 & Hernandez et al., 2019). Among the technologies based on renewable energy, photovoltaic panels (PV) are considered the most environmentally convenient and the main source of energy. The PV industry is experiencing significant growth due to the lower cost and higher efficiency of the technology (Jiang et al., 2021). In addition to the reduction of greenhouse gas emissions, photovoltaic installations also have some co-benefits, such as increasing soil moisture under the PV panels, enhancing water use efficiency, and enabling co-location for agriculture and energy production (Stefano et al., 2018; Barron-Gafford et al., 2019; Delfanti et al., 2016; Hassanpour et al., 2020; Marrou et al., 2013).

However, there are increasing concerns regarding the PV industry, particularly regarding its potential effects on air temperature (Broadbent et al., 2019; Taha, 2013), albedo (Li et al., 2022; Nemet, 2009), net radiation (Li et al., 2022), soil moisture, and soil temperature (Adeh et al., 2018; Yavari et al., 2022; Yue et al., 2021), as well as evapotranspiration (Feistel et al., 2022; Marrou et al., 2013a), biomass (Armstrong et al., 2016; Liu et al., 2019), and soil chemical and physical properties (Choi et al., 2020; Lambert et al., 2021), including infiltration and runoff (Pisinaras et al., 2014). Understanding the potential impact of PV installations on local hydroclimate and soil is crucial for sustainable development and enhancing the efficiency of PV technology.

The expansion of solar parks has garnered increasing attention due to their potential influence on local hydrological processes and microclimates. The establishment of large-scale solar installations can lead to changes in land surface characteristics, such as shading and modifications in land use, impacting the surrounding climate

(Broadbent et al., 2019; Taha, 2013). Consequently, these alterations can affect evapotranspiration rates, leading to fluctuations in local temperature and humidity levels (Wu et al., 2020). Furthermore, the presence of solar panels can reduce incoming solar radiation reaching the ground, potentially influencing soil moisture levs and disrupting the natural runoff patterns (Cook & McCuen, 2013; Yue & Guo, 2021 & Armstrong et al., 2016).

Through an investigation into the relationship between accurate evapotranspiration estimation and the impacts of solar parks, this research aims to provide a comprehensive understanding of how renewable energy developments interact with water resources and the environment. The findings of this study will significantly contribute to informed decision-making, guiding sustainable integration strategies for solar parks while mitigating potential adverse effects on local hydrological and ecological systems.

Solar parks (PV) have been observed to influence various local climate parameters, including temperature (Barron-Gafford et al., 2016), humidity (Wu et al., 2020), wind speed (Armstrong et al., 2016), solar radiation (Nemet, 2009; Millstein & Menon, 2011), evapotranspiration, runoff, and percolation (Pisinaras et al., 2014), as well as soil moisture (Makaronidou, 2020). These alterations in climatological and hydrological variables, induced by solar parks, present additional environmental challenges that could potentially impede the smooth transition towards renewable energy.

To address these challenges, it is essential to monitor the potential impacts of solar parks on hydroclimatological conditions. Given the high potential for solar energy production in Sicily (Farinelli, 2004), monitoring the potential impacts of solar energy infrastructure on hydroclimatological elements becomes crucial. However, conducting experimental monitoring and measurements on very large-scale solar parks can be both expensive and labor-intensive. To overcome such challenges, indirect measurements, such as evapotranspiration estimation methods, can be supportive. However, it is also necessary and prerequisite to evaluate the performance of different evapotranspiration estimation methods that use various

climatological variables before the utilization methods against the Penman-Monteith method, which is considered as the standard method for estimating evapotranspiration (Alexandris et al., 2008; Almorox, 2018; Antonopoulos & Antonopoulos, 2018; Chen et al., 2005; Gong et al., 2006; Schrier et al., 2011; Seginer, 2002).

Furthermore, it is essential to analyze the trends in different climatological variables and evapotranspiration to support climate change mitigation efforts, including the transition to renewable energy sources like solar power. Simultaneously, sensitivity analysis can help identify the contribution of evapotranspiration sensitivity in regions highly susceptible to drought.

Considering the large-scale solar parks proposed by Ambiens Energy Srl (the funder of this PhD course) and Italy's ambitious renewable energy transition program by 2050, effective stormwater management is essential for designing solar energy infrastructure in Sicily. Additionally, it is important to understand how solar parks respond to runoff in the Mediterranean climate, specifically in Sicily's climate.

Therefore, this study aims to evaluate evapotranspiration estimation methods for indirectly monitoring the potential impact of solar parks on evapotranspiration. It will also analyze the trends in evapotranspiration and climatological elements, assess sensitivity to evapotranspiration trends, and simulate the impact of solar parks on runoff in Sicily's climate.

1.2 Aims of the research

There is a highly increasing demand for renewable energy, which holds high promise in reducing greenhouse gas emissions. In addition to the reduction of greenhouse gas emissions, renewable energy-based projects also provide additional ecosystem services, such as increasing soil moisture, enhancing water use efficiency, and enabling co-location for agriculture and energy production (Stefano et al., 2018; Barron-Gafford et al., 2019; Delfanti et al., 2016; Hassanpour et al., 2020; Marrou et al., 2013).

However, potential adverse effects of large-scale solar parks have not properly addressed in literature yet. For example, some studies showed that the PVs have impacts on the air temperature (Broadbent et al., 2019; Taha, 2013), albedo (Li et al., 2022; Nemet, 2009),

net radiation (Li et al., 2022), soil moisture and soil temperature (Adeh et al., 2018; Yavari et al., 2022; Yue et al., 2021), evapotranspiration (Feistel et al., 2022; Marrou et al., 2013a), biomass (Armstrong, Ostle, et al., 2016; Liu et al., 2019), soil chemical and physical properties (Choi et al., 2020; Lambert et al., 2021), infiltration and runoff (Pisinaras et al., 2014).

The aim of the research is to contribute to understanding the role that PV (Photovoltaic) systems can play in mitigating climate change and to develop methodologies/methods for understanding their hydrological impacts in Sicily climate.

To sum up, the specific objectives of this dissertation are:

- Evaluate the reference evapotranspiration estimation methods for the assessment of hydrological impacts of photovoltaic farms.
- Analyse the trend and identify of the meteorological factors influencing reference evapotranspiration.
- Assess the trends of potential evapotranspiration at multiple timescales and locations.
- Assess the impact of photovoltaic solar parks on stormwater runoff using EPA-SWMM

1.3 Research methodology

Estimation and investigation of evapotranspiration trends are essential for water resource management in agriculture, climate variability analysis, and other hydroclimate-related projects. Additionally, the estimation and analysis of the spatio-temporal trends in evapotranspiration support understanding Earth's energy budget, agricultural water management, water resource management, and climate change studies (Dezsi & Mîndrescu, 2018; Dong et al., 2020; Han et al., 2018; He et al., 2013; Hui-mean & Yusof, 2018; Kingston et al., 2009; Li et al., 2017; Nam et al., 2015).

Given that measures of evapotranspiration are challenging, expensive, labor-intensive, and time-consuming, scientists and researchers worldwide have conducted studies aimed at estimating evapotranspiration. The main categories of evapotranspiration estimation methods include direct methods (field water balance approach and soil moisture depletion approach) and indirect methods (empirical/statistical methods, micrometeorological methods, and remote sensing methods) (Henok et al., 2015; Choudhary, 2018; Mokhele et al., 2013; Gharsallah et al., 2013; Hatfield et al., 2016; Long & Singh, 2012; Ochoa-sánchez et al., 2019; Tanner, 1967).

There are several empirical evapotranspiration estimation methods, which can be categorized into radiation-based, temperature-based, and aerodynamics-based models. Researchers employ these methods based on the availability of meteorological data and on the purpose of their task.

Some of the most commonly used evapotranspiration estimation methods are described below:

- Penman-Monteith Method: The Penman-Monteith method is considered the standard method for estimating evapotranspiration. It takes into account various factors such as solar radiation, air temperature, humidity, wind speed, and vegetation characteristics. It is based on the energy balance equation and requires weather data input.
- Priestley-Taylor Method: The Priestley-Taylor method is a simplified version of the Penman-Monteith method that estimates evapotranspiration using only the net radiation and air temperature. It assumes that the ratio of actual evapotranspiration to potential evapotranspiration is constant.
- Hargreaves Method: The Hargreaves method is a widely used empirical method that estimates evapotranspiration based on temperature data only. It is simple to use and requires daily maximum and minimum air temperature data.
- Blaney-Criddle Method: The Blaney-Criddle method is another empirical method that estimates evapotranspiration using temperature and reference crop coefficients. It is commonly used in areas where weather data is limited.
- FAO-56 Method: The Food and Agriculture Organization (FAO) developed the FAO-56 method, which is based on the Penman-Monteith equation. It provides guidelines and standardized procedures for estimating evapotranspiration in different agroclimatic regions.

These evapotranspiration estimation methods are essential for monitoring evapotranspiration dynamics and trends associated with land use changes, such as the recent expansion of renewable energy infrastructure. Simultaneously, the expansion of solar parks has garnered increasing attention due to their potential influence on local hydrological processes and microclimates. The establishment of large-scale solar installations can lead to changes in land surface characteristics, such as shading and modifications in land use, impacting the surrounding climate (Broadbent et al., 2019; Taha,

2013). Consequently, these alterations can affect evapotranspiration rates, leading to fluctuations in local temperature and humidity levels (Wu et al., 2020). Furthermore, the presence of solar panels can reduce incoming solar radiation reaching the ground, potentially influencing soil moisture levels and disrupting the natural runoff patterns (Cook & McCuen, 2013; Yue & Guo, 2021 & Armstrong et al., 2016).

This study evaluated the performance of different evapotranspiration estimation methods such as, Hargreaves and Samani (HS), Baier-Robertson (BR), Priestley and Taylor (PT), Makknik (MKK), Turc (TUR), Thornthwaite (THN), Blaney and Criddle (BG), Ritiche (RT) and Jensen and Haise (JH) against the FAO-PM using the Nash–Sutcliffe efficiency (NSE), Coefficient of Determination (R^2), Mean Absolute Error (MAE), Mean Basis Error (MBE), and Root Mean Square Error (RMSE) at Ambiens S.r.l. Environmental Lab in Piazza Armerina, Sicily, Italy.

The Mann-Kendall test with serial autocorrelation removal by Trend-free pre-whitening (TFPW) was applied to analyse evapotranspiration trends and the basic meteorological variables on which they depend. Sen's slope was also used to examine the magnitude of the trend of evapotranspiration and its related meteorological variables at multiple temporal scales (monthly, seasonal, and annual). The study used the meteorological data obtained from the Agrometeorological Information Service of Sicily (SIAS, http://www.sias.regione.sicilia.it/), having 46 meteorological stations (which have completed data for the computation of evapotranspiration) distributed all over the region.

To examine the response of PV systems to runoff, the study took into account different sizes of the installation, soil types, input hyetographs, and ground cover by adjusting the surface roughness using the EPA SWMM software. The EPA-SWMM is a free and open-source software developed by the United States Environmental Protection Agency (US-EPA). The release n. 5.1 of the software was used in this study (Rossman 2015, 2016). It is a dynamic rainfall-runoff model used for single event or continuous simulation. The runoff component of SWMM operates on a collection of subcatchment areas that receive precipitation and generate runoff, after computation of water losses.

1.4 Outline of the Dissertation

This thesis is organized as an article-based thesis, consisting of a compilation of interconnected articles that were generated during the Ph.D. program. This implies that some repetitions are present in the material presented in the thesis. For instance, in the methodology of chapters 3, 4, and 5, FAO Penman-Monteith method to estimate reference evapotranspiration is repeated. I would like to ask readers' forgiveness for this inconvenience. The dissertation is divided into seven chapters.

Chapter 1 consists of an overview of the study, objectives, research methodology and outline of the dissertation.

Chapter 2 presents an overview of the literature review addressing the main themes covered in this thesis. It covers the concept of evapotranspiration, methods for estimating evapotranspiration, trends in evapotranspiration, the impacts of PV on local climate (temperature, humidity, solar radiation, and wind speed), hydrology (runoff, evapotranspiration, and infiltration), and soil moisture and temperature. In relation to the article-based thesis, each article chapter has an introduction section. These introduction sections may contain some unavoidable repetition with the literature review.

Chapters 3 to 6 presents articles that have been published in international journals The details of each article are listed below.

Chapter 3 presents an evaluation of different evapotranspiration estimation models applicable to PV infrastructure, considering the future potential impacts of PV on evapotranspiration. This chapter, the most common evapotranspiration estimation methods Hargreaves and Samani (HS), Baier-Robertson (BR), Priestley and Taylor (PT), Makknik (MKK), Turc (TUR), Thornthwaite (THN), Blaney and Criddle (BG), Ritiche (RT) and Jensen and Haise (JH) were evaluated against the FAO-PM estimation method. This article has been published, and the full information is provided below:

Aschale, T.M.; Sciuto, G.; Peres, D.J.; Gullotta, A.; Cancelliere, A. Evaluation of Reference Evapotranspiration Estimation Methods for the Assessment of Hydrological Impacts of Photovoltaic Power Plants in Mediterranean Climates. Water 2022, 14, 2268. https://doi.org/10.3390/w14142268.

Chapter 4 presents the trends of different climatological elements and reference evapotranspiration and identifies the main sensitive climatological element for reference evapotranspiration. Moreover, this chapter also addressed the contribution and sensitivity of evapotranspiration to different climatological variables, with specific location and time. This article has been published, and the full information is provided below:

Aschale, T.M.; Peres, D.J.; Gullotta, A.; Sciuto, G.; Cancelliere, A. Trend Analysis and Identification of the Meteorological Factors Influencing Reference Evapotranspiration. Water 2023, 15, 470. https://doi.org/10.3390/w15030470.

Chapter 5 examines the spatiotemporal trend of potential evapotranspiration in multiple stations across Sicily. This chapter updated the spatiotemporal trend of potential evapotranspiration over Sicily, which had limited information regarding the recent patterns of climate change in the region. This article has been published, and the full information is provided below:

Aschale, T.M.; Palazzolo, N.; Peres, D.J.; Sciuto, G.; Cancelliere, A. An Assessment of Trends of Potential Evapotranspiration at Multiple Timescales and Locations in Sicily from 2002 to 2022. Water 2023, 15, 1273. https://doi.org/10.3390/w15071273.

Chapter 6 assesses the response of ground-mounted photovoltaic solar parks to runoff using the open-source EPA SWMM. This chapter simulated the potential impacts of the PV on runoff taking into account different different sizes of the installation, soil types, input hyetographs, and ground cover, by changing the surface roughness. This article has been published, and the full information is provided below:

Gullotta, A., Aschale, T. M., Peres, D. J., Sciuto, G., & Cancelliere, A. (2023). Modelling Stormwater Runoff Changes Induced by Ground-Mounted Photovoltaic Solar Parks: A Conceptualization in EPA-SWMM. Water Resources Management, 1-14. https://doi.org/10.1007/s11269-023-03572-3.

Chapter 7 presents the main conclusions and recommendations for future research and development.

Chapter 2

Literature review

Abstract

The literature review section of the thesis illustrates various aspects related to evapotranspiration, including definition of evapotranspiration, estimation models for evapotranspiration, sensitivity of evapotranspiration to different climatological elements, and spatio-temporal trends of evapotranspiration. Human-induced factors highly contribute to the spatio-temporal variability of evapotranspiration in different areas. Perhaps, the recently highly expanded renewable energy infrastructure, like photovoltaic solar parks, will alter evapotranspiration and other hydroclimatic parameters, such as local climate (temperature, humidity, wind speed, solar radiation), runoff, evapotranspiration, infiltration, and soil moisture. This literature part emphasized also to figure out the potential impacts of photovoltaic panels on local climate variables such as air temperature, humidity, wind speed, and solar radiation, as well as their effects on hydrology (runoff, infiltration, and evapotranspiration) and soil moisture and temperature.

Furthermore, this chapter presents the latest research findings regarding the potential impacts of photovoltaic systems on local hydroclimate and soil. It also highlights the discrepancies found in the research and explores possible reasons for these variations in the findings.

2.1 Evapotranspiration and estimation models

Reference evapotranspiration (ETo) is a pivotal part of the hydrological cycle and the most crucial physical processes in natural ecosystems and environmental system in our planet (Ochoa-sánchez et al., 2019). It enables to figure out the energy and water exchange in vegetation (Glenn et al., 2010; Zhang et al., 2001), soil surface (Parajuli et al., 2019), land surface (Alexander et al., 2020; Di et al., 2014), and atmosphere (Dickinson, 1974; Long & Singh, 2012; Mueller et al., 2011). Estimation and measurements of ETo are essential for understanding the in-earth energy budget, agricultural water management, water resource management and climate change studies (Dezsi & Mîndrescu, 2018; Dong et al., 2020; Han et al., 2018; He et al., 2013; Hui-mean & Yusof, 2018; Kingston et al., 2009; Li et al., 2017; Nam et al., 2015).

Reference evapotranspiration (ET_o) is a measurement used in hydrology and agriculture to estimate the amount of water that would be evaporated and transpired by a standardized reference crop under specific weather conditions (Malamos et al., 2015; Matzneller et al., 2010; Peng et al., 2017; Zhang et al., 2020). It represents the water demand of a well-watered, actively growing grass or crop with an assumed height, surface resistance, and leaf area index. ET_o is usually expressed in millimetres per day (mm/day) or in inches per day (in/day). It is influenced by various weather factors such as temperature, humidity, solar radiation, and wind speed.

ET_o is used as a baseline standard evapotranspiration to figure out the crop water requirements and irrigation scheduling. Once the reference evapotranspiration for a specific location is known, crop coefficients can be applied to determine the actual evapotranspiration (AET) of a particular crop in that area. AET is indispensable to manage irrigation systems efficiently and determining the water needs of different crops throughout their growth stages (Čadro et al., 2017; Pandey et al., 2016; Rodrigues & Braga, 2021; Wu et al., 2021).

The ET_o is derived from elaboration of data recorded by meteorological stations equipped with sensors for weather variables. These data can be used by farmers, water resource managers, and researchers to make informed decisions regarding water allocation, crop selection, irrigation planning, and water conservation strategies. It is worth to notice that reference evapotranspiration is a theoretical value based on a standardized reference crop, and actual evapotranspiration of specific crops may vary depending on various factors such as crop type, stage of growth, canopy cover, and management practices.

Potential evapotranspiration (PET) is also another important parameter for evapotranspiration. It is defined as the amount of water that could be potentially evaporate and transpire from a specific area if water availability were not a limiting factor (Hidalgo et al., 2005; Rwasoka et al., 2011). In other words, PET is a measure of the water demand by vegetation and the evaporation from the land surface under ideal conditions, assuming a well-watered surface and adequate energy availability (Stefanidis & Alexandridis, 2021; Xiang et al., 2020a; Zongxing et al., 2014). It considers different climatological elements which influence evaporation and transpiration rates, including temperature, humidity, wind speed, and solar radiation. These factors determine the PET for a given location and time.

The estimation of PET is important in various fields, including agriculture, hydrology, and water resources management. It helps in determining irrigation needs, scheduling

irrigation, estimating water availability, and assessing the water balance of a region (Hidalgo et al., 2005; Todisco & Vergni, 2008). By comparing the potential evapotranspiration with the actual evapotranspiration, one can evaluate the water deficit or surplus in a specific area (Minacapilli et al., 2009; Xiang et al., 2020).

Both the PET and ET_o are typically estimated using empirical formulas or models that incorporate meteorological data such as temperature, relative humidity, wind speed, and solar radiation. The most used and standard method for estimating PET and ET_o is the Penman-Monteith equation (FAO-PM), which is recommended by the Food and Agriculture Organization (FAO) of the United Nations.

With the difficulty of estimate and measure the ETo, scientists and researchers conducted different studies in different parts of the world. There are different methods and approaches available in literature to measure and estimate the ETo. The main categories of evapotranspiration computation groups are direct (field water balance approach and soil moisture depletion approach) and indirect methods (empirical/ statistical methods, micrometeorological methods and remote sensing methods (Henok et al., 2015; Choudhary, 2018; Mokhele et al., 2013; Gharsallah et al., 2013; Hatfield et al., 2016; Long & Singh, 2012; Ochoa-sánchez et al., 2019; Tanner, 1967).

These different estimation approaches of ETo have some limitations mainly related to different climate zones, intention of the study, the spatial scale of the study, time and laborious expenses, and availability of input data. Given the time-consuming, cost, and laborious expenses scientists emphasized empirical/statistical analysis using different empirical approaches. Among these approaches, the most common and convenient are:

- Eddy-covariance (EC) (Anapalli et al., 2018; Ding et al., 2010; Gebler et al., 2015; Gharsallah et al., 2013; Hatfield et al., 2016; Hirschi et al.,2017; Liu et al., 2013; Moorhead et al., 2019; Shusen et al., 2014; Ochoa-sánchez et al., 2019; Alan, 1994; Shi et al., 2008)
- Bowen ratio energy balance (BREB) (Dicken et al., 2012; Inman-bamber & Mcglinchey, 2003; Savage, 2010; Alan, 1994; Shi et al., 2008; Todd et al., 2000; Yunusa et al., 2004; Zeggaf et al., 2008),
- Penman-Monteith Evapotranspiration (FAO56-PM) (Almorox, 2018; Beven, 1979; Cai & Santos, 2007; Choudhary, 2018; Est & Gavil, 2009; Gao et al., 2018; Gong et al., 2006; Hatfield et al., 2016; Jim et al., 2004; Kingston et al., 2009; Mccoll, 2001; Monteith, 2017; Ochoa-sánchez et al., 2019; Res et al., 2005;

Sabziparvar et al., 2013; Schrier et al., 2002; Sentelhas et al., 2010; Sharifi & Dinpashoh, 2014; Shi et al., 2008; Snyder et al., 2004; Sumner & Jacobs, 2005; Tanner, 1967; Tegos et al., 2015; Di et al., 2014; Westerhoff, 2015; Yin et al., 2008)

- Thornthwaite method (Mulualem & Liou, 2020; Dezsi & Mîndrescu, 2018; Dong et al., 2020; He et al., 2013; Hui-mean & Yusof, 2018; Res et al., 2005; Schrier et al., 2011) and
- Hargreaves method (Antonio et al., 2014; Hui-mean & Yusof, 2018; Jim et al., 2004; Kingston et al., 2009; Monteith, 2017; Parajuli et al., 2019; Snyder et al., 2004; Tanner, 1967).

The EC method provides the continuous measurements of long-term fluxes above the canopy at the high temporal resolution. The main limitations of EC include underestimation compared to lysimeter measurements due to errors in turbulent flux measurements (Anapalli et al., 2018; Ding et al., 2010; Gebler et al., 2015; Hirschi et al., 2017; Hatfield et al., 2016; Shi et al., 2008), interruptions during weakly turbulent periods, especially at night (Hirschi et al., 2017; Lee et al., 1996), limited spatial coverage in measurements, making it difficult for model validation at a national scale (Shusen et al., 2014). It is time-consuming, labor-intensive, and costly (Savage, 2010), and involves complex data processing and data quality control methods (Liu et al., 2013).

BREB is also another estimation method of evapotranspiration and it is used in different studies. The main limitations of BREB include the influence of boundary layer stability (Dicken et al., 2012), which can result in poor outcomes for large canopies (Dicken et al., 2012; Yunusa et al., 2004). Additionally, temperature and humidity gradients are small and difficult to measure with sufficient resolution for accurate flux estimation (Alan et al., 1994). The method also tends to underestimate compared to lysimeter data (Zeggaf et al., 2008) and overestimate latent heat fluxes (Blad & Rosenberg, 1976; Inman-bamber & Mcglinchey, 2003; Shi et al., 2008). It requires highly accurate measurements of temperature and vapor pressure gradients, particularly for very rough canopies like forests, when turbulent mixing is significant (Pitacco et al., 1992). Moreover, it is less effective after the growing season (Todd et al., 2000).

Thornthwaite method has also some limitations. For instance, it underestimates evapotranspiration under arid conditions (Hashemi & Habibian, 1978; Subedi & Chávez, 2015), it is not appropriate for estimating oasis evapotranspiration, a condition of advection

of dry hot air to a moist vegetated area (Camargo, 1989), not enough to consider vapor flux and heat balance (Palmer et al., 1958), and underestimation with adjective condition (Al-sudani, 2019).

Hargreaves method has also some limitations like underestimation and overestimation (Givoani et al., 2012; Sepaskhah & Razzaghi, 2009; Subedi & Chávez, 2015) influenced by growing seasons and inconsistency in seasonality (Nikam et al., 2014), overestimation (Quej et al., 2019), low quality results specifically in climates with high humidity and extremely high or low wind speeds (Quej et al., 2019)

The FAO56-PM has been established as a standard for calculating reference evapotranspiration (ET0) (Nikam et al., 2014). This method required air temperature, relative humidity, solar radiation and wind speed data inputs, and produced high quality output results of ETo compared with other empirical estimation methods (Alexandris et al., 2008; Almorox, 2018; Cai et al., 2007; Gong et al., 2006; Res et al., 2005; Schrier et al., 2011; Seginer, 2002). This method is also approved by FAO and American Society of Civil Engineers (ACSE) as the best and comprehensive method when the data inputs are available (Al-sudani, 2019; Almorox, 2018; Anapalli et al., 2018; Jim et al., 2004; Hashemi & Habibian, 1978; Quej et al., 2019; Sharifi & Dinpashoh, 2014; Snyder et al., 2004; Subedi & Chávez, 2015). The FAO56-PM is also recommended for its simplicity in computational processes, as it only utilizes temperature data. It has shown generally good accuracy in describing spatiotemporal characteristics of ETo. Moreover, it performs better with high-quality data and larger farmland sizes to produce more accurate results (Peng et al., 2017). The main challenge of FAO56-PM is the high requirement of data (temperature, wind speed, solar radiation, and relative humidity).

There are many studies related to estimation of evapotranspiration in Mediterranean climate (Est & Gavil, 2009; Gharsallah et al., 2013; Kingston et al., 2009; Moorhead et al., 2019; Subedi & Chávez, 2015). These studies used different methods and approaches for estimation of evapotranspiration also in relation to the purpose of the study. In the central Spanish Pyrenees (Hess & White, 2009) study stated that even though the FAO56-PM challenging high quality of data, this resulted for FAO56-PM method offers a more accurate estimation of reference evapotranspiration than the Hargreaves formula. From 1995 and 1996 maize growth-seasons at Zaragoza, Spain (Utsetet al., 2004) compared the FAO56-PM with to Priestley–Taylor (PT) and the study result revealed that PT-ET0 values were significantly lower than FAO56-PM calculations.

Katerji et al., (2006), tried to calculate the ETo using two models daily and hourly based by consider FAO56-PM baseline. Their results showed that FAO56-PM not much sounding for short period of time rather 10 days and above is more accurate (Katerji & Rana, 2006). The EC showed that underestimated under certain environmental conditions and highly sensitive to the choice of the correction method applied (Perez-priego et al., 2017). According to (Rana & Katerji, 2000) study, they tried to assesses and evaluate six ETO estimation and measurement methods in Mediterranean regions. Based on their study result, FAO56-PM is suitable for the Mediterranean region and monthly and seasonal temporal scale analysis. In the Padana Plain (Northern Italy) (Gharsallah et al., 2013) study result showed that the FAO56-PM has provided better results compare with other estimation and measurements approaches. Some studies also used the FAO56-PM method as the reference to compare and evaluate other methods by considering that the best standard in Mediterranean climates (Alexandris et al., 2008; Samaras & Reif, 2014).

The above studies showed that FAO56-PM is the best method for estimation of ETo and seasonal variation analysis for long time (above 10 days). Moreover, it is the best method for analysis seasonal and monthly variations in the Mediterranean climate (Rana & Katerji, 2000).

2.2 Impacts of photovoltaic panels on local hydroclimate

There is high demand for renewable resources to overcome greenhouse gasses emission of fossil fuel and climate change combating (Edalat & Stephen, 2017; Grippo et al., 2020). Many countries and governments emphasize wind and solar energy to reduce the impact of climate change. Solar photovoltaic (PV) power generation is increasing throughout the world and has significant contribution for the development of renewable energy (Armstrong et al., 2016; Armstrong et al., 2014; Cagle et al., 2020.; Hernandez et al., 2019). The PV industry is highly developed with related to reduction of its cost and high demand of the technology (Jiang & Chen, 2021).

In 2015, Europe generated a power more than 8.2 GW from the solar plants (Dunlop & Roesch, 2020). Germany, Italy, and France hold the lion's share among EU countries. While globally the solar plant is generated around 37.6 GW in 2014 (EU, 2014). Italy has also a great potential for solar energy related to distance from the equator compared with to other EU countries (Farinelli, 2004). In 2014, Italy was

one of the leading countries in solar power coverage of domestic electricity supply, and estimated 8% the total electricity generation of the country (EU, 2014).

The PVs have a great role for environmental sustainability. The most promising significance of PVs are reducing the emission of greenhouse gases (Cagle et al., 2020; Choi et al., 2020; Delfanti et al., 2016; Kibaara, 2016; Zhiyong et al., 2012; Pisinaras et al., 2014) and cut off the emission of fossil fuel (Chowdhury & Kibaara, 2016; Pisinaras et al., 2014), non-generating liquid or solid waste products (Liu, 2019; Tsoutsos et al., 2005) and they are also cost effective compared with to other source of energy (Delfanti et al., 2016; Martín-Chivelet, 2016; Ong et al., 2013). The reduction the emission of greenhouse gases (CO_2, CH_4, N_xO and chlorofluorocarbons) and providing sustainable energy are the two-primer objectives of the PVs.

Studies also showed that the PVs have additional environmental benefits with the connection of the establishment of PVs. The PVs shaded areas increase the soil water content and reduce evaporation rate compared with to PVs unshaded area in semi-arid of Xingqing District, in the Ningxia Hui Autonomous Region, China (Liu, 2019). Results of This study also revealed that the PVs enable to not only supply clean energy but also to bring unintended ecological benefits in the future. The PV also improves the air quality by balancing the energy and decreasing the emission of greenhouse gases (Taha, 2012).

Hassanpour et al., (2020) addressed the potential impact of agrovoaltic solar panels in microclimatology, soil moisture, water usage and biomass in semi-arid environment. Their result showed that areas under PVs have higher soil temperature than areas far away from PVs and higher biomass concentration (90%) and 328% water-efficiency under PVs area. They also illustrated the Water Use Efficiency (WUE). It was calculated as the biomass produced per unit of water used.

Taha (2012) simulation study results showed that there were no adverse impacts on air temperature and urban heat islands from largescale PV deployment; instead, results showed that solar PV can cool the urban environment by 0.2 °C in Los Angeles. The analysis result for 30 consecutive years of Landsat satellite imagery

across the Lower Colorado Desert, showed that there was no effect of solar energy development on vegetation canopy cover based on normalized difference vegetation index (NDVI) values (Potter, 2016). Another study (Armstrong, Burton, et al., 2016) result showed that during the summer season, they observed cooling, of up to 5.2 °C, and drying under the PV arrays compared with gap and control areas. While, during the winter gap areas were up to 1.7 °C cooler compared with under the PV arrays and control areas in Westmill Solar Park, UK.

The PVs facilities which are installed in degraded lands, are useful for reuse of degraded land. Moreover, the PVs will be installed with agricultural land and energy production for co-location for agriculture and energy production (Stefano et al., 2018; Barron-gafford et al., 2019; Delfanti et al., 2016; Hassanpour et al., 2020; Marrou et al., 2013).

Solar plants have been shown to create positive biodiversity impacts when compared to other types of intensive land use. For example, solar plants in the UK previously used for agriculture were found to have a greater diversity of flora and birds when managed through grazing (Bennun et al., 2021; Hernandez et al., 2014). The PV technology also resulted in land use changes in different parts of the world. For instance, in the UK, Europe, and globally, it led to land use changes for ground-mounted solar PV in 2013, which covered approximately 15–79 km^2, 204–1019 km^2 and 554–2772 km^2, respectively (Armstronget al., 2016). Even though the PVs have great efficiency to reduce the emission of greenhouse to the atmosphere, it has also adverse impacts on vegetation (Armstrong et al., 2016), microclimate (Armstrong et al., 2014), hydrology (Pisinaras at al., 2014), soil chemical and physical characteristics and temperature (Armstrong et al., 2014; Delfanti et al., 2016; Hassanpour et al., 2020), energy budget (Wu et al., 2020) , soil erosion (Wiesinger et al., 2018), air quality (Taha, 2013), landscape values (Bevk & Golobič, 2020) , and aesthetic values (Torres-sibille et al., 2009).

The effects of PV panels on soil temperature and moisture were studied by Yue and Guo in 2021. The study found that the PV panels increased the average soil temperature during winter but decreased it during the other three seasons.

Moreover, their studies showed that at the sites without shaded areas, the average soil moisture under the shaded by fixed tilt PV panels and under the shaded by oblique single-axis PV panels increased by 14.7% and by 11.1%, respectively. In desert areas, the daily range of soil temperature at a depth of 5–10 cm at a solar farm was lower than that in areas without the PV farm (Yang et al., 2017). The temperatures over a PV plant were regularly 3–4 °C warmer than wildlands at night (Barron-gafford et al., 2016). Under the PV panels mean air and soil temperature during the growing season were cooler compared to the gap between the PV panel rows, by approximately 2 °C and 4 °C, respectively (Makaronidou, 2020). The diurnal air temperature and relative humidity ranges in the PV power plant were greater than those outside the PV power plant (Wu et al., 2020).

Studies showed that the land use change because of PV will adversely impact on habitat fragmentation and disruption the genetic resource movement like pollination, disturbance regulation and storm protection, water supply especially flow direction, biodiversity, land scarcity, food production system, surface water and beautiful sceneries (Murphy-mariscal et al., 2018; Turney & Fthenakis, 2021). The natural CO_2 sequestration of capacity of the vegetation is decreased because increasing and installation the PV at Lecce, Southern Italy (Antonella et al., 2014). There are different monitoring systems that are adopted to synthesize the PV impacts on environment. Studies applied different approaches such as literature review, monitoring experiment and in situ measurements. The effects of PVS on environment have different temporal scale such as during construction, operation and decommissioning of the PV facilities (Murphy-mariscal et al., 2018).

2.2.1 The impacts of PVs on air temperature, humidity, wind direction and speed, and radiation

The PV panels have impacts on air temperature and microclimate. Taha (2012) studied the impacts of PVs on air temperature using mesoscale and meso-urban meteorological models. The results showed that large-scale deployment of solar PV arrays has no adverse impacts on the atmosphere, solar conversion efficiency of

20% or higher. Moreover results showed that PV arrays can cool the air and that a very high-density deployment of PV can cause some warming but also larger cooling. The PVs reduced the albedo, and this results in the PV values for climate mitigation solutions underlying on how its deployed and installed (Nemet, 2009). The temperature, albedo, and cloud cover impacts of PVs were assessed in the Mojave Desert of California using the coupled climate Weather Research and Forecasting (WRF) model (Millstein & Menon, 2011). The result showed that the desert surface albedo was darkened, causing local afternoon temperature increases of up to +0.4 ◦C. Due to the solar arrays, local and regional wind patterns within a 300 km radius were affected. Statistically significant but lower magnitude changes to temperature and radiation could be seen across the domain due to the introduction of the solar arrays. The addition of photovoltaic arrays caused no significant change to summertime outgoing radiation when averaged over the full domain, as interannual variation across the continent obscured more consistent local forcing (Millstein & Menon, 2011).

Taha, (2012) simulation study result showed that there were no adverse impacts on air temperature and urban heat islands from largescale PV deployment rather than resulted for solar PV can cool the urban environment by 0.2 0C in Los Angeles.

Using the HIS-PV (Heat In the Solar PV park) model (Makaronidou, 2020) the annual incoming shortwave radiation was strongly affected by solar park installation; control received 60% more solar radiation than under and 8% more than the gap across all tested zones ($p < 0.001$).

Studies showed that contradicting with related to the impact of PVs on air temperature. In temperate regions it results increasing of temperature because of PVs and resulted for urban heat island (Barron-Gafford et al., 2016a) while in semi-arid regions the temperature is cooling because of the PVs (Millstein & Menon, 2011; Taha, 2013; Turney & Fthenakis, 2011). This might happen with different experimental designs. For instance, Barron-gafford, (2016) measured the air temperature from 2.5 heights while Taha, (2013) measured the air temperature from 5m heights. The variability in experimental design and measurement heights has

also led to discrepancies in the results of various studies. This scenario has been verified (Gao et al., 2016).

On the other hand, there is also increase and decrease of the air temperature because of the PVs in deserts areas of the Gonghe PV Power Plant in Qinghai, China (Wu et al., 2020). In their experimental campaign, they installed air temperature and soil moisture and temperature sensors in under the PVs, gap between the two PVs rows and another reference points to analyze the response of air temperature for the PVs. The result showed that the overall daytime air temperature in the PV power plant had changed slightly (increased and decreased), while the night-time temperature dropped significantly. Specifically, in spring and summer, the daytime temperature increased slightly, with a maximum increase of 0.34 ◦C; in autumn and winter, the daytime temperature decreased slightly, with a maximum decrease of 0.26 ◦C; in all seasons, the night-time temperature decreased, with a maximum decrease of 1.82 ◦C during the winter night.

This study (Wu et al., 2020) also examined the relative humidity with the same experimental set up; the result showed that the relative humid in the PV power plant generally increased; except for a slight decrease in summer, the daytime and night-time relative humidity in spring, autumn, and winter always increased.

In Qinghai Province (China) the Golmud solar park was also monitored by measuring under the PV site and outside of the PV area (far away 645 m from the PV site) (Yang et al., 2017). In the PV site they measured wind direction, air temperature, humidity and solar radiation from 10 m height and they measured the same variables from 2 m height except solar radiation (which was measured from 1.5 m height). On the other hand, in the area without PV site (reference that was 645 m far away from the PV site), wind speed and direction measurements were taken at a height of 3 m , while air temperature and humidity measurements were taken at a height of 2 m . The measurement taken at a height of 1.5 m was solar radiation. The result of this experiment showed that the mean daily albedo in PV site is 0.19, while it is 0.26 in the area without PV. The annual mean net radiation in the PV site is clearly higher than that of the region without PV (Yang et al., 2017).

Moreover, daytime air temperature measured from 2 m height in the two sites is essentially the same during winter, while during the other seasons, the daytime air temperature in the PV site is higher than that in the region without PV, with the maximum difference occurring during the summer. However, the nighttime air temperatures at height of 2 m during the four seasons in the solar farm are higher than those in the region without PV. The monthly average 2-m air temperature in the solar farm is higher than that in the region without PV.

In Westmill Solar Park (UK) (Armstrong et al., 2016) measurement points - under the PV, gap between the two PV and reference point far away the PV area- were established. From these points, they measured hourly air temperature and relative humidity data for one year from the height of 0.5 meter. The result showed that the diurnal variation in both temperature and humidity during the summer was reduced under the PV arrays.

Using the two eddy covariance observational towers, Barron-gafford et al., (2019) analyzed the impact of PVs on surface temperature and energy balance in the southern Arizona. The results showed that the average daily maximum 1.5 m (height of the recorder) air temperature at the PV array was 1.38C warmer than the reference (i.e., non-PV) site, whereas no significant difference in 1.5 m (height of the recorder) night-time air temperature was observed. Moreover, the PV modules significantly reduce ground heat flux QG storage and night-time release, as the soil beneath the modules is well shaded.

The wind speed at the gap between the PVs is slowed down by 63% annually compared to the control areas of the PVs (reference areas of the PV) (Armstrong, Burton, et al., 2016) in the UK Grassland. There is also increase of wind speed from the above and a decrease in the magnitude of the afternoon south-westerly winds under the panels due to changes of the albedo and the surface roughness in desert environments (Millstein & Menon, 2011). Moreover, in temperate environment, Fthenakis & Yu, (2013) showed that heating and cooling of the air temperature inside the solar park was a function of wind speed, which was south-westerly and seemed to be affected by the physical presence of the solar park.

The microclimatic conditions between panel mounts were found to be more extreme than in the surrounding desert yet beneath the panel's temperature is lower and relative humidity higher than outside the panel area (Anna et al., 2017).

2.2.2 The impacts of PVs on runoff, percolation, and evapotranspiration

During construction of the PV and its facilities, there are impacts on surface-water flow pathways and water quality, particularly when projects are sited on bajadas, individual alluvial fans, floodplains, or near washes. Moreover, the PV required cooled water (in arid desert areas) and washing water for the PVs to clean the plates; these will result in water stress in the area (Murphy-mariscal et al., 2018). Recent studies in Southwestern US showed that the water use for dust removal is the main component (60%-99%) of water consumption in the PV installation (Hernandez et al., 2015). By using HIS-PV (Heat In the Solar PV park) model, Makaronidou, (2020) showed that in the area which are completely shaded by the PVs the potential evapotranspiration was strongly affected in the Arid (46% less) and the Equatorial ((35% less)) zone, compared to the area outside of the PV park (significant level $p < 0.001$).

The PVs has also adverse impacts on geohydrological resources including the erosion of topsoil, that facilitate for the sediment load or turbidity in local streams, reduction in the filtration of pollutants from air and rainwater, the reduction of groundwater recharge, or the increased likelihood of flooding (Chiabrando et al., 2009; Turney & Fthenakis, 2011).

The PVs also has direct effects on hydrological cycle like runoff, percolation, and evapotranspiration. The study (Pisinaras et al., 2014) in Vosvozis river basin in North Greece, identified, conceptualized and quantified the PV response by using SWAT model for hydrological cycle like evapotranspiration, percolation and runoff. The results showed that the general trend observed both in basin and sub-basin scale is that surface runoff and percolation increase, while evapotranspiration decreases. In general, the coverage of 1% basin area with PVPs does not significantly affect the hydrologic budget of the basin, as surface runoff changes ranged between 0.9 and 1.27 mm, while the corresponding ranges for

evapotranspiration and percolation were 2.3 to 5.2 mm and 0.17 to 0.52 mm, respectively. Moreover, the study predicted the long-term potential impact of the PVs on local climate using Regional Climate Model (RCM) simulation. This simulation from 2011 to 2100 showed that surface runoff and percolation potential are significantly increased at the local scale.

2.2.3 The impacts of PVs on soil moisture, soil temperature, and soil erosion

Makaronidou, (2020) monitored and modelled the spatiotemporal impacts of PV panels during growing and non-growing seasons using five linear transects, each running perpendicular between two PV panel rows at solar PV park in Wiltshire, UK, during 2015-2016. The results showed that the areas which are completely shaded by the PV panels mean air and soil temperature during the growing season were cooler compared to the gap between the PV panel rows, by approximately 2 °C and 4 °C, respectively. Moreover, the soil moisture under the panels was higher during growing season compared to the gap. Under the PV panels, soil bulk density was higher, and the organic matter lower, likely the result of compaction and vegetation management during and after construction. In contrast, the induced microclimate showed no spatial effect on leaf area index (LAI) nor on the net ecosystem exchange (NEE) and the water (H2O) vapor fluxes.

In the desert areas of Gonghe PV power plant, Qinghai Province, China (Yue & Guo, 2021); analyzed the PVs impacts on soil temperature and moisture by measuring within a depth of 0–0.4 m from the three types of PV shading conditions: shaded by fixed- tilt (FIX) PV panels, shaded by oblique single-axis (OSA) PV panels, and no shading. The results revealed that both soil temperature and moisture under PV shading were significantly affected compared with those at sites without shading. PV panels increased the average soil temperature during winter but decreased it during the other three seasons. Whereas, the moisture result showed that PV panels have positive effects on soil moisture. Compared with that at the sites without shaded areas, the average soil moisture under the FIX PV panels and under the OSA PV panels increased by 14.7% and by 11.1%, respectively.

In Qinghai Province, China, the Golmud solar park also studied by measuring in PV site and without (far away 645 m from the PV site) (Yang et al., 2017). In the PV site measured the soil temperature at 5, 10, 20, 40, 80, and 180 cm were recorded in the solar farm. Moreover, the area without PV site (reference that 645 m far away from the PV site), taken the soil temperature measurements at 5, 10, 20, 40, 80, and 180 cm were recorded in the region without a PV array. The result of this monitoring system revealed that the daily range of soil temperatures at a depth of 5– 10 cm in the PV site is lower than that in the region without a PV farm. The annual range of soil temperatures at a depth of 5–180 cm in the PV site is higher than that in the region without PV. The soil temperatures at different depths in winter in the PV site are clearly lower than those in the region without PV. The daily mean of soil temperatures at a depth of 5-80 cm from October 2012 to March 2013 in the PV site is clearly lower than that in the region without a PV array (Yang et al., 2017).

Moreover, on Westmill Solar Park, UK (Armstrong et al., 2016) established 3 sites (under the PV, gap between the two PV and reference point far away the PV area. From these sites, they measured soil temperature and moisture from 10 cm above and below the surface for one year. The result of this study showed that during autumn and winter the soil in the gap area was, on average, 1.7 °C cooler than the control and under PV throughout the diurnal cycle.

The PVs also have their adverse and positive impacts on soil erosion. The PVs will protect (during operation) the soil erosion especially in the desert areas from wind erosion (Zhiyong et al., 2012). They also have adverse impacts during the construction time by damaging and destroying the soil strata and vulnerable for erosion especially the sand soils texture profile.

Beyond the soil moisture and temperature, there are also studies conducted the impact of the PVs on soil chemical and physical characteristics. After 7 years of revegetation in Colorado, US (Choi et al., 2020); the carbon and nitrogen remained lower in the PV soil than in the reference soil (outside from the PVs area) and contained a greater fraction of coarse particles. Moreover, the PV modules

introduced heterogeneity in the soil moisture distribution, with precipitation accumulating along the lower edges of panels.

In Rabbit Hills agrivoltaic solar of Oregon State Campus (Hassanpour et al., 2020), analysed and quantified the impact of agrivolatic (agriculture and PV) on soil temperature, moisture and air temperature and biomass. The result showed that there were significant differences in mean air temperature, relative humidity, wind speed, wind direction, and soil moisture were observed. Areas under PV solar panels maintained higher soil moisture throughout the period of observation. Moreover, there was also a significant increase in late season biomass areas under the PV panels (90% more biomass), while areas under PV panels were significantly more water efficient (328% more efficient).

Table 2.1 Summary of the potential impacts of PVs on hydroclimate and soil

PVs impacts on hydrology	PV impacts on soil	PV impacts on microclimate
➢ High consumption of water for cleaning and cooling (Murphy-mariscal et al., 2018). ➢ PVs shaded areas, the potential evapotranspiration was strongly affected in the Arid (46% less and the Equatorial ((35% less)) zone, relative to the control; ($p < 0.001$) (Makaronidou, 2020). ➢ Erosion resulted for sediment load or turbidity in local streams, reduction in the filtration, low ground water recharge, flooding, increasing runoff. (Chiabrando et al., 2009; Turney & Fthenakis, 2011). ➢ Surface runoff and percolation increase, while evapotranspiration decreases; and surface runoff and percolation potential are significantly increased at the local scale (Pisinaras et al., 2014).	➢ In growing seasons, the soil temperature of the PVs shaded areas were much cooler than other areas ; while the soil moisture were higher than the PVs unshaded areas(Makaronidou, 2020; Hassanpour et al., 2020). ➢ Moreover, under the PVs shaded areas have higher bulk density and lower organic matter, C & N compared with to PVs unshaded (Makaronidou, 2020; Choi et al., 2020). ➢ PV shaded are higher soil temperature in winter seasons, and lower in other seasons; have positive effects on soil moisture (Yue & Guo, 2021). ➢ Lower daily range, and higher annual range of soil Temp in PV shaded areas compared to unshaded (Yang et al., 2017).	➢ Solar PV arrays has no adverse impact on the atmosphere, solar conversion efficiency of 20% or higher (Taha, 2012) ➢ PVs reduced the albedo (Nemet, 2009). ➢ Desert surface albedo was darkened, afternoon Temp increase, wind pattern with 30 km changed (Millstein & Menon, 2011). ➢ Both reference (60%) and gap areas (8%) have more radiation than under shaded areas (Makaronidou, 2020). ➢ Relative humidity slightly decreased in summer; and the daytime and night-time relative humidity in spring, autumn, and winter always increased (Wu et al., 2020).

2.2.4 The impacts of PVs on biodiversity and ecosystem

The large development of PVs will be impacted in the areas where high biological endemism (species with very limited distributions that are often highly adapted to their environments), fragile habitats, and high solar resources co-occur, such as the Mojave Desert in the southwestern United States (Murphy-mariscal et al., 2018). During construction and operation there is removal of aboveground biomass and in mortality of wildlife or species displacement especially when grading and scraping. Moreover, it will disturb the soil profile and resulted for the destruction of the soil biota. The PV and its facilities will impact on birds, mammals, insects, reptiles and plants (Murphy-mariscal et al., 2018). These biodiversity will be impacted by the PVs and resulted for habitat fragmentation, panels and mirrors ("lake effect"), and fences (Hernandez et al., 2019). The PVs also impacted through making barriers on the movements of species, vegetation cleared (construction), and disturbance on the ecosystem interaction of organisms (Armstrong et al., 2016, 2014; Hernandez et al., 2014; Makaronidou, 2020; Potter, 2016; Turney & Fthenakis, 2021). Dust suppressants, rust inhibitors, antifreeze agents, and herbicides will deplete the biodiversity in long-term either regional or local level (Abbasi & Abbasi, 2000).

The PV will be impacted during construction and operation time. The drastic damage will happen during the construction time (Zhiyong et al., 2012); the machinery and transport vehicles will destroy most vegetation coverage and habitat, cause environmental vibration and noise, which will scare the animals will migrate from their habitat.

The PVs development asl adversely impacted on aquatic habitat and biota. The PV will impacts on them through loss, fragmentation, or prolonged drying of ephemeral water bodies and drainage networks resulting from the loss of desert washes during the construction of its facility (Grippo et al., 2020). It resulted to attract aquatic insects and water- birds, potentially resulting in mortality.

Experimental studies showed that the species diversity, with both lower under the PV arrays (completely shaded by the PV panels) (Armstrong et al., 2016).

Photosynthesis and net ecosystem exchange in spring and winter were also lower under the PV arrays. This study also revealed that the solar plant revegetated with grassland showed that species diversity was lower under PV panels as a result of differences in soil and air temperature

According to IUCN (2021) report the PVs have the following adverse impacts on biodiversity and ecosystem service of on biosphere. These are loss of habitat through clearance or displacement of land, bird collision with solar panels, and transmission lines, bird and bat mortality through electrocution on distribution lines, displacement due to attraction to reflective surface of solar panels, wildlife mortality due to attraction to evaporation ponds, barrier effects to terrestrial biodiversity movement, habitat degradation due to changes in hydrology and water availability and quality, pollution (e.g. dust, light, noise and vibration, solid/liquid waste), indirect impacts from displaced land-uses, induced access or increased economic activity, associated ecosystem service impacts, habitat alteration due to changes in microclimatic effect of solar panels and introduction of invesive and alien species.

2.3 Discrepancies of the findings

Most of the studies applied comparisons of PVs between PVs shaded areas, gap areas and reference areas. The results showed that there were discrepancies of the impact of PVs on the PVs shaded area's on hydroclimatic, soil and biodiversity pattern.

The shaded areas under the PV panels showed an increase in air temperature from heights of 0.5 meters to 2.7 meters compared to reference areas (Adeh et al., 2018). It was observed that the annual air temperature was consistently higher (Fthenakis & Yu, 2013). At night, the shaded areas were regularly 3–4 °C warmer than wildlands (Barron-Gafford et al., 2016). From a height of 1.5 meters, the average daily temperature was 1.3°C warmer (Broadbent et al., 2019). Additionally, higher daytime air temperatures were observed in all seasons except winter, along with

higher nighttime temperatures in all seasons and higher monthly temperatures (Yang et al., 2017).

Studies have also confirmed that there was no change air temperature between PVs shaded and reference areas (Taha, 2013); from 1.5m height record the air temperature (Broadbent et al., 2019); and daytime air temperature in winter (Yang et al., 2017). In contrast, the PVs shaded areas also showed decreasing of air temperature during summer season (Armstrong et al., 2016) from 1.2 m and 2.0 meters height (Adeh et al., 2018).

Relative humidity also showed discrepancies between the PV shaded and reference area. The relative humidity of the PVs shaded areas showed that lower compared with to the reference areas from 0.5, 1.2, 2 and 2.7 meters heights (Adeh et al., 2018); decreasing trend in summer season (Armstrong et al., 2016); and general decreasing trend of relative humidity (Pisinaras et al., 2014). On the other hand , the relative humidity also showed higher values on full day, and during spring, winter, autumn seasons (except slight decreasing in summer season) (Wu et al., 2021).

The biodiversity and the biomass of the PVs shaded areas showed decreasing compared with to reference areas (Armstrong et al., 2016). The net ecosystem and photosynthesis also lower in spring and winter season under the PV shaded areas compared with to the reference area (Armstrong et al., 2016). Moreover, the PV shaded areas affected the aquatic ecosystem because of the loss, fragmentation, or prolonged drying of ephemeral water bodies and drainage networks resulting from the loss of desert washes within the construction footprint of the facility (Grippo et al., 2015). Additional adverse impacts of PVs on biodiversity and ecosystem are habitat degradation, birds and wildlife mortality and displacement, invasive species, barrier for the integration of ecosystem, light, noise and other pollution (Armstrong et al., 2014; Bennun et al., 2021; Hernandez et al., 2014). On the other hand, the PVS also resulted in an increasing of vegetation population and also resulted increasing of precipitation (Li et al., 2018); and biomass, microhabitat index and species richness were showed higher values because the area was desert

and arid (Liu et al., 2019).

The PVs shaded areas showed that lower amount of incoming short radiation and net solar radiation (Adeh et al., 2018); upward long-wave radiation at night and similar amount at daytime , lower average surface albedo (Li et al., 2022); lower albedo (Yang et al., 2017); lower photosynthetically active radiation (PAR) (Liu et al., 2019); and decrease of incident solar radiation reaching the ground surface (Pisinaras et al., 2014). In contrast, studies also showed that the PVs shaded areas showed that higher amount daytime net radiation (Broadbent et al., 2019); annual mean net radiation (Yang et al., 2017), average net radiation of the underlying surface (Li et al., 2022); and the daytime net shortwave radiative forcing increases (Jiang et al., 2021).

The PV shaded areas configured higher soil water content and low evaporation (Liu, 2019; Liu et al., 2019); lower evapotranspiration and better water efficiency (Marrou et al., 2013a); discrepancy in the soil moisture distribution, with precipitation accumulating along the lower edges of panels (Choi et al., 2020); and significantly more water efficient (328%) (Adeh et al., 2018). The PVs shaded areas also did not significantly affect the hydrologic budget of the basin, as surface runoff changes ranged between 0.9 and1.27mm, while the corresponding ranges for evapotranspiration and percolation were −2.3 to −5.2 mm and 0.17 to 0.52 mm, respectively (Pisinaras et al., 2014).

The wind speed and direction were also affected by the PV infrastructure. The shaded areas under the PV panels predominantly exhibited a southward direction (Adeh et al., 2018; Armstrong et al., 2016; Fthenakis & Yu, 2013; Makaronidou, 2020; Millstein & Menon, 2011; Turney & Fthenakis, 2011) because related to the orientation of the panels. Moreover the PVs area wind speed showed that higher speed (Adeh et al., 2018; Jiang et al., 2021). On the other hand the wind direction of the southernly is getting decreased by 38% from 10m height of observation (Jiang et al., 2021).

The PVs have also affected the soil -physical and chemical characteristics. The study result showed that the carbon and nitrogen remained lower in the PV soil than

in the reference soil and contained a greater fraction of coarse particles (Choi et al., 2020). PVs shaded areas increased the average soil temperature during winter but decreased it during the other three seasons and the soil moisture was higher all seasons under the PVs shaded areas (Yue et al., 2021); higher soil moisture in a year from 20-60 cm depth (lower soil moisture less than 20 cm depth) (Adeh et al., 2018); and higher annual range of soil temperature (Yang et al., 2017). The PVs areas also showed that decreasing of soil temperature (Liu et al., 2019); lower soil temperature all seasons except winter season (Armstrong et al., 2016); and lower daily range of soil temperature (Yang et al., 2017).

To sum up, these finding discrepancies are resulted with the different climate zones and types, instrumentation and experiment procedures, duration and timing of data recording and duration of analysis (Figure 2.1).

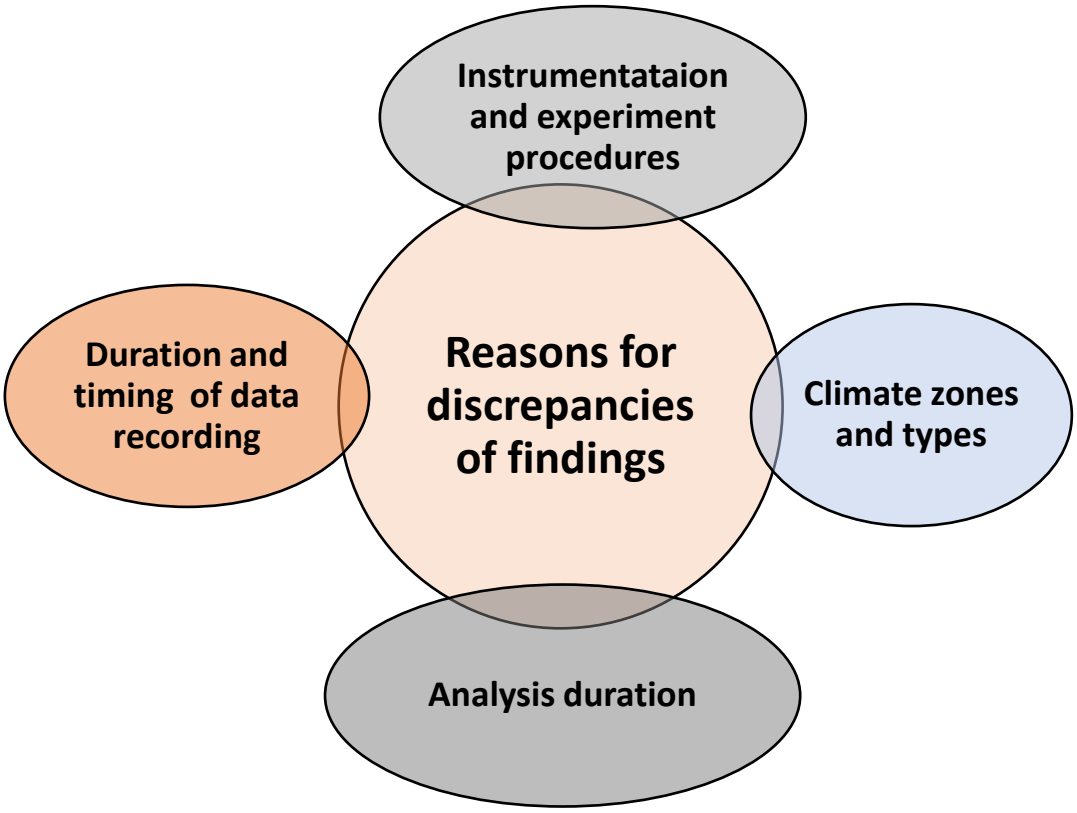

Figure 2. 1 The reason for discrepancies of findings regarding the impacts of PVs on different hydroclimate, soil and biodiversity.

2.4 Conclusion

The PV infrastructure is growing at an alarming rate worldwide, with a focus on efficiency to reduce greenhouse gas emissions into the atmosphere. However, there is a lack of awareness regarding the potential adverse impacts of PVs on hydrology, climate, soil, biodiversity, and other environmental components. Studies have shown that PVs can have both negative and positive impacts on climate, soil, and hydrology, as well as instances where no significant changes occur.

The impact of PVs on local air temperature varies. Research by Taha (2013) indicates that there is no change in air temperature due to PVs. However, a comparison between shaded PV areas and unshaded areas reveals daily, seasonal, and annual variations in air temperature. In desert areas, the shaded PV areas tend to be much warmer than the unshaded areas in the afternoon, while in temperate zones, the PV areas are cooler than the unshaded areas during summer seasons. These temperature variations also occur during winter, summer, and growing and non-growing seasons. In temperate regions, PVs contribute to increased temperatures, leading to urban heat islands, whereas in semi-arid regions, PVs contribute to cooling. PVs also affect radiation, with shaded areas receiving less solar radiation compared to unshaded areas. Furthermore, relative humidity increases both during the day and night due to PVs, except in the summer season. Additionally, PVs slow down and decrease wind speed compared to areas without PVs, which regulates air temperature and affects albedo under the PVs due to reduced wind speed.

The PV infrastructure requires cooled water in arid desert areas and washing water to clean the PV panels. This results in water storage and stress in the area. PVs also have an impact on the geohydrological environment, causing topsoil erosion, increased turbidity in local streams, reduced filtration of pollutants from air and rainwater, decreased groundwater recharge, and an increased likelihood of runoff flooding. PVs contribute to increased surface runoff and percolation while decreasing evapotranspiration.

PVs also affect soil by regulating soil temperature and moisture, as well as causing

soil erosion and destruction of soil strata during PV infrastructure construction. For example, the soil temperature and organic content under the PV panels are significantly lower during the growing season compared to areas not covered by PV panels. Additionally, soil moisture and soil bulk density under the panels are higher during the growing season compared to the gaps. Moreover, the magnitude of the impact of PVs on soil varies with soil depth. For instance, the daily range of soil temperature at a depth of 5-10 cm is lower in the PV areas compared to unshaded areas, whereas the annual range of soil temperatures at a depth of 5-180 cm in the PV site is higher than that in regions without PVs.

In conclusion, PVs have potential impacts on microclimate, soil, and hydrology. However, discrepancies in findings exist due to different monitoring systems, climatic zones, and experimental designs.

Chapter 3

Evaluation of Reference Evapotranspiration Estimation Methods for the Assessment of Hydrological Impacts of Photovoltaic Power Plants in Mediterranean Climates

Abstract:

Large-scale photovoltaic (PV) power plants may affect the hydrological cycle in all its components. Among the various components, evapotranspiration is one of the most important. As a preliminary step for assessing the impacts of PV plants on evapotranspiration, in this study, we performed an evaluation study of methods for estimating reference evapotranspiration (ETo). FAO and ASCE recommend the Penman–Monteith (PM) method for the estimation of ETo when the data for all involved variables are available. However, this is often not the case, and different empirical methods to estimate ETo, requiring mainly temperature data, need to be used. This study aimed at assessing the performance of different temperature- and radiation-based empirical ETo estimation methods against the standardized PM ETo method in an experimental photovoltaic power plant in Piazza Armerina, Sicily, Italy, where a meteorological station and a set of sensors for soil moisture were installed. The meteorological data were obtained from the Ambiens Energy srl Environmental Lab from July 2019 to end of January 2022. By taking the ETo estimations from the PM method as a benchmark, the study assessed the performance of various empirical methods. In particular, the following methods were considered: Hargreaves and Samani (HS), Baier and Robertson (BR), Priestley and Taylor (PT), Makkink (MKK), Turc (TUR), Thornthwaite (THN), Blaney and Criddle (BG), Ritchie (RT), and Jensen and Haise (JH) methods, using several performance metrics. The result showed that the PT is the best method, with a Nash–Sutcliffe efficiency (NSE) of 0.91. The second method in order of performance is HS, which, however, performs significantly worse than PT (NSE = 0.51); nevertheless, this is the best among methods using only temperature data. BG, TUR, and THN underestimate ETo, while MKK, BG, RT, and JH showed overestimation of ETo against the PM ETo estimation method. The PT and HS methods are thus the most reliable in the studied site.

Keywords: statistical performance metrics; Penman–Monteith method; empirical methods; PV panels

3.1 Introduction

Recently, the solar photovoltaic (PV) plant areas have been increasing globally, as they are seen as a valid source of renewable energy production (Armstrong et al., 2014, 2016; Cagle et al., 2020; Edalat & Stephen, 2017; Grippo et al., 2015; Hernandez et al., 2019). These PV panels contain directly produced energy from the incoming solar radiation (Barron-Gafford et al., 2016; Nemet, 2009; Yang et al., 2017). The PV will be influenced and attributed on the amount of solar radiation on the existing local climate system (Barron-Gafford et al., 2016; Broadbent et al., 2019; Yang et al., 2017). This solar radiation is also a crucial part of reference evapotranspiration (ETo). Solar radiation highly contributed to the trend and sensitivity of evapotranspiration compared with the other climatological elements (Luo et al., 2021; MÉszáros & Miklánek, 2006). Therefore, before we estimate and analyze the impact of PV on evapotranspiration, it is necessary to carefully select which empirical estimations should be applied on the study area.

The ETo process is entirely linked to the exchange of water and energy within land, soil, atmosphere, and biosphere (Gebler et al., 2015; Moeletsi et al., 2013; Ochoa-Sánchez et al., 2019). ETo can be estimated by using earth–atmosphere energy balance aerodynamics principles or by more simplistic empirical models (Moeletsi et al., 2013; Pandey et al., 2016). The estimation of ETo can be carried out either directly (field water balance approach and soil moisture depletion approach) or indirectly (empirical/statistical methods, micrometeorological methods, and remote sensing methods) (Alemu et al., 2015; Choudhary, 2018; Gharsallah et al., 2013; Hatfield et al., 2016; Long & Singh, 2012; Moeletsi et al., 2013; Tanner, 1967). Empirical estimation of ETo is very helpful to understand the spatiotemporal configuration of hydrological cycle and climatological components and for water use, agricultural, ecological applications, and other developmental projects (including large-scale photovoltaic panels) (Chen et al., 2005; Moeletsi et al., 2013; Xu & Singh, 2002). An accurate estimation of ETo is important to improve the understanding of water and energy exchange processes between land and atmosphere that are relevant for many scientific disciplines and agricultural management (Gebler et al., 2015).

Mediterranean climate studies have evaluated the ETo empirical estimation methods against the PM method and filed measurements (Est & Gavil, 2009; Gharsallah et al., 2013; Kingston et al., 2009; Moorhead et al., 2019; Subedi & Chávez, 2015). With reference to the Central Spanish Pyrenees, Hess and White (2009) found that the FAO56–PM method offers a more accurate estimation of reference evapotranspiration than the Hargreaves formula against the field lysimeter measurement. From 1995 and 1996, a study on the maize growth seasons

at Zaragoza, Spain (Utset et al., 2004), compared the FAO56–PM with Priestley–Taylor (PT), and the study revealed that PT ETo values were significantly lower than the FAO56–PM calculations.

Katerji and Rana (2000) calculated the ETo by using the FAO56–PM method from hourly and daily data. The result of this study showed that the FAO56–PM was not effec- tive for timescales shorter than 10 days, whereas for greater intervals, it was more accurate. Katerji and Rana (2000) evaluated ten ETo estimation methods in Mediterranean regions by field lysimeter measurements; the results showed that the FAO56–PM is sufficiently accurate for the Mediterranean region at monthly and seasonal temporal–scale analysis, and the second for performance was the Hargreaves–Samani method (1985) (Rana & Katerji, 2000). Gharsallah et al. (2013), with reference to two sites in the Padana Plain, Northern Italy, showed that the FAO56–PM provides better results than other indirect estimation methods against lysimeter measurements. The FAO–PM method also showed the highest R2 (0.96) value compared to radiation-based models of Makkink and Priestley–Taylor, against scintillometer measure- ments in Sicily (Agnese et al., 2012). The FAO–PM method is used as a standardized method for comparison of other temperature, radiation, and mixed (radiation and temperature) based methods in different areas of the world (Nikam et al., 2014; de Melo & Fernandes, 2012; Lang et al., 2017; Pandey et al., 2016; Xu & Singh, 2002).

A study in Alentejo, Southern Portugal (Rodrigues & Braga, 2021), also evaluated nine ETO estimation empirical methods; the result showed that the HS radiation adjustment coefficient (kRs) produced the best performance against the FAO56–PM. In addition to the ETo empirical estimation methods, machine learning also proved to be helpful to estimate the ETo. A study in Valenzano, Southern Italy, showed that the k-Nearest Neighbor (kNN) machine learning technique had the best performance only when using temperature data input, compared with the Artificial Neural Networks (ANNs) and Adaptive Boosting (AdaBoost) models to predict daily potato crop evapotranspiration against the gravimetric measurement and FAO–PM method (Yamaç & Todorovic, 2020). Yamaç and Todorovic (2020) conducted a study that also confirmed that ANN showed the highest performance with temperature, wind speed, solar radiation, and relative humidity data inputs compared with the machine learning techniques against the FAO–PM method and gravimetric measurement. The study in Ranichauri (India) and Dar El Beida (Algeria) compared the artificial neural network (ANN)-embedded grey wolf optimizer (ANN–GWO), multi-verse optimizer (ANN–MVO), particle swarm optimizer (ANN–PSO), whale optimization algorithm (ANN–WOA), and ant lion optimizer (ANN–ALO) hybrid machine learning approaches against the FAO–PM standard; the result showed that the ANN–GWO-1 model with five input variables (Tmin, Tmax, RH, Us, Rs) provided better estimates at both study stations (RMSE

= 0.0592/0.0808, NSE = 0.9972/0.9956, PCC = 0.9986/0.9978, and WI = 0.9993/0.9989) (Tikhamarine et al., 2019).

The empirical estimations of ETo have their advantage and disadvantageous. In general, except for the FAO–PM method, they do not need full meteorological data; rather, they will use either one or two input data. This will be considered as an advantage, especially in developing countries (Mulualem & Liou, 2020; Tellen, 2017). The main disadvantage is over- or underestimation in different climate systems. For instance, Hargreaves–Samani showed both under- and overestimation in Mediterranean climate (Todorovic et al., 2013). The Priestley–Taylor, Thornthwaite, and Blaney–Criddle models showed overestimation by 0.2 mm per day, while the Makkink and Hargreaves–Samani models showed an underestimate 0.2 mm per day in Peninsular of Malaysia (Goh et al., 2021).
In the Goulburn-Murray Irrigation Area (GMIA) of Southeastern Australia (Azhar & Perera, 2011), one study evaluated Hargreaves (HAR), improved Hargreaves (IHA), FAO-24 Radiation (RAD), Ritchie-type (RIT), FAO-24 Class-A Pan with pan coefficients of Doorenbos and Pruitt (PEV) and empirical regression coefficient (SEV), combination methods McIlroy (McI), FAO– Penman with wind functions of Watts and Hancock (W–H) and Meyer (M_PY), and the Penman–Monteith (P–M); and the result showed that there were both underestimations and overestimations in the two sample sites. In arid regions across Iran, Irmak (Irmak et al. 2003), Hargreaves–Samani (Hargreaves and Samani 1985), and Hargreaves (1975) equations showed the best performance compared to 13 other commonly applied empirical methods against the FAO–PM method (Nazari et al., 2020). A study in Southern Manitoba (Ndulue & Ranjan, 2021), aassessed the performance of the 14 commonly used ETo estimation methods, and the result showed that Valiantzas-1, Valiantzas-3, Irmak, Valiantzas-2, and Priestley–Taylor models scored the best in regard to performance against the FAO–PM method.
Specifically in Sicily, by using the scintillometer measurements, six ETo empirical estimation methods were compared in Southwest Sicily (Minacapilli et al., 2016a), obtaining the following ranking in respect to performance: FAO–PM, Priestley–Taylor, Makkink (1957), and Turc. Closely similar analyses compared radiation based and aerodynamic-radiation based ETo estimation methods against scintillometer measurements; the result showed that the radiation-based model of Priestley–Taylor had the best performance (Agnese et al., 2012). In a study conducted in the semi-arid Mediterranean areas of the Belice Basin, Sicily (Bartholy, 1997), it was reported that the Hargreaves method gave a better performance compared with remote sensing data against the filed measurement.
The abovementioned studies conducted in Sicily used radiation-based methods. How- ever, temperature- and aerodynamics/radiation-based methods still remain

poorly evaluated. To test the hypothesis of this study, besides the FAO–PM method, we applied other ETo empirical estimation methods and substituted when there was a lack of data to apply to the FAO–PM method. Therefore, the objective of this study was to evaluate the nine ETo empirical estimation methods, which include temperature-, radiation-, and aerodynamics/radiation-based methods against the FAO56–PM method and to apply the best-performing method for future research work about the impact of PVs infrastructure on evapotranspiration in Ambiens S.r.l. Lab, near Piazza Armerina, Sicily.

3.2 Methodology

Study area

In this study we analyze the data collected at the experimental site in Piazza Armerina, Sicily, Italy, owned by Ambiens S.r.l. The site has the aim at large-scale PV plants impacts on local hydroclimate and soil in Piazza Armerina, Sicily. A meteorological station has recorded every 10 min temperature (°C), relative humidity (%), air pressure (hPa), wind direction, wind speed (m/s), and solar radiation (w/m^2) from 1 July 2019 to 14 January 2022 for 929 days record data. The sensors that were used to record the variables were a thermo-hygrometer, barometer, anemometer, rain gauge, and pyranometer. The site is located at 37°20′42.19” N, 14°24′16.11” E, and has an altitude of 558 m a.s.l (Figure 3.1).

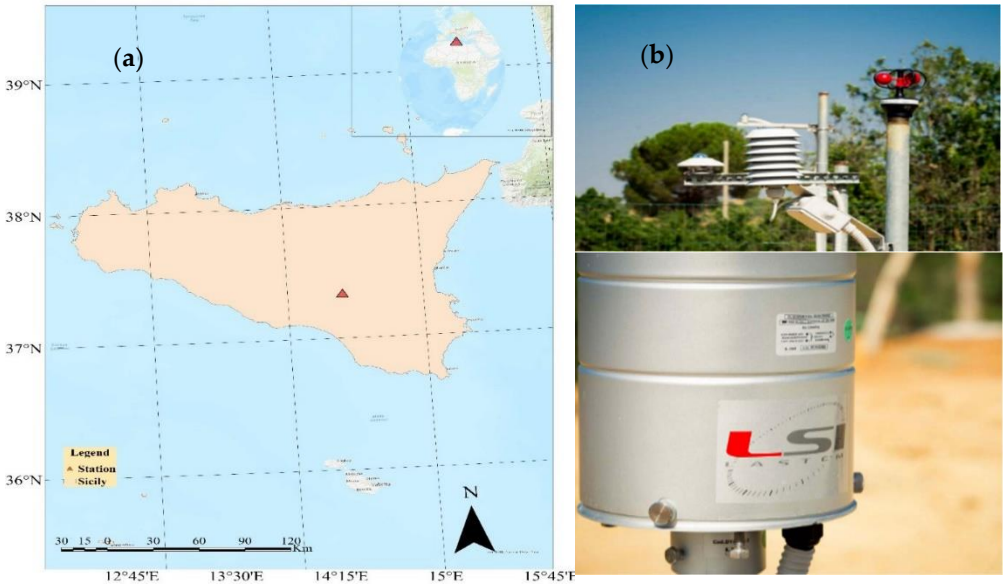

Figure 3. 1 (**a**) Location of the experiment site and (**b**) on-site view of the meteorological station.

The climate of Sicily is typically Mediterranean along the coasts, with hot but not torrid summers, mild and short winters, and moderate annual rainfall (average around 750 mm), occurring mainly from October to March. The annual average temperature along the coast is between 17 and 18.7 °C, with July being the hottest month (Torina et al., 2006). It is also characterized by hot and dry summer and mild and rainy winter (Bonaccorso et al., 2015).

The study used maximum, minimum, and mean temperature; solar radiation; relative humidity; and wind speed for the FAO56–PM method and other ETo estimations methods depending on their necessary variables. The data for these variables were obtained from the mentioned meteorological station. The data cover the period from July 2017 to 31 January 2022 for all four meteorological variables.

The Standardized ETo Estimation (FAO/Penman–Monteith) Method

The FAO–PM has been established as a standard for calculating reference evapo- transpiration (ETo) (Nikam et al., 2014). The method requires air temperature, relative humidity, solar radiation, and wind speed data and is usually reported as the most accurate compared to other empirical ETo estimation methods (Alexandris et al., 2008; Almorox, 2018; Antonopoulos & Antonopoulos, 2018; Chen et al., 2005; Gong et al., 2006; Schrier et al., 2011; Seginer, 2002).

This equation is simplified by integrating the original Penman–Monteith equation and the equations of the aerodynamic and canopy resistance, yielding the following FAO/Penman–Monteith equation:

$$ETo = \frac{0.408\Delta(R_n - G) + \gamma \frac{900}{T + 273} U_2(e_s - e_a)}{\Delta + \gamma(1 + 0.34\, U_2)} \ldots\ldots\ldots\ldots\ldots\ldots\ldots\ldots\ldots 3.1$$

where:

ETo is the reference evapotranspiration (mm day^{-1}), R_n is the net radiation at the crop surface [MJ m^{-2} day^{-1}], G is the soil heat flux density [MJ m^{-2} day^{-1}], T is the air temperature at 2 m height [°C], U_2 is the wind speed at 2 m height [m s^{-1}], e_s is the saturation vapor pressure [kPa], e_a is the actual vapor pressure [kPa], e_s–e_a is the saturation vapor pressure deficit [kPa], Δ is the vapor pressure curve slope [kPa °C^{-1}], and γ is the psychrometric constant [kPa °C^{-1}].

Moreover, 900 and 0.34 are, respectively, the constants by considering the clipped grass reference crop, while for the alfalfa crop, they are 1600 and 0.38, respectively (FAO 1998).

Selected ETo Estimation Methods

Considering the effectiveness of the Mediterranean climate and Sicily climate, the study selected ten ETo empirical estimation methods, including temperature-based, radiation-based, and the mixed-based (aerodynamic radiation) methods (Table 3.1).

Table 3. 1 Selected ETo empirical estimation methods which are compared with against the FAO56–PM method with their equation, reference, and other information.

Method	Model Type	Abbreviation	Formula	Timescale	Parameters
Hargreaves and Samani (1985)	Temp	HS	$0.0023R_a(T_{avg} + 17.8)\ (T_{max} - T_{min})^{0.5}$	Daily	T_{max}, T_{min}, φ
Baier and Robertson (1965)	Temp	BR	$0.157T_{max} + 0.158(T_{max} - T_{min}) + 0.109\ R_a - 5.39$	Daily	T_{max}, T_{min}, φ
Priestley and Taylor (1972),	Rad	PT	$1.26\ \frac{\Delta}{\Delta+\gamma}\frac{R_n-G}{\lambda}$	Daily	T_{max}, T_{min}, φ, T_{avg}
Makkink (1957)	Rad	MAK	$0.61\frac{\Delta}{\Delta+\gamma}\frac{R_s}{2.45} - 0.12$	Daily	T_{avg}, R_s
Turc (1961	Rad	TUR	$0.013(\frac{T_{avg}}{T_{avg}+15})\ (R_s + 50)$	Daily	T_{avg}, R_s
Thornthwaite (1957)	Temp	THN	$16\ (10\frac{T_{avg}}{I})^a \times \frac{N}{360}$	Monthly	T_{max}, T_{min}, φ
Blaney and Criddle (1950)	Temp	BG	$p\ (0.457T_{avg} + 8.128)$	Monthly	T_{avg} and p (FAO document)
Ritchie (1972)	Rad	RT	$\frac{\Delta}{\Delta+\gamma}R_n$	Daily	R_s
Jensen and Haise (1963)	Rad	JH	$R_s(0.0252T_{avg} + 0.078)$	Daily	T_{avg}, R_s

Note:

Temp, temperature-based method; Rad, radiation-based method; T_{max}, maximum temperature; T_{min}, minimum temperature; T_{avg}, mean temperature; φ, latitude; I, annual heat index, defined as the summation of 12 values of the monthly heat; N, maximum number of sunshine hours in the month (h/d); a, empirical exponent function of the annual heat index, I ($a = 6.75 \times 10^{-5}I^3 + 7.71 \times 10^{-7}I^2 + 1.79 \times 10{-}2I + 0.492$); Ra, extraterrestrial radiation (MJ m^{-2} day^{-1}); Rs, solar radiation (MJ m^{-2} day^{-1}); *p*, mean daily percentage of annual daytime hours. For Jensen and Haise (1963), R_S should be changed in mm d^{-1} (Rs mm d^{-1} = 0.408×Rs in MJ m^{-2} day^{-1}); e^o, mean saturation vapor pressure for a day in KPa; G = soil heat flux density, MJ m^{-2} d^{-1} (for this study the value zero because of its daily analysis); Δ,

slope of the vapor pressure curve, kPa·°C^{-1}; γ is psychrometric constant, kPa·°C^{-1}; λ, latent heat of vaporization (MJ kg^{-1}); R_n, net radiation at the crop surface, MJ m^{-2} d^{-1}(Table 3.1).

Statistical Analysis

To evaluate the best ETo estimation methods against the FAO–PM international stan-dard method, we considered the following metrics: Nash–Sutcliffe efficiency (NSE), Akaike Information Criterion (AIC), Bayesian Information Criterion (BIC), Willmott index (d), Coefficient of Determination (R^2), Mean Absolute Error (MAE), Mean Basis Error (MBE), and Root Mean Square Error (RMSE). The NSE is a widely used and potentially reliable statistic for assessing the goodness of fit of hydrologic models (McCuen et al., 2006). The NSE ranges from −∞ to 1. When NSE is close to 1, the quality of the method for estimating ETo is perfect. When NSE is less than 0, the estimation is worse than the observed mean, and thus it is not reliable (Peng et al., 2017).

$$NSE = 1 - \frac{\sum_{i=1}^{n}(O_i - P_i)^2}{\sum_{i=1}^{n}(O_i - \bar{O})^2}, \quad 3.2$$

$$R^2 = \left\{ \frac{\sum_{i=1}^{n}(O_i - \bar{O})\,(P_i - \bar{P})}{\sqrt{\sum_{i=1}^{n}(O_i - \bar{O})^2} * \sqrt{\sum_{i=1}^{n}(P_i - \bar{P})^2}} \right\}^2, \quad 3.3$$

$$MAE = \frac{\sum_{i=1}^{n}(|O_i - P_i|)}{n}, \quad 3.4$$

$$RMSE = \sqrt{\frac{\sum_{i=1}^{n}(P_i - O_i)^2}{n}}, \quad 3.5$$

$$MBE = \bar{P} - \bar{O}\,. \quad 3.6$$

$$AIC = -2lnL + 2k \quad 3.7$$

$$BIC = -2lnL + kln\,(n) \quad 3.8$$

$$d = 1 - \frac{\sum_{i=1}^{n}(P_i - O_i)^2}{\sum_{i=1}^{n}(|P'_i| + |O'_i|)^2} \quad 3.9$$

where P_i are the values obtained from the ETo estimation methods to be assessed O_i are the reference ones, derived from the FAO–PM method, $\bar{P}$ and $\bar{O}$, are the

respective arithmetic mean and *n* is sample size. $Additionally, P'_i = P_i - \overline{O}$ and $O'_i = O_i - \overline{O}$.

Moreover, in AIC and BIC, n means number of values, *L* is the maximum value of the likelihood function for the model, and *k* is the number of free parameters in the model.

3.3 Results

Assessing ETo empirical estimation methods' performance is essential in relation todiscrepancies of performance in different climate systems (Utset et al., 2004). Temperature- and radiation-based empirical ETo estimation methods have different performances. Table 3.2 showed that the average daily ETo value of PM is highly similar to the ETo values of the PT and HS methods, respectively. The NSE values (Table 3.2) showed that the PT and HS have the best performance over other methods, with values of 0.91 and 0.51, respectively, against the PM ETo method. The other methods showed negative values of NSE. The negative values of NSE imply that the methods are not recommended or not well calibrated against the PM method (Gupta & Kling, 2011; Jain & Sudheer, 2008; McCuen et al., 2006).

Table 3. 2 Statistical indicators for the performance of the ETo estimation methods against the FAO–PM ETo estimation method.

	PM	***HS***	***BR***	***PT***	***MKK***	***TUR***	***RIT***	***JH***	***THN***	***BG***
average	2.32	2.88	1.65	2.39	2.86	1.26	4.61	3.68	65.36	4.39
NSE		0.51	−1.01	0.91	−0.51	−0.49	−4.42	−4.58	−1.74	−6.44
RMSE (mm/d)		0.80	1.63	0.34	1.41	1.41	2.68	2.72	41.50	2.22
AIC		−681.4	1537.6	−3363.02	1435.9	147 4.8	2902.02	3285.2	90.32	19.42
BIC		−674.04	1544.94	−3355.7	1443.3	1482.14	2909.4	3292.6	92.8	21.91
Willmott index		0.651	0.318	0.865	0.499	0.37	0.18	0.034	0.577	0.4514
MAE (mm/d)		0.66	1.30	0.26	0.95	1.20	2.32	1.84	36.34	1.94
MBE (mm/d)		0.56	−0.67	0.06	0.54	−1.06	2.29	1.36	−9.23	1.94
R^2		0.75	0.01	0.94	0.40	0.35	0.94	0.29	0.18	0.42

Note: The THN values are the overall monthly average of ETo, while the BG values are the monthly daily average ETo values; and others empirical methods have daily ETo values.

The AIC values result also confirmed that PT and HS are the lowest values, with -3633.02 and -681.4, respectively, compared with the other ETo empirical estimation method. The AIC and BIC values showed the lowest values, meaning that they are the best models compared with other models (Fan & Thomas, 2013; Gul et al., 2021; L. Zhang et al., 2019). Moreover, the BIC value results for PT and HS showed the lowest values, with 3355.7 and 674.04, and this implies that the PT was the best model, and the HS was the second best compared with other models against the FAO–PM ETo estimation method. The Willmott Index result also showed that the PT method was the highest, with a value of 0.865, and the second highest was HS, with the value of 0.651, when compared with other ETo empirical estimation methods (Table 3.2). The highest value of Willmott Index means that the model has the best performance against the standard model (de Melo & Fernandes, 2012; Pandey et al., 2016; Tikhamarine et al., 2019; Valipour, 2015).

The RMSE values result (Table 3.2) showed that the PT and HS were the lowest values, with 0.34 mm per day and 0.8 mm per day errors, respectively; while the THN also showed that with 41.5 mm in monthly scale. The JH and RIT illustrated the highest RMSE, with 2.72 mm per day and 2.68 mm per day errors (most likely greater than the daily average PM ETo value). The MAE values of PT, HS, and MKK showed that less than 1 mm per day errors with 0.26, 0.66, and 0.95 mm per day, respectively. Meanwhile, in monthly scale, the THN also showed that 36.34 mm per month MAE value. Moreover, the MBE values of PT, MKK, and HS showed values close to zero, with 0.06, 0.54, and 0.56 mm per day errors, respectively, against the PM ETo method. While RIT showed the poorest performance of MBE values against the PM ETo method with 2.29 mm per day overestimate error.
The coefficient determination of the ETO estimation methods against the PM ETO estimation method was evaluated. The result (Table 3.2) showed that the PT, RIT, and HS values highly correlated with the PM ETo with 0.94, 0.94, and 0.75 R^2 values. On the other hand, the BR and THN have the lowest correlation with PM ETo values, with 0.01 (there is no correlation) and 0.18, respectively. In general, the performance result showed that the PT is the best method compared with other methods against the PM ETo method. The second better ETo estimation method is the HS. This showed that the radiation-based method (PT) is better than

the temperature- based methods in the study area. Among temperature-based methods, the HS showed the best performance compared to other methods. The PT confirmed the highest performance: NSE = 0.91, RMSE = 0.34 mm per day error, MAE = 0.26 mm per day error, MBE = 0.06 mm per day error, and R^2 = 0.94; followed by HS NSE = 0.51, RMSE = 0.80 mm per day error, MAE = 0.66 mm per day error, MBE = 0.56 mm per day error, and R^2 = 0.75 (Table 3.2).

To sum up, the performance assessment statistical metrics result showed that the PT and HS configured equivalence; TUR, THN, and BR showed underestimations (Figure 3.2); and RT, BG, JH, and MKK configured an overestimation of ETo against the PM ETo estimation method (Figure 3.2).

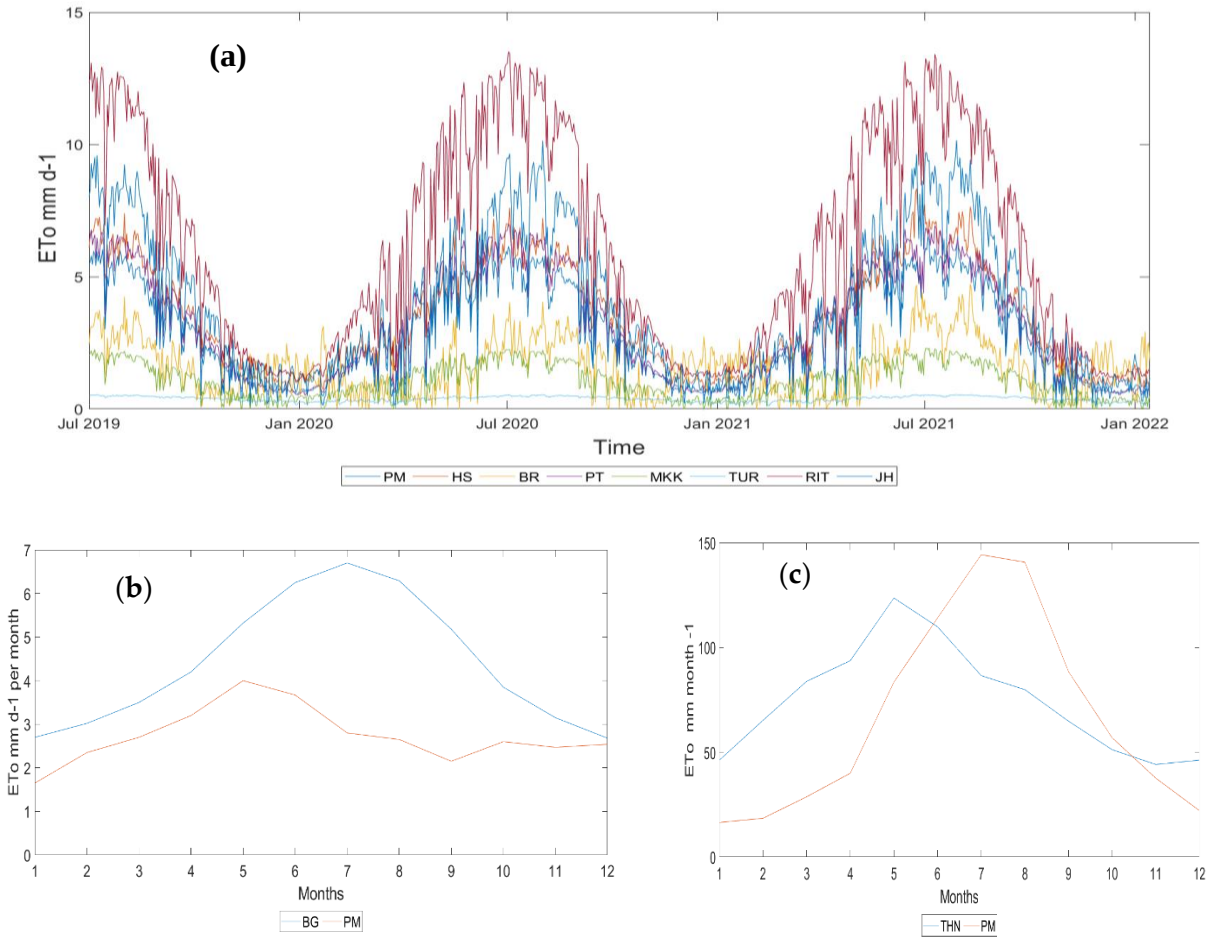

Figure 3. 2 Comparison of PM ETo time-series data to other ETo estimation

methods: (**a**) daily ETo in mm for PM, PT, BR, HS, JH, MKK, RIT, and TUR from 1 July 2019 to 14 January 2022; (**b**) average daily ETO per month for PM and BG from 1 July 2019 to 14 January 2022; (**c**) monthly ETo in mm for PM and THN from 1 July 2019 to 14 January 2022. N.B.: BG and THN are calculated based on monthly timescale, and the others were daily scale.

The R^2 is highly supportive the correlation between the observed and estimated model. Table 3.2 showed that the correlation between the FAO–PM ETo estimation method and other temperature- and radiation-based ETo estimation methods. The result showed that the PT and RIT showed the highest R^2 values (both 0.94) compared with other methods (Table 3.2). Both RIT and PT are radiation-based models, and net radiation (R_n) was the main input for them. The HS also has the second highest R^2 value (0.75) compared with other ETo estimation methods (the first highest from temperature based ETo estimation methods). Additionally, BR, THN, and JH are the lowest R^2 values 0.01, 0.18, and 0.29, respectively (Table 3.2). Specifically, BR showed that there is no significant correlation to the PM ETo estimation method. TUR, MKK, and BG estimation methods showed a moderate correlation to the PM ETo estimation method, with R^2 values 0.35, 0.40, and 0.42, respectively (Table 3.2).

3.4 Discussion

Hargreaves and Samani (1985)

The Hargreaves and Samani (1985) (which we denote as HS in this study) is the second better performance compared to other ETo estimation methods. This method showed good performance against the FAO–PM ETo estimation method (Nikam et al., 2014) in a humid subtropic climate on monthly evapotranspiration. The result showed that the Hargreaves and Samani (1985) method R^2 value was 0.889 and the highest compared to Thornthwaite (1957), Turc (1962), and Priestley–Taylor (1972) against the standard FAO–PM ETo estimation method. It also showed relatively similar values to the PM ETo values in Sichuan Basin and Tibetan Plateau in China compared with the Makkink, Abtew, Priestley–Taylor, Thornthwaite, Hamon, Linacre (Lin), and Blaney–Criddle methods against the standard PM method (Lang et al., 2017) during a warm, temperate monsoonal summer, on the seasonal and yearly scale. In Southern Italy, namely in Campania, Basilicata, Apulia, Calabria, and Sicily, the Hargreaves and Samani (1985) showed a better performance in regard to MAE and Bias (0.52 and 0.03 mm per day, respectively) values compared with the Makkink ETo method (0.55 and −0.11 mm per day, respectively) values against the PM method with the values (Senatore et al., 2015) in a hot summer Mediter- ranean climate. The Hargreaves–Samani

method showed higher than that obtained by the modified Thornthwaite method against the lysimeter measurement in Shiraz, Iran (Sepaskhah & Razzaghi, 2009). It showed also the second performance compared with other temperature-based meth-ods next to the PM temperature-based method, with the values of R^2 = 0.68, NSE = 0.68, MAE = 0. 92 mm d^{-1}, and RMSE = 0.74 mm d^{-1}) (Quej et al., 2019) in a tropical savanna climate.

Baier–Robertson (1965)

The Baier–Robertson (1965) result showed less than the average of the PM method (1.65 mm per day) and underestimated the ETo daily values (Table 3.2). It showed that the RMSE, MAE, MBE, and R^2 values are 1.63, 0.30, −0.67, 0.01 mm d^{-1}, respectively. This showed that there is also an insignificant correlation between the PM method and the Baier–Robertson (1965). In the central hilly region of Ivan Sedol, eastern hilly region of Sokolac, central of Bugojno, and central of Sarajevo, the Baier–Robertson (1965) showed that underestimation of ETo into daily scale compared with both radiation- and temperature-based empirical methods (Čadro et al., 2017) in a temperate humid climate, humid boreal, and Mediterranean climate.

Priestley–Taylor (1972)

Priestley–Taylor method showed that the highest performance compared to all other ETO estimation methods, using different statistical metrics evaluation (Table 3.2). The Priestley–Taylor showed the highest correlation with the PM ETo method in daily ETo scale compared with the Makkink, de Bruin–Keijman, modified Penman, Hargreaves–Samani, Jensen–Haise, and Blaney–Criddle methods in Northern Greece (Antonopoulos and Antonopoulos, 2018) in the Mediterranean climate. In South- west Sicily olive groves, the Priestley–Taylor showed a better performance next to the PM method against the scintillometer filed measurements in daily ETo (Minacapilli et al., 2016) in a hot summer Mediterranean climate.

Makkink (1957)

The NSE value of the Makkink (1957) showed a negative value (−0.51), that the Makkink (1957) should not be recommended to estimate ETo in the study area. This method also showed a negative value (−0.2) for NSE and was not considered from the proposed estimation method across different regions of China (Peng et al., 2017) in monthly and annually ETo. This method

overestimated compared to the standard PM method: 2.86 and 2.32 mm daily average ETo (Table 3.2). In Northern Greece Makkink (3.179 mm per day) also showed a higher daily average value than the PM method (2.824 mm per day) (Antonopoulos & Antonopoulos, 2018). It also showed negative values (−1.857) for NSE in Southwestern China (Lang et al., 2017). The MBE result of the MAK was also lower than the HS in the Southern Italy (Senatore et al., 2015).

Turc (1961)

Turc (1961) showed an underestimation and lesser daily average values compared with the standardized PM method and a negative value of NSE (Table 3.2). For the grassland central part of Serbia, this method also showed underestimated daily ETo values and was lower than the PM method (Tellen, 2017) in daily ETo under the warm, temperate humid climate. The index of agreement of the TUR was also the lowest in different regions in the northern and southern areas of Mostar in Bosnia and Herzegovina (Čadro et al., 2017).

Thornthwaite (1957)

The Thornthwaite (1957) monthly analysis result showed that the NSE = −1.74 and R^2 = 0.18 (Table 3.2), and it underestimated compared to the PM method. It showed that there was a poor correlation between the PM method and the Thornthwaite method (1967). This method is also not recommended based on its result of the NSE. In three regions of Southwestern China, it also showed NSE negative values against the PM method in seasonal ETo (Lang et al., 2017).

Blaney and Criddle (1950)

The Blaney and Criddle (1950) overestimated and had the following values: NSE= −6.44, and RMSE = 2.22 mm per day, and R^2 = 0.42 (Table 3.2). It also showed higher average values than the PM method. It showed a negative NSE value in three regions of Southwestern China (Lang et al., 2017). It showed higher average values than the PM method in Northern Greece (Antonopoulos & Antonopoulos, 2018).

The performance of the BG also categorized as bad in Minas Gerais, Brazil against to the PM method (de Melo & Fernandes, 2012) in daily ETo under the tropical climate.

Ritchie (1972)

The Ritchie (1972) result was highly correlated with the PM method, including the PT, because both used net solar radiation as the main input for their estimation method. Despite the R^2, it showed a lower performance, with a negative NSE value (−4.42), and it is not recommended for ETo estimated in the studied area because of its NSE negative value. It showed overestimated, and the mean daily ETo values were two times those of the PM method's ETo value, 4.61 mm per day. In Northeastern India, it was evaluated in three sites against the PM method; it had higher average values compared with the PM method (Pandey et al., 2016). Additionally, it showed highest values of R^2 (0.98) in the Jowai site compared to other ETo estimation methods (Pandey et al., 2016) in daily ETo under humid summers, severe monsoons, and mild winter climate. Additionally, it showed highest values of R^2 (0.98) in the Jowai site compared to other ETo estimation methods (Pandey et al., 2016). It showed also the second highest R^2 (0.98) value compared with the other 22 ETo estimation methods against the PM method in Iran (Valipour, 2015) in daily ETo, under a subtropical climate.

Jensen and Haise (1963)

The Jensen and Haise (1963) method of this study showed a lower performance on the statistical metrics assessment (Table 3.2). It showed overestimated and higher mean values (3.68 mm per day) than the PM method. Moreover, it also showed a negative NSE value (−4.58) and is, thus, not suitable for the studied site ETo estimation method (Table 3.2). In Northern Greece, a similar performance was observed when comparing the temperature- and radiation-based methods (Antonopoulos & Antonopoulos, 2018). It is considered to be the most unsuitable method when compared with other temperature- and radiation-based methods against the PM method in different parts of Northeastern India (Pandey et al., 2016). It also showed the second highest value RMSE (1.67 mm per day) next to the original Penman method (2.52) compared with other methods in Uberaba-MG, Brazil (de Melo & Fernandes, 2012).

3.5 Conclusions

The aim of this study was to identify the best ETo estimation methods for future works that will assess the impact of the PV on evapotranspiration and decide which meteorological instrumentation should be installed under PVs. The study assessed the performance of different ETo estimation methods against the PM method in an experimental PV site in Piazza Armerina, Sicily, Italy. Different statistical performance assessment metrics were considered for the evaluation of both temperature- and radiation-based methods against the PM method. The study assessed the performance of 10 methods based on various statistical metrics, i.e., Nash–Sutcliffe efficiency (NSE), Coefficient of Determination (R2), Mean Absolute Error (MAE), Mean Basis Error (MBE), and Root Mean Square Error (RMSE). The results showed that the Priestley–Taylor method (1972) (radiation-based) was the best method, with an NSE = 0.91, RMSE = 0.34 mm/d, MAE = 0.26 mm/d, MBE = 0.06 mm/d, and R2 = 0.94. The AIC, BIC, and Willmott Index results also confirmed that the PT and the HS were the first and second best performing models against the PM method, respectively. The second method which showed the best performance was that of Hargreaves and Samani (1985) (temperature-based), with an NSE = 0.51, MSE = 0.80 mm/d, MAE = 0.66 mm/d, MBE = 0.56 mm/d, and R2 = 0.75. Baier–Robertson (1965), Turc (1961), and Thornthwaite (1957) showed underestimations, while the Makkink (1957), Blaney– Criddle (1950), Ritiche (1972), and Jensen–Haise (1963) showed overestimation of ETo against the PM ETo estimation method. Hence, the Priestley–Taylor (1972) and Hargreaves– Samani (1985) methods are the most recommended methods if not all variables required for the PM method are available.

Chapter 4

Trend Analysis and Identification of the Meteorological Factors Influencing Reference Evapotranspiration

Abstract:

Investigating the trends of reference evapotranspiration (ETo) is fundamental importance for water resource management in agriculture, climate variability analysis, and other hydroclimate-related projects. Moreover, it would be useful for understanding the sensitivity of such trends to basic meteorological variables, as the modifications of these variables due to climate change are more easily predictable. This study aims to analyze ETo trends and sensitivity in relation to different explanatory meteorological factors. The study used a 17 year-long dataset of meteorological variables from a station located in Piazza Armerina, Sicily, a region characterized by a Mediterranean climate. First, the FAO-Penman-Monteith method was applied for estimation of ETo. Next, the Mann-Kendall test with serial autocorrelation removal by Trend-free pre-whitening (TFPW) was applied to analyze ETo trends and the basic meteorological variables on which they depend. Sen's slope was also used to examine the magnitude of the trend of monthly ETo and its related meteorological variables. According to the obtained results, ETo only showed a downward trend of 0.790 mm per year in November, while no trend is shown in other months or on seasonal and annual time scales. Solar radiation (November and Autumn) and rainfall (Au-tumn) showed a downward trend. The other meteorological variables (minimum temperature, maximum temperature, mean temperature, wind speed, and relative humidity) showed an upward trend both at monthly and seasonally scale in the study area. The highest and lowest sensitivity coefficients of ETo in the study area are obtained for specific humidity and wind speed, respec-tively. Specific humidity and wind speed give the highest (44.59%) and lowest (0.9%) contribution to ETo trends in the study area. These results contribute to understanding the potential and possible future footprint of climate change on evapotranspiration in the study area.

Keywords: climate change; reference evapotranspiration; Mann-Kendall test; sensitivity analysis; contribution rate

4.1 Introduction

Reference evapotranspiration (ETo) is a pivotal part of the hydrological cycle and of the most crucial physical processes in natural ecosystems and environmental systems on our plane (Ochoa-Sánchez et al., 2019). The reference surface of ETo considered the hypothetical grass reference crop to have an assumed crop height of 0.12 m, a fixed surface resistance of 70 s $m^{-1,}$ and an albedo of 0.23. ETo enables one to calculate the energy and water exchanges in vegetation (Glenn et al., 2010; Zhang et al., 2020), soil surface (Parajuli et al., 2019), land surface (Ellsäßer et al., 2020; He et al., 2013), and atmosphere (Dickinson, 1984; Long & Singh, 2012; Mueller et al., 2011). Estimation and measurements of ETo contribute greatly to our understanding of earth's energy budget, agricultural water management, water resource management, and climate change studies (Dezsi & Mîndrescu, 2018; Dong et al., 2020; Han et al., 2018; He et al., 2013; Hui-mean & Yusof, 2018; Kingston et al., 2009; Li et al., 2017; Nam et al., 2015). There are different methods and approaches for measuring and estimating ETo. These methods can be divided into two main groups: direct methods (field water balance approach and soil moisture depletion approach) and indirect methods (empirical/statistical methods, micrometeorological methods, and remote sensing methods (Alemu et al., 2015; Choudhary, 2018; Gharsallah et al., 2013; Hatfield et al., 2016; Long & Singh, 2012; Moeletsi et al., 2013; Ochoa-Sánchez et al., 2019; Tanner, 2015).

Moreover, it is of fundamental importance to analyze the trends in reference evapotranspiration in order to understand the potential impacts of climate change on ETo. Different methods for analyzing trends in hydroclimate variables over space and time are available in the literature. Both parametric and non-parametric methods were applied for hydroclimate time series analysis in different part of the world (Alemu et al., 2015; Gul et al., 2021; Tegos et al., 2015; Z. Yang et al., 2011). In parametric methods, linear regression is used for trend analysis for different meteorological variables including ETo (Gocic & Trajkovic, 2014; Gul et al., 2021; Yang et al., 2011). These parametric methods are helpful for explaining the relationship between two or more variables using a linear relationship (Gocic & Trajkovic, 2014). However, parametric methods require data to be independent and normally distributed, while non-parametric trend tests only require data to be independent and can tolerate outliers in the data (Shadmani et al., 2012). One of the most commonly applied non-parametric tests for assessing trend significance is the Mann Kendhall test (MK-test) (Mann, 1945; Kendhall, 1975; (Ahmad et al., 2015; Gul et al., 2021; Kamal & Pachauri, 2019; Shadmani et al., 2012; Blain et al., 2014; Zhang et al., 2020).

The MK-test allows one to determine whether or not the trend is monotonic, in terms of monthly, seasonal, and annual time series of evapotranspiration, as well as

other hydro-climatological variables (Ahmad et al., 2015; Bouklikha et al., 2021; Buhairi, 2010; Caloiero et al., 2020; Merabtene et al., 2016). Additionally, to investigate trend magnitude, Sen's slope is widely used as a non-parametric method, including in ETo analysis (Ghafouri-Azar et al., 2018; Gocic & Trajkovic, 2014; Gul et al., 2021; Ndiaye et al., 2020; Sonali & Kumar, 2016). Meanwhile, sensitivity analysis is also essential for identifying the most influential factors in cases where a monotonic trend is present(Ndiaye et al., 2020).

In addition to estimation of ETo, there are studies concerning the trend and magnitude of ETo in different parts of the world. By applying the MK test and Sen's Slope, ETo trends showed different configurations on a monthly, seasonal, and annual scale. The annual trend of ETo increases as the temperature increases in different studies (Ghafouri-Azar et al., 2018; Gul et al., 2021; Ndiaye et al., 2020; Shadmani et al., 2012; Z. Yang et al., 2011; Zhang et al., 2020a). There are also studies showing a downward trend of ETo as related to temperature. Such situations are called "Evapotranspiration Paradox" because this behavior contrasts with the upward trend of global temperature (Ndiaye et al., 2020; Sonali & Kumar, 2016; Yang et al., 2011). In seasonal trend analysis, ETo showed downward trends in summer in many parts of the world (Gul et al., 2021; Ndiaye et al., 2020; Shadmani et al., 2012). In monthly significant trend analysis, there are different pattern configurations in different studies.

With reference to the Mediterranean area, there are studies showing that climate variables and extreme events are changing (Liuzzo et al., 2015). There are also some studies conducted to assess and compare different estimation methods of ETo in Sicily (Aschale et al., 2022; Borzì et al., 2020; Mario Minacapilli et al., 2007; Negm et al., 2017; Minacapilli, et al., 2017; Provenzano & Ippolito, 2021). There are also studies about the amount of ETo and its configuration for different crops in Sicily (Consoli et al., 2006; Minacapilli et al., 2009).

In general, ETo has shown both increasing (Ghafouri-Azar et al., 2018; Gul et al., 2021; Ndiaye et al., 2020; Shadmani et al., 2012; Yang et al., 2011; Zhang et al., 2020a), and downward trends across the world, as documented in several studies (Ndiaye et al., 2020; Sonali & Kumar, 2016; Yang et al., 2011). On the other hand, there are also different areas showing the absence of trends for ETo. ETo trends are subject to both spatial and temporal variations (monthly, seasonally, and annually). Further studies analyzing and comparing trends of monthly, seasonal, and annual ETo are needed, especially with reference to the Mediterranean climate. Many previous studies in other regions do not investigate the main factors affecting ETo trends. Therefore, this study, apart from estimating ETo trends at multiple temporal scales, we provide some additional insights to provide a better understanding of the evapotranspiration dynamics by analyzing the sensitivity and contribution rate of each variable to evapotranspiration trends. To this aim, we refer to ETo estimations

made by the Penman-Monteith formula. Analysis is carried out using the data collected in an experimental site located in Piazza Armerina, Sicily, Italy. In addition to these points, it may be also mentioned that, in many previous studies, the sensitivity of ETo trends to air humidity is carried out respective to relative humidity. However, this relative humidity represents a measure of the actual amount of water vapor in the air compared to the total amount of vapor that can exist in the air at its current temperature (Willett et al., 2007). It implies that air will have a higher relative humidity if the air is cooler, and a lower relative humidity if the air is warmer. Hence, this study will examine the sensitivity and contribution rate of specific humidity for ETo rather than that for common relative humidity, because specific humidity is always considered a measure of the actual amount of water vapor (moisture) in the air, regardless of air temperature (Hobbins, 2016).

4.2. Data and Methods

4.2.1. The FAO-Penman-Monteith Method

The FAO-PM has been established as a standard for calculating reference evapotranspiration (Nikam et al., 2014). This method requires air temperature, relative humidity, solar radiation, and wind speed data input and is produced high quality output results of ETo compared to other empirical ETo estimation methods (Alexandris et al., 2008; Almorox, 2018; Chen et al., 2005; Schrier et al., 2011; Seginer, 2002). This method was also approved by the FAO and the American Society of Civil Engineers (ACSE) as the best and most comprehensive method, to be used when the necessary data inputs are available (Al-sudani, 2019; Almorox, 2018; Anapalli et al., 2018; Hashemi & Habibian, 1979; Jim et al., 2004; Quej et al., 2019; Sharifi & Dinpashoh, 2014; Subedi & Chávez, 2015).

A simplified equation was recommended by the FAO (Allen et al., 1998) with the FAO-56 Penman-Monteith Equation, by assuming some constant parameters for a clipped grass reference crop. In particular, the reference crop was assumed to be a hypothetical crop with crop height of 0.12 m, a fixed surface resistance of 70 s $m^{-1,}$ and an albedo value (i.e., portion of light reflected by the leaf surface) of 0.23.

This simplified equation is obtained by integrating the original Penman-Monteith equation and the equations of the aerodynamic and canopy resistance:

$$ETo = \frac{0.408\Delta(R_n - G) + \gamma \frac{900}{T + 273} U_2 (e_s - e_a)}{\Delta + \gamma(1 + 0.34\, U_2)} \qquad 4.1$$

where: ETo is reference evapotranspiration (mm day^{-1}),(R_n) is the net radiation at the crop surface [MJ m^{-2} day^{-1}], G is the soil heat flux density [MJ m^{-2} day^{-1}], T is the air temperature at 2 m height [°C], U_2 is the wind speed at 2 m height [m s^{-1}],

e_s is saturation vapor pressure [kPa], e_a is actual vapor pressure [kPa], $e_s - e_a$ is the saturation vapor pressure deficit [kPa], Δ is the vapor pressure curve slope [kPa °C^{-1}], and γ is the psychrometric constant [kPa °C^{-1}].

4.2. 2 Sen's Slope Estimator

Sen's slope is a method for estimating the magnitude of a trend in time series data (Ahmad et al., 2015; Ghafouri-Azar et al., 2018; Gocic & Trajkovic, 2014; Gul et al., 2021; Hu et al., 2019; Kamal & Pachauri, 2019) by evaluating the slope of the trend (Sen, 1968). This study used a 0.05 significance level confidence. When |Z| > 1.96, the null hypothesis is rejected, and the trend is significant at 5%. If a trend is detected in the data series, its amount can be evaluated by the slope of the trend (β in the following). Hence, the magnitudes of the trends in ETo were studied using Sen's slope estimator:

$$\beta = Median\left(\frac{X_i - X_j}{i - j}\right) \; for \; all \; i > j \qquad 4.2$$

where X_i and X_j are the data values at times i and j, respectively. While the value of $\beta > 0$, the time series of the ETo and other climatic factors are increasing and the vice versa.

4.2.3 Mann-Kendall Test

The Mann-Kendall test is the most effective method for supporting statistically significant trend tests for different hydro-climatological time series analysis and is widely applied in the literature (Alemu et al., 2015; Dong et al., 2020; He et al., 2013; Hui-mean & Yusof, 2018; Nam et al., 2015; Peng et al., 2017). The main advantage of the MK test is that it does not require the data to follow any statistical distribution and not sensitive to extreme values(Alemu et al., 2015; Diop et al., 2016; Ndiaye et al., 2020). The test is based on two hypotheses: the null hypothesis (Ho) which supposes that the test is stationary and no trend exists, and the alternative hypothesis (H1), which rejects Ho and indicates the existence of a trend. Mann-Kendall's statistical S is given by the following formula:

$$S = \sum_{k=1}^{n-1} \sum_{j=k+1}^{n} Sgn(X_j - X_k) \qquad \textbf{\textit{4.3}}$$

where X_k and X_j are the values of the variable at time k and j, respectively, n is the length of the series and Sgn() is the sign function, defined as follows:

It has been documented that when n > =10, the statistic S is approximately normally distributed with the mean E(S) = 0, and its variance is:

$$Var\ (s) = \frac{n(n\ -\ 1)(2n\ +\ 5) - \sum_{i=1}^{m} t_i(\ t_i - 1)(2t_i + 5)}{18} \qquad 4.4$$

where n is the number of data points, m is the number of tied groups (a tied group is a set of sample data having the same value), and t_i is the number of data points in the i^{th} group.

The standardized test statistic (Z) is computed as follows:

$$Z = \begin{cases} \frac{S-1}{\sqrt{Var(S)}}, if\ S > 0 \\ 0, if\ S = 0 \\ \frac{S+1}{\sqrt{Var(S)}}, if\ S < 0 \end{cases} \qquad 4.5$$

The null hypothesis, H_0, meaning that no significant trend is present, is accepted if the test statistic (Z) is not statistically significant, i.e., $-Z_{\alpha/2} < Z < Z_{\alpha/2}$, where $Z_{\alpha/2}$ is the standard normal deviate.

$$\mathrm{Sgn}(X_j - X_k) = \begin{cases} 1\ if\ (X_j - X_k) > 0 \\ 0\ if\ (X_j - X_k) = 0 \\ -1\ if\ (X_j - X_k) < 0 \end{cases} \qquad 4.6$$

To overcome the limitation of the MK test related to autocorrelation of the original data that could affect the outcome of the test (Zhang et al., 2020), a trend-free prewhitening (TFPW) algorithm was applied. This method enables removing serial dependence, which is one of the main problems in testing and interpreting time series data (Ahmad et al., 2015; Wu et al., 2021; Zhang et al., 2020). Trend-free prewhitening includes the following steps:

Calculate the first-order coefficient of autocorrelation (r):

$$Y_t = X_t - \beta_t \quad 4.7$$

$$r = \frac{\sum_{t=1}^{n-1}(X_t - \bar{X}_t)(X_{t+1} - \bar{X}_{t+1})}{\sqrt{\sum_{t-1}^{n-1}(X_t - \bar{X}_t)^2}\sum_{t-1}^{n-1}(X_{t+1} - \bar{X}_{t+1})^2} \quad 4.8$$

Remove any trend items from the time series variables to form a sequence without trend items:

Supplement the trend term β_t to obtain a new sequence without an autocorrelation effect:

$$Y_t \acute{=} Y_t - r_1 Y_{t-1} + \beta_t \quad 4.9$$

where:

X_t is the value of the variable at time t of the time series, n is the length of the data, and $\bar{X}_t$ is the aver-age value. To assesses significance of the trend, the original MK test is applied to Y_t.

4.2.4. Sensitivity Analysis

Sensitivity analysis enables one to calculate the influence of climatic variables on ETo (Darshana et al., 2013; Irmak et al., 2006; Liang et al., 2008; Patle et al., 2020; Sharifi & Dinpashoh, 2014). The sensitivity coefficient is the rate of variation in ETo with respect to meteorological variables (Ndiaye et al., 2020; Patle et al., 2020). It is a quantitative parameter that represents the effect degree of change of ETo when one or several related meteorological factors are changed (Li et al., 2017). To precisely determine the sensitivity of ETo to humidity, it needs to differentiate the specific humidity from the relative humidity. The relative humidity does not show the humidity exactly; rather it consists of humidity and temperature on its partition. Hence, this study used specific humidity (SHU) to precisely determine and examine the sensitivity and contribution of humidity to the ETo trend in this study.

The specific humidity is computed as follows:

$$e = 6.112 \exp\frac{17.6\,T_d}{T_d + 243.5} \quad 4.10$$

$$q = \frac{0.622\,e}{p - (0.378\,e)} \quad 4.11$$

where *e* is vapor pressure in mbar, T_d the dew point in °C, p the surface pressure in mbar, and q the specific humidity in kg/kg.

The dew point temperature is also computed as follows:

$$e_s = 6.112 * \exp\frac{17.67T}{T + 243.5} \quad 4.12$$

Otherwise, for Equation (4.10) we can use the following:

$$e = e_s\frac{RH}{100} \quad 4.13$$

$$T_d = \frac{\log\left(\frac{e}{6.112}\right) * 243.5}{17.67 - \log\left(\frac{e}{6.112}\right)} \quad 4.14$$

where T is the mean temperature in °C, e_s is saturation vapor pressure in mbar, e is vapor pressure in mbar, and RH is relative humidity in percent.

T_{max} and T_{min} contribute differently to the ETo trend. The FAO PM equation (Equation (3.1)) includes the e_s saturation vapor pressure [kPa], e_a actual vapor pressure [kPa], and their difference (e_s−e_a saturation vapor pressure deficit [kPa]). These terms are computed using the T_{max} and T_{min}.

The sensitivity coefficient equation is:

$$Sv_i = \lim_{v_i \to 0}\left(\frac{\Delta ETo/ETo}{\Delta v_i/v_i}\right) \quad 4.15$$

where Sv_i is the sensitivity coefficient of v_i, ΔETo is the variation in ETo, v_i is the meteorological factor, and Δv_i is the variation in v_i.

The positive or negative sensitivity coefficient means that ETo increases or decreases with the increase or decrease of a climatic variable. The values of the sensitivity coefficient (SVI) for a particular climatic parameter show the magnitude of the sensitivity of ETo in variation in that parameter. The larger the absolute value of the sensitivity coefficient, the larger the effect of a given variable on ETo (Liang et al., 2008; Patle et al., 2020; Sharifi & Dinpashoh, 2014; Wu et al., 2021).

Moreover, (Lenhart et al., 2002) the range of variation of the sensitivity coefficient was divided into four levels, as shown in Table 4.1.

Table 4. 1 Classification of the sensitivity coefficient.

Sensitivity Coefficient	**Sensitivity Level**
$0.00 \leq \lvert \boldsymbol{Sv_i} \rvert < 0.05$	Negligible
$0.05 \leq \lvert \boldsymbol{Sv_i} \rvert < 0.2$	Moderate
$0.2 \leq \lvert \boldsymbol{Sv_i} \rvert < 1$	High
$1.00 \leq \lvert \boldsymbol{Sv_i} \rvert$	Very high

4.2.5. Contribution Rate

This is computed by multiplying the sensitivity coefficient of a single meteorological factor by its relative change rate (Li et al., 2017). If the contribution rate results >0, then the change of the factor means that ETo is increasing, which means that the factor had a positive contribution to the variation of ETo. If the contribution rate <0, then the change in the factor means that ETo is decreasing, and that the factor had a negative contribution (Li et al., 2017) .

$$Conv_i = Sv_i * RCv_i \quad (4.16)$$

$$RCv_i = 100\frac{n * Trendv_i}{|av_i|}100 \quad (4.17)$$

where, Conv_i is the contribution rate of v_i, RCv_i is the relative change rate in v_i, n is the number of years, av_i is the mean value of v_i, and Trendv_i is the annual trend in v_i.

4.2.6 Study Area and Data

The proposed approach was applied to an experimental site located in Piazza Armerina (Sicily, Italy). The climate in this area is typically Mediterranean, with hot but not torrid summers, mild and short winters, and moderate annual rainfall mainly occurring in the period from October to March (Bonaccorso et al., 2015). The annual average temperature along the coast is between 17 and 18.7 °C, with July being the hottest month (Torina et al., 2006). The maximum (T_{max}) and minimum temperature (T_{min}), relative humidity (RH), wind speed (WS), and solar radiation (SR) data were obtained from Piazza Armerina meteorological station installed and managed by the Sicilian Agro-meteorological informative service (Servizio Informativo Agrometeorologico Siciliano—SIAS, http://www.sias.regione.sicilia.it/, accessed on July 20, 2022). The astronomical location of the meteorological site is 37.382171° N and 14.3666704° E, and its elevation is 697 m a.s.l. (Figure 1). The dataset consisted of 17.25 years of dailydata covering the period from December 1, 2003 to February 28, 2021, for all variables.

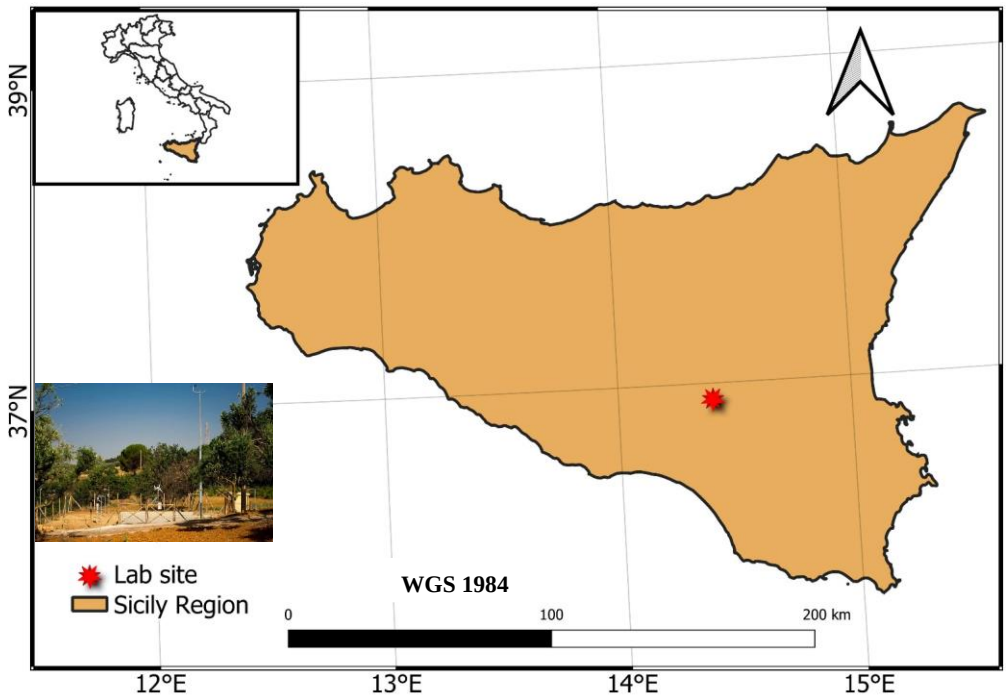

Figure 4. 1. Location of the study area.

4.3. Results

The Penman Monteith was applied for estimation of ETo in the 17-year timeframe of analysis. The result showed that maximum daily ETo was 14.47 mm per day on June 24, 2007 (Figure 4.2A), and the minimum daily ETo was 0.24 mm per day on January 4, 2016.

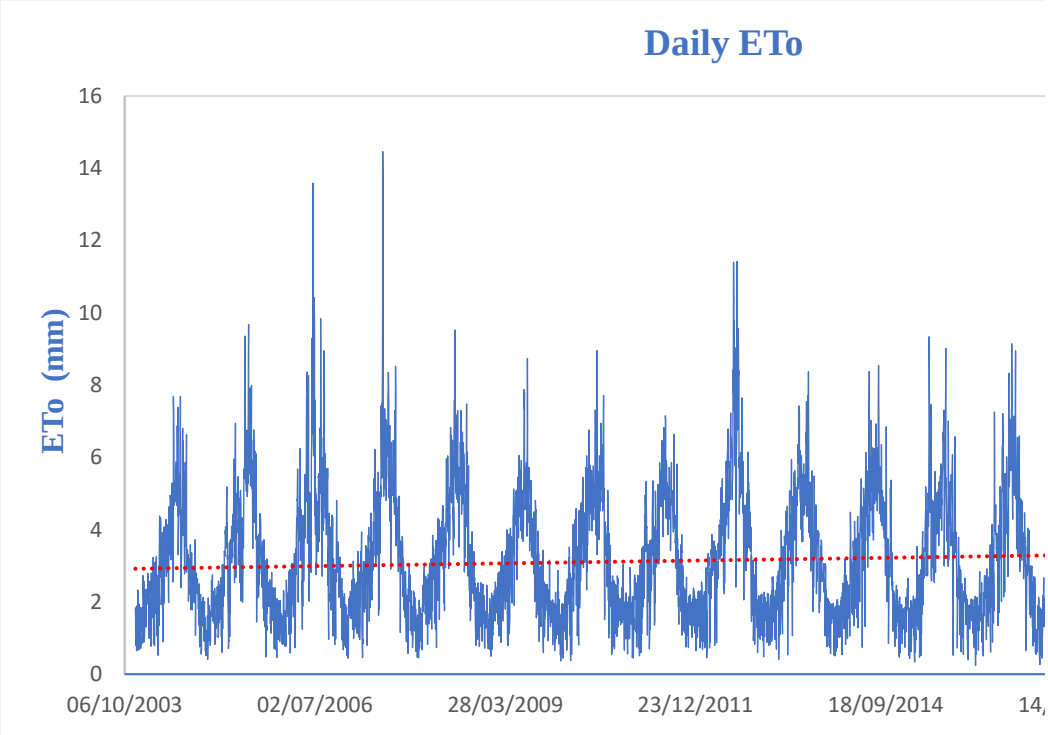

(A)

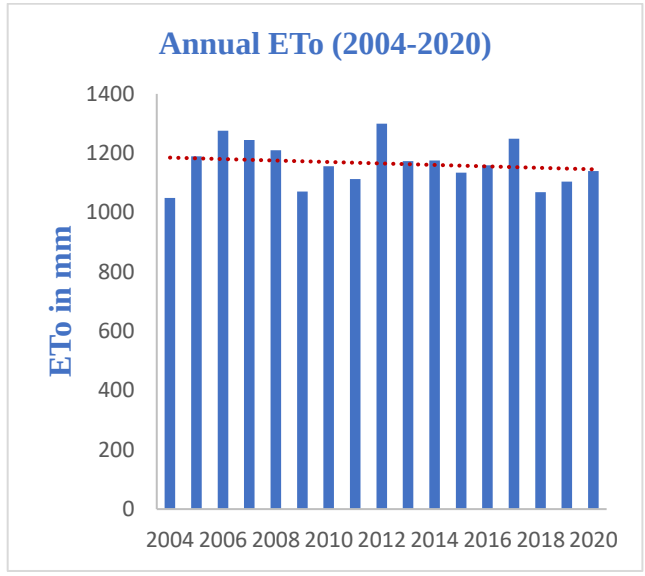
Annual ETo (2004-2020)
ETo in mm
1400
1200
1000
800
600
400
200
0
2004 2006 2008 2010 2012 2014 2016 2018 2020

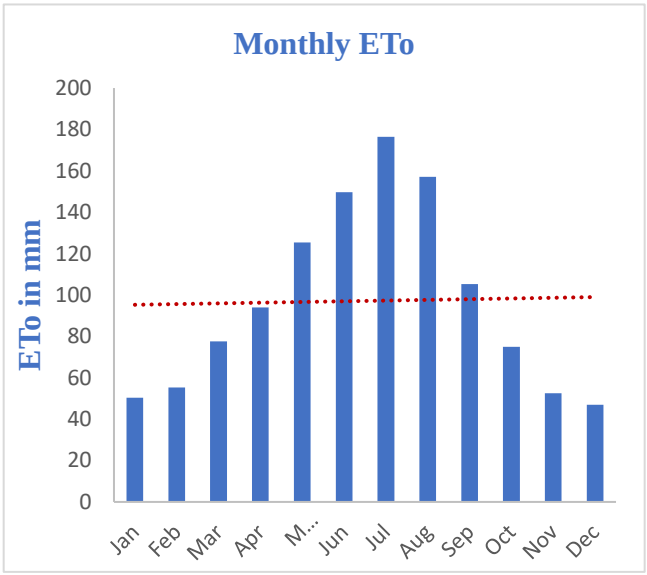
Monthly ETo
ETo in mm
200
180
160
140
120
100
80
60
40
20
0
Jan
Feb
Mar
Apr
M...
Jun
Jul
Aug
Sep
Oct
Nov
Dec

(B)

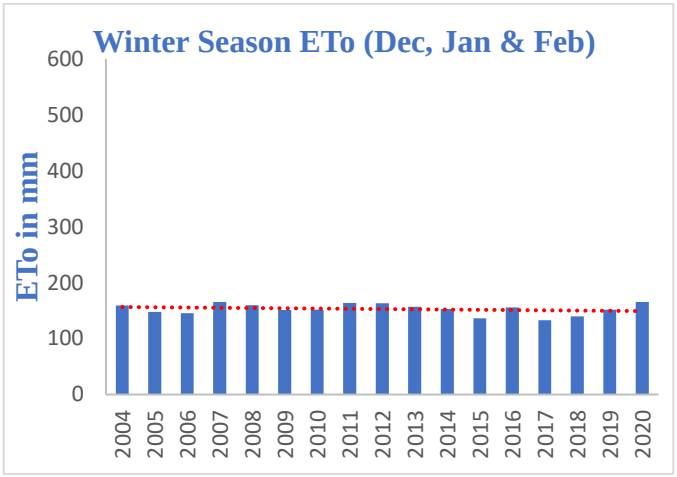
Winter Season ETo (Dec, Jan & Feb)
ETo in mm
600
500
400
300
200
100
0
2004
2005
2006
2007
2008
2009
2010
2011
2012
2013
2014
2015
2016
2017
2018
2019
2020

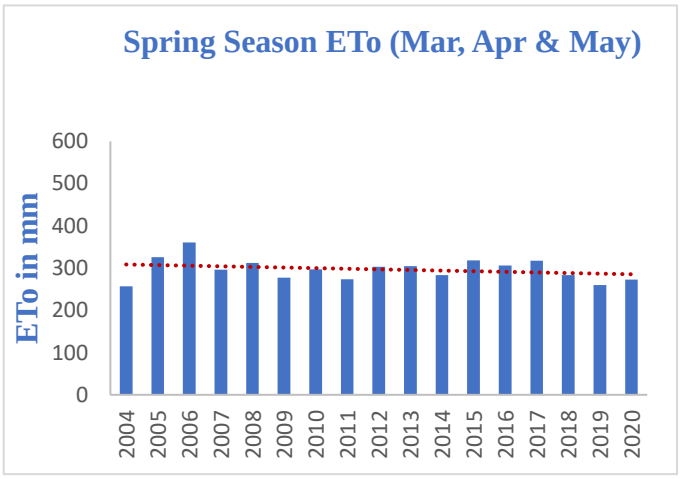
Spring Season ETo (Mar, Apr & May)
ETo in mm
600
500
400
300
200
100
0
2004
2005
2006
2007
2008
2009
2010
2011
2012
2013
2014
2015
2016
2017
2018
2019
2020

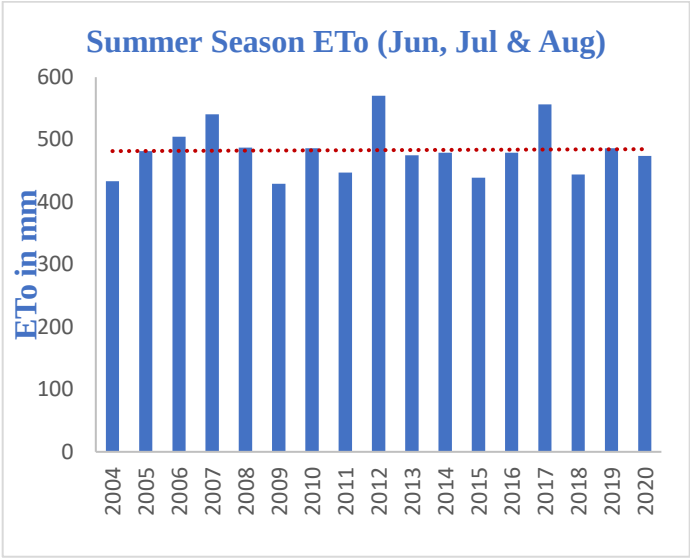
Summer Season ETo (Jun, Jul & Aug)
ETo in mm
600
500
400
300
200
100
0
2004
2005
2006
2007
2008
2009
2010
2011
2012
2013
2014
2015
2016
2017
2018
2019
2020

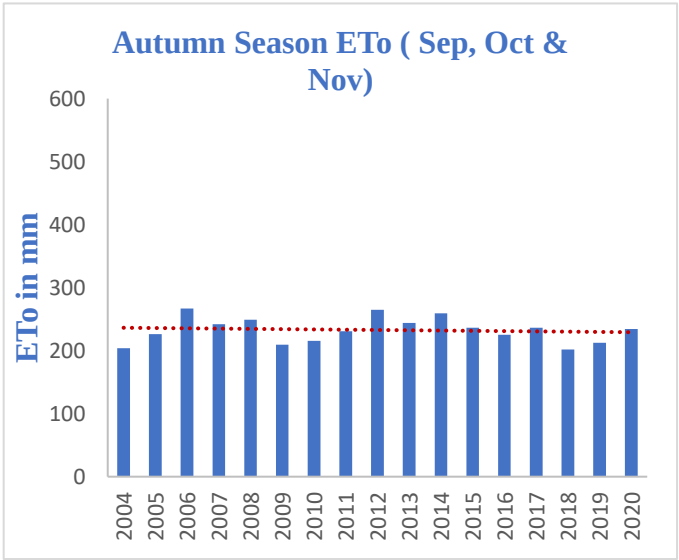
Autumn Season ETo (Sep, Oct & Nov)
ETo in mm
600
500
400
300
200
100
0
2004
2005
2006
2007
2008
2009
2010
2011
2012
2013
2014
2015
2016
2017
2018
2019
2020

(**C**)

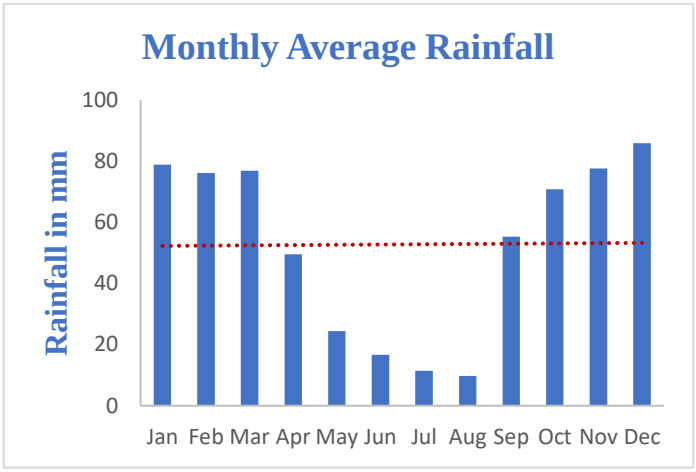

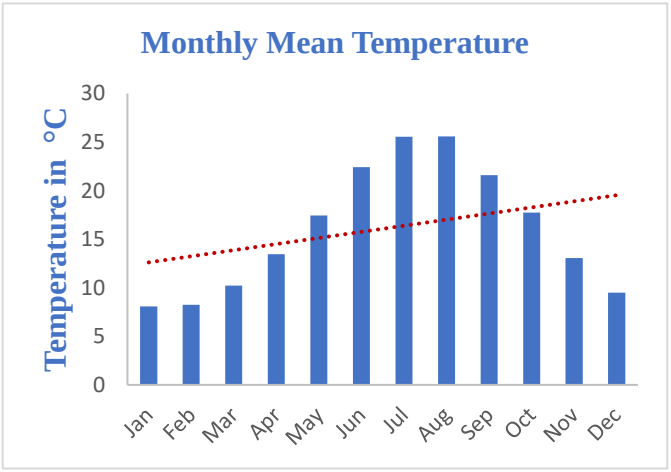

(**D**)

Figure 4. 2**.** Daily ETo (**A**), Annual ETo and Monthly ETo (**B**), Seasonal ETo (**C**), and Monthly Climatology (**D**).

4.3.1 Sen's Slope (Magnitude of the Trend)

Climatic variables and ETo showed both negative and positive trends in seasonal and monthly scale analysis. The ETo showed a negative downward trend in November of 0.790 mm per year. The T_{max} increased in March (0.10 °C) and September (0.14 °C) (monthly trend analysis), and spring (0.10 °C) and summer (0.09 °C) (seasonal trend analysis). The T_{min} also increased in August (0.09 °C) and September (0.07 °C). The T_{mean} trend also increased in September (0.10 °C) in monthly analysis and in spring (0.07 °C), and summer (0.06 °C) in the seasonal analysis. The SR showed a downward trend in November (0.09 MJ/m^2), at the monthly scale, and in Autumn (0.076 MJ/m^2), at the seasonal scale. The WS also showed an upward trend in January (0.054 m/s), May (0.038 m/s), June (0.021 m/s), July (0.043 m/s), November (0.040 m/s), and December (0.042 m/s), as well as in

winter (0.037 m/s) and spring (0.029 m/s). The HU trend also increased in March (0.711%), April (0.543%), May (1.169%), June (0.741%), July (1.012%), August (0.824%), September (0.816%), October (0.614%), and December (0.412%), as well as in spring (0.840%) and summer (0.942%). The RF also decreased in Autumn by 14.019 mm in the seasonal trend analysis.

4.3.2. MK-Test Trends of Meteorological Factors and ETo

Table 4.2 shows the results concerning trend significance, as obtained from the MK-Test. The T_{max} exhibits positive trends for March and September and spring and summer, while no significant trends were obtained for other time series. The T_{min} presents positive monthly trends in August and September, and no other significant trends were observed. For Tmean, there was no significant trend except for September and spring and summer. Conversely, SR presents a negative trend in November and in Autumn. As regards WS, positive trends were observed on both seasonal and monthly scales. On the monthly scale, January, May, June, July, November, and December showed positive trends; for the remaining months no trend is evidenced. The HU also has a positive significant trend in March, April, May, June, July, August, September, October, and December, as well as in spring and summer. Rainfall showed a negative trend only in Autumn. The trend of ETo is negative only in November, and non-significant in the other cases.

Table 4. 2 MK trend test result with 95% significance level.

	Jan	Feb	Mar	Apr	May	Jun	Jul	Aug	Sep	Oct	Nov	Dec	Win	Spr	Sum	Aut	Annual
T_{max}	1.1	1.19	**2.27**	1.44	0.91	1.77	1.61	1.69	**2.43**	0.78	1.69	1.86	1.77	**2.14**	**1.98**	1.49	1.31
T_{min}	0.08	0.95	0.99	0.62	−0.49	−0.21	1.19	**2.18**	**2.14**	0.01	1.36	−0.37	0.12	0.33	1.03	1.4	1.19
T_{mean}	0.12	1.03	1.94	1.36	0.29	0.45	1.69	1.77	**2.35**	0.29	1.77	0.62	0.95	**2.51**	**2.18**	1.49	1.58
SR	−0.95	−0.54	−0.7	0.62	−1.65	−0.33	−0.78	−1.2	−1.07	−1.44	**−2.02**	0.95	−0.12	−0.87	−0.91	**−2.6**	−1.44
WS	**2.68**	0.99	1.03	1.28	**2.76**	**2.18**	**2.97**	1.73	0.77	0.95	**2.39**	**2.23**	**2.76**	**2.02**	0.95	0.86	0.95
HU	0.41	0.5	**2.27**	**2.27**	**2.12**	**2.84**	**3.17**	**2.39**	**2.12**	**2.02**	1.22	**2.02**	0.86	**2.21**	**2.03**	1.31	1.31
ETo	−1.85	−0.95	−1.11	0.45	−1.28	−0.62	0.54	0.21	0.45	0.04	**−2.51**	−0.95	−0.54	−0.78	−0.21	−0.54	−0.78
RF	−0.04	0.45	−0.62	−1.19	0.29	−0.49	0.46	0.64	−0.21	0.33	0.95	0.5	−1.28	−0.29	−0.04	**−2.6**	−1.61

Win = winter; Spr = spring; Sum = summer; Aut = Autumn. Red color text = showed decreasing/upward trend.

4.3.3. Sensitivity of ETo to Climatic Factors

As the study stated above, for ETo estimation, T_{max}, T_{mean}, T_{min}, SR, WS, and SHU were used as input climatological variables. ETo showed different levels of sensitivity to these climatological variables. In particular, the result showed that SHU, $T_{mean,}$ and T_{max} have a very high sensitivity level, with sensitivity coefficients of 2.68, 1.46, and 1.35 respectively. The RS and T_{min} also showed a high sensitivity level, with the sensitivity coefficient of 0.53 and 0.28 respectively. In contrast, the sensitivity level of wind speed was negligible, with a value of 0.02 for the sensitivity coefficient (Table 4.3).

Table 4. 3 Sensitivity coefficient of climatic factor for ETo.

Climatological Element	Sensitivity Coefficient |x|	Sensitivity Level
Net solar radiation	|0.53|	High
Maximum temperature	|1.35|	Very high
Minimum temperature	|−0.28|	High
Mean temperature	|1.46|	Very high
Specific humidity	|−2.68|	Very high
Wind speed	|0.02|	Negligible

4.3.4. Contribution Rate of Climatic Factors for the Variation of ETo

The above-mentioned climatic factors have different contribution rates for the ETo trends at different temporal scales. Figure 4.3 shows that the contribution rate of SHU, SR and T_{min} are negative, with values of 91.73, 2.48, and 1.06, respectively. On the other hand, T_{max}, $T_{mean,}$ and WS contribute positively with an 11.2, 9.74, and 0.9 contribution rate. This result shows that SHU has the highest contribution to the decrease of ETo and maximum temperature has the highest contribution to the increase of ETo in the study area.

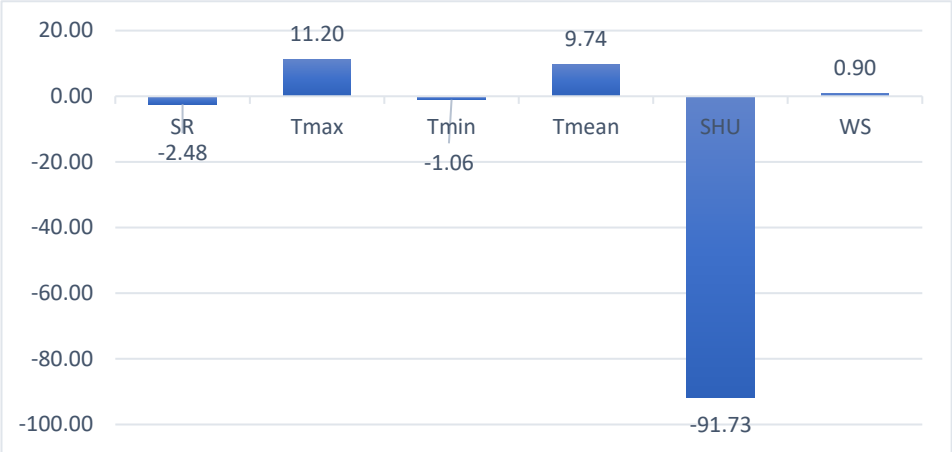

Figure 4. 3. Contribution of climatological factors to ETo.

4.4. Discussion

4.4.1. Trend of Climatic Factors and ETo

Globally, studies conducted by many authors showed that there is an upward trend of mean, maximum, and minimum temperature (Jain & Kumar, 2012; Mohammad & Goswami, 2019; Mondal et al., 2015; Saboohi et al., 2012; Subash & Sikka, 2014; Xu et al., 2008) . Our study also revealed that there were monthly and seasonal temperature upward trends at the experimental site in Sicily (Figure 4.4B). This is in line with similar research results showing an upward trend in temperature in Sicily (Liuzzo et al., 2017; Mohammad & Goswami, 2019). The studies cited also showed a decreasing rainfall trend in autumn in Sicily. In particular, from 1921 to 2012 there was a downward trend of rainfall throughout the island in autumn (Liuzzo et al., 2016) and a downward trend at the annual scale (Liuzzo et al., 2015). Moreover, a seasonal decrease in rainfall has been shown and documented in Sicily and Calabria (Caloiero et al., 2020). Our study revealed that there was an increase in monthly and seasonal minimum temperature. Globally, in about the 37% of the landmasses from 1951–1990 the minimum temperature and maximum temperature increased by 0.84 °C and 0.28 °C respectively (Jones, 1995). Similar results are also documented in several studies for different parts of Italy. From 1865 to 1996 southern Italy showed an upward trend of the minimum and maximum temperature, especially in southern Italy (Brunetti et al., 2000). Moreover, from 1952 to 1990, Bologna showed an increase of 0.7 °C in 48 years in annual mean temperature and an increase in higher minimum and maximum temperature (Ventura et al., 2002). In Calabria (southern Italy), trend analysis results showed an increase in maximum and the minimum temperature specifically in the summer and spring seasons (from

1951 to 2010) (Caloiero et al., 2017). This result is in line with our study since the maximum temperature showed a positive trend in summer and spring (Table 4.2). The maximum temperature also had a positive trend in Sardinia from 1982 to 2011 (Caloiero & Guagliardi, 2021). This study confirmed that there is an upward trend in mean temperature in summer, spring, and in the month of September (Table 4.2). The mean temperature of Sicily from 1924 to 2013 also showed an upward trend in summer and spring (Liuzzo et al., 2017).

This study showed that there was increasing monthly and seasonal trend of relative humidity. In Ravenna, Italy, for the period 1989 to 2008, relative humidity had an upward trend (Mollema et al., 2012). Moreover, by considering the past and projected future data from 1971 to 2050, relative humidity also had an upward trend for Sicily (Segnalini et al., 2013). Similar results showing an increase in relative humidity were confirmed in different part of the world (Abu-Taleb et al., 2007; Kousari et al., 2011; Singh et al., 2008). Unlike other main meteorological factors, solar radiation showed a downward trend in November and in autumn (Table 4.2). Southern Italy showed a decrease in solar radiation after the mid-1980s (Sanchez-lorenzo et al., 2015). In China from the 1960s to 2010s, solar radiation showed a downward trend (Che et al., 2005; Zhou et al., 2018); and globally also showed a downward trend in solar radiation after the 1980s as well as the trend known as "global dimming" (Ohmura, 2009).

Like the most climatological elements, wind speed also showed an upward trend both in monthly and seasonal analysis (Table 4.2). Comprehensive studies that analyzed several meteorological sites showed both upward and downward trends in wind speed. Meanwhile, these studies also showed that there were increases in wind speed in monthly as well as seasonal timescales (Eymen & Köylü, 2019; Jiang et al., 2010; Klink, 2002; Laib et al., 2018). However, the study which analyzed 24 meteorological sites seasonal, monthly, and annually in Iran from 1975 to 2005 showed a downward trend in wind speed in most of its stations (Kousari et al., 2011).

Table 4.2 showed that there was a downward trend in monthly reference evapotranspiration in November. This result is known as the "evaporation paradox". There are many studies discussing a monthly, seasonal, and annual downward trend in ETo. For instance, studies conducted in China (Wu et al., 2021; Yang et al., 2011), India(Darshana et al., 2013; Sonali & Kumar, 2016), and Senegal (Ndiaye et al., 2020) revealed a downward trend in ETo seasonally, monthly, and annually. In Iran, a downward trend in seasonal and monthly trend was also found (Shadmani et al., 2012), and specifically in November (Tabari et al., 2011). In general, this study did not show seasonal or annual trends other than for November.

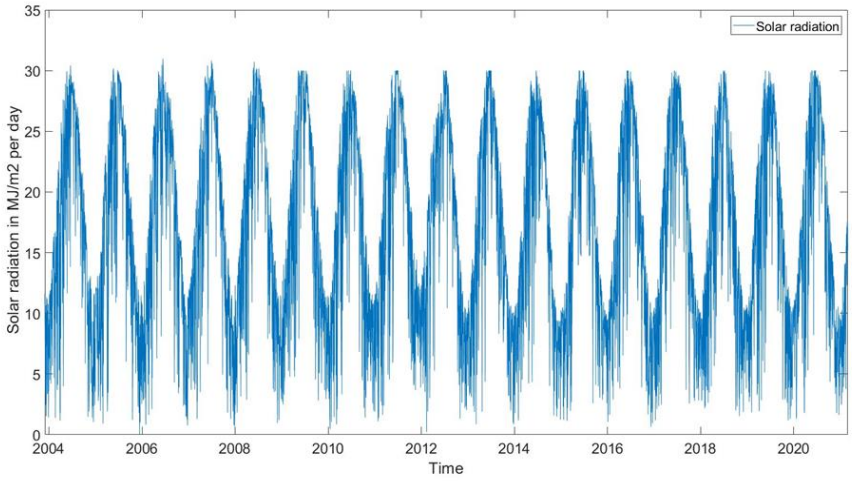
Solar radiation
Solar radiation in MJ/m2 per day
Time
0
5
10
15
20
25
30
35
2004
2006
2008
2010
2012
2014
2016
2018
2020

(**A**)

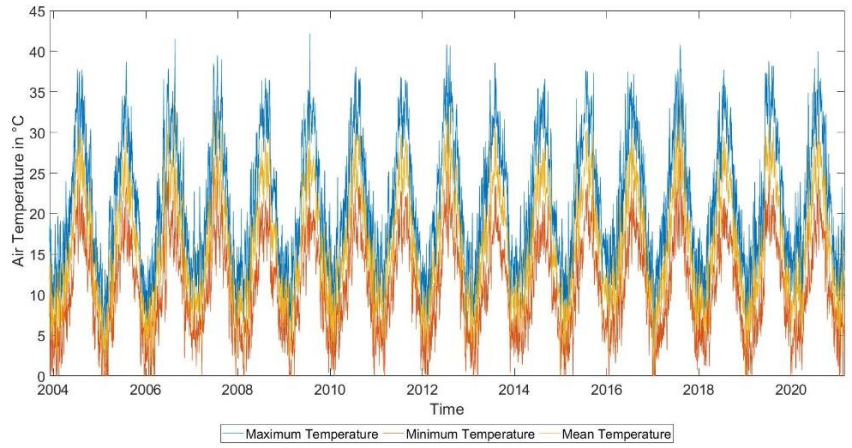
Air Temperature in °C
Time
Maximum Temperature
Minimum Temperature
Mean Temperature
0
5
10
15
20
25
30
35
40
45
2004
2006
2008
2010
2012
2014
2016
2018
2020

(**B**)

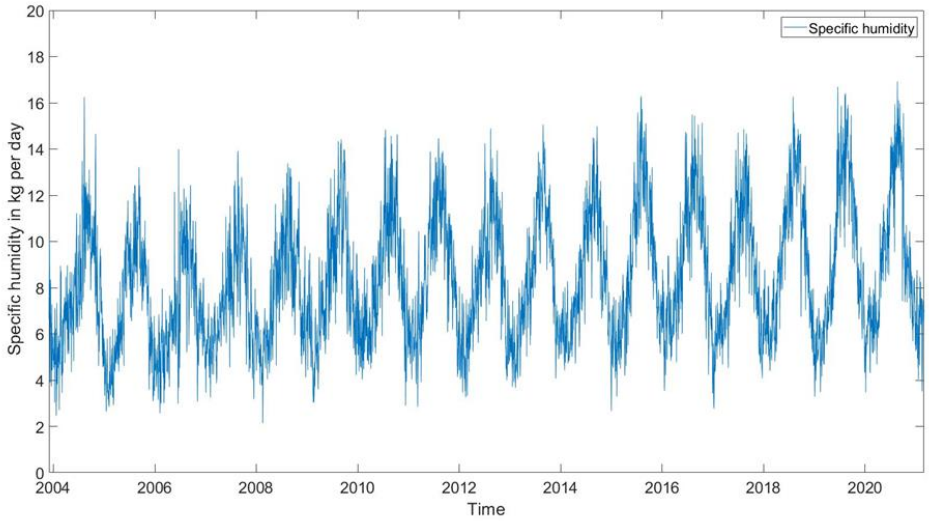
Specific humidity
Specific humidity in kg per day
Time
0
2
4
6
8
10
12
14
16
18
20
2004
2006
2008
2010
2012
2014
2016
2018
2020

(**C**)

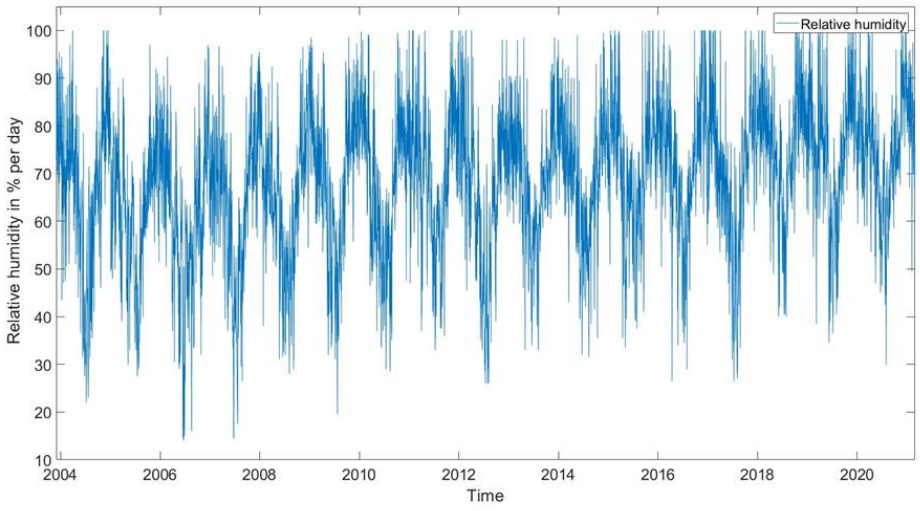
Relative humidity
Relative humidity in % per day
Time
10
20
30
40
50
60
70
80
90
100
2004
2006
2008
2010
2012
2014
2016
2018
2020

(**D**)

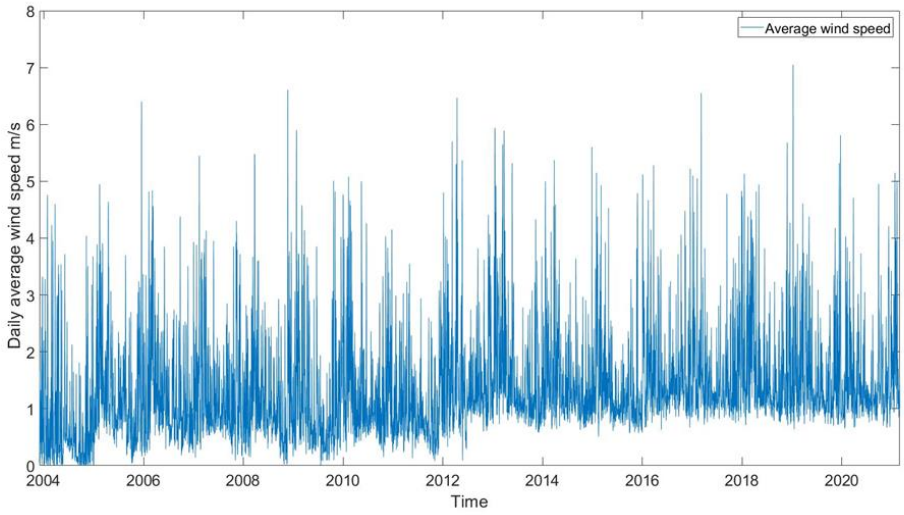

(**E**)

Figure 4. 4**.** Daily timeseries of climate variables from December 1, 2003–December 28, 2021: (**A**–**E**) are Solar radiation, Air temperature (maximum, minimum, and mean temperature), Relative humidity, Specific humidity, and Wind speed, respectively.

4.4.2. Sensitivity of ETo and Contribution Rate of Climatological Elements

The sensitivity analysis of ETo for climatic factors showed different magnitudes of sensitivity. The main and very high-level sensitivity in ETo trends was observed for specific humidity, mean temperature, and maximum temperature. Specific humidity was the most sensitive climatic factor for ETo trends in the study area. On the other hand, wind speed had a negligible sensitivity climatic factor for ETo trend. Likewise, relative humidity was the highest sensitivity climatic factor in the Loess Plateau of Northern Shaanxi, China (Li et al., 2017); in the Tao'er River Basin, China (Liang et al., 2008); and in the Yellow River Basin, China (Yang et al., 2011). Mean temperature was also one of the most sensitive factors for ETo in Iran (Sharifi & Dinpashoh, 2014); in the Tarim River basin, in Central Asia (Wu et al., 2021) and in the Yellow River Basin, China (Yang et al., 2011).

Similarly maximum temperature was also the another prime sensitivity climatic factor for ETo in Senegal (Ndiaye et al., 2020); the Himalayan region of Sikkim, India (Patle et al., 2020); the Tarim River basin, Central Asia (Wu et al., 2021), and in the Tons River Basin in Central India (Darshana et al., 2013). Wind speed also showed the lowest sensitivity in Santa Barbara (Irmak et al., 2006); the Himalayan region of Sikkim, India (Patle et al., 2020) and in the Tarim River basin, Central Asia (Wu et al., 2021).

This study showed that specific humidity, solar radiation, and minimum temperature contributed negatively to the trend of ETo; whereas maximum

temperature, mean temperature, and wind speed contributed positively to ETo in the study area (Figure 4.3). The contribution values showed that the absolute value of the climatic factors showed the contribution magnitude. Hence specific humidity is the climatological factor that contributed the most to monthly decrease in ETo in November. On the other hand, wind speed made the least contribution to ETo in the study area. Maximum temperature was prominent in ETo in the Loess Plateau of Northern Shaanxi, in China and the Tarim River basin, in Central Asia; and wind speed was the factor that contributed less to ETo in the Loess Plateau of Northern Shaanxi, China (Li et al., 2017).

4.5. Conclusions

In this study, referring to the FAO Penman-Monteith method for estimating reference evapotranspiration, we investigated the trends and sensitivity of ETo to meteorological variables. This analysis is important as there is a lack of similar studies. Also, in a climate change context it is key to understand the main climatological factors controlling such an important process for water resources management as evapotranspiration (Peres et al., 2019). The analysis considered the data collected at a Mediterranean climate site in Sicily, Italy (Piazza Armerina). The results show that there was no annual trend for all the analyzed variables. Trends are present only at the sub-annual scale (monthly or seasonally). Significant trends at the monthly and seasonal time scales were exhibited for all variables other than minimum temperature and ETo. ETo showed a significant trend only monthly, for November (ETo), and minimum temperature only monthly, for August and September.

The sensitivity analysis also showed that specific humidity, mean temperature, and maximum temperature are those factors that have a greater influence on ETo. Sensitivity to wind speed is negligible. In terms of the contribution of the climatic factors for ETo trends, specific humidity, solar radiation, and minimum temperature contribute negatively to ETo. On the other hand, maximum temperature, mean temperature, and wind speed contribute positively. These results contribute to understanding the potential and possible future footprints of climate change on evapotranspiration in the study area. On the one hand, the fact that no significant trends are exhibited by ETo seems to imply that the impacts of climate change have not left a relevant footprint on this hydrological variable. On the other hand, given the high sensitivity of ETo to temperature, it must be expected that ETo will be highly impacted by climate change in the future; as temperature is expected to increase by 2–3 °C in Sicily, depending on emission scenario (Peres et al., 2020; Pere et al., 2022). Moreover, the study in Pertouli and Taxiarchis in Greece also exhibited an increase in the potential evapotranspiration (PET) from 1974 to 2016 (Stefanidis & Alexandridis, 2021). Further development of this study will consider

more meteorological stations in Sicily, as well as other sources of data, to extend the length of the series and thus to improve the significance of trend assessments. Moreover, investigation could be extended, where data is available, to actual evapotranspiration.

Chapter 5

An assessment of trends of Potential Evapotranspiration at multiple timescales and locations in Sicily from 2002 to 2022

Abstract

Climate change and the related temperature rise can cause an increase of evapotranspiration. Thus, the assessment of Potential evapotranspiration (PET) trends is important to identify possible ongoing signals of climate change, in order to develop adaptation measures for water resource management and improving irrigation efficiency. In this study, we capitalize on the data available from a network of 46 complete meteorological stations in Sicily that cover a period of about 21 years (2002-2022) to estimate PET by the Food and Agriculture Organization (FAO) Penman-Monteith method at the daily time scale in Sicily Island (southern Italy). We then analyse the trends of PET and assess their significance by the Sen's Slope and the Mann Kendall test, at multiple temporal scales (monthly, seasonal, and annual). Most of the locations do not show significant trends. For instance, at the annual timescale only 5 locations have a significantly increasing trend. However, there are many locations where the monthly trend is statistically significant. The number of locations where monthly trend is significant is maximum for August, where 18 out of these 46 stations have an increasing trend. In contrast in March there are no locations with significant trends. The location with the highest increasing trend of PET indicates a trend slope of 1.73, 3.42, and 10.68 mm/year at monthly (August), seasonal (Summer), and annual timescales, respectively. In contrast, decreasing PET trends are present only at monthly and seasonal scales, with a maximum of respectively -1.82 (July) and -3.28 (Summer) mm/year. Overall, the findings of this study are useful for climate change adaptation strategies to be pursued in in the region.

Keywords: Climate change; temperature; drought; irrigation; Mediterranean area, Penman-Monteith

5.1 Introduction

Global warming induced by greenhouse gas emissions is claimed to be key contributor to changes in the global climate (IPCC., 2019; Fischer et al., 2021; Hoegh-Guldberg et al., 2018). The Fifth Assessment report by (AR5) discusses how the last three decades have been successively warmer at the Earth's surface than any preceding decade since 1850 (IPCC, 2013). Global warming is claimed to influence the entire hydrological cycle (Huang et al., 2015; Liu et al., 2018; Wang et al., 2017; Zuo et al., 2012). Assessments of Potential evapotranspiration (PET) show that evapotranspiration can be considerably influenced by global climatic changes (Bian et al., 2020; Ding & Peng, 2021; Wang et al., 2017; Zongxing et al., 2014). The IPPC 6th technical report showed that there is an increasing of the evapotranspiration due to growing atmospheric water demand will decrease soil moisture over the Mediterranean region (Arias et al., 2021).

Evapotranspiration is also a key variable for the estimation of the energy budget in the earth-atmospheric system and the water balance in a given region (Han et al., 2015; Wang et al., 2017; Zhao et al., 2018; Zongxing et al., 2014). PET refers to evaporation and transpiration over a surface under certain meteorological conditions with considering sufficient water, unlimited soil water supply. Moreover, PET is important for scientific research on hydro-climatology, irrigation planning and water resource management (Bian et al., 2020; Huang et al., 2015; Liu et al., 2018).

Understanding of the spatiotemporal trends of PET is a crucial part of in climatology, water resource management and irrigation planning (Guo et al., 2020). Both decreasing and increasing trends of PET have been detected in different parts of the world (Chu et al., 2019; Li et al., 2013; Luo et al., 2021; Maruyama et al., 2004; Shadmani et al., 2012; Zuo et al., 2012). PET is expected to increase due to climate change. Nevertheless, decreasing trends have been identified, leading to the so-called "evapotranspiration paradox" (Bian et al., 2020; Huang et al., 2015; Jerin et al., 2021; Luo et al., 2021; Ndiaye et al., 2020), and it was detected in several regions worldwide, especially in various areas of China (Han et al., 2015; Bian et al., 2020; Zongxing et al., 2014; Zuo et al., 2012; Chu et al., 2019; Zhao et al., 2018). For the Mediterranean climate, Palumbo et al., (2011), showed that 14 studies confirmed prevailing positive trends, 4 studies negative trends, and three studies no trends. From 1961 to 2016, the trend of the reference evapotranspiration from 18 meteorological stations of Slovenia was analysed and the result showed that samples are mostly increasing and statistically significant while no consistent trend could be detected (Maček et al., 2018). In the western French Mediterranean area, the PET showed an increasing trend at monthly, seasonal (Spring) and annual

scale from 1970-2006 (Chaouche et al., 2010).

Mediterranean area also showed there was an increasing trend of PET from 1950 to 2020, and significantly contributed for drought intensification in the region (Wang et al., 2022). The actual evapotranspiration also showed a trend in humid and subhumid Mediterranean climate of North Algeria from 1961 to 1990 (Aieb et al., 2022). Moreover, for the Mediterranean future projections of the PET also confirmed that there will be increasing trend (Zeng et al., 2022). Additionally, in Greece the PET showed an increasing trend (Stefanidis & Alexandridis, 2021); in southern Italy showed increasing trend in growing season (Liuzzo, Viola, et al., 2016). According to Liuzzo et al. (2016), there were seasonal differences of the spatiotemporal trend of PET in different areas of Mediterranean climate. For instance, in southern Italy, an increasing trend was observed in correspondence of the growing season, while no trend was observed during the non-growing season. However, the mentioned study needs to updated as it considers an outdated period and only 3 locations in Sicily.

In this study, we advance from previous studies by considering a dataset that covers a recent period (last 21 years, up to 2022), and 46 locations spread in Sicily. This allows an unprecedented systematic and robust assessment of PET trend in this region, which is prone to droughts and presents several critical due to climate change (Peres et al., 2019). In particular, in the present study we analyse the PET trends in Sicily at multiple locations (i.e., those of meteorological stations managed by the SIAS - Servizio Informativo Agreometeorologico Siciliano, the Agrometeorological Informative Service of Sicily) at the monthly, seasonal and annual temporal scales.

This study was organized: introduction, the study area and the data are described, and the methodology is delineated (Section 2). This section explains the methods for computing PET and the statistical methods for assessing the magnitude and the significance of trends. Then, in Section 3 results are presented analysing various time scales. Section 4 discusses the results with a comparison to other regions in the globe. Finally, Section 5 presents some conclusions and an outlook.

5.2 Material and Study Area

Figure 5.1 shows the study area, Sicily Island. The climate of Sicily is typically Mediterranean, with hot but not scorching Summers, mild and brief Winters, and moderate rainfall from October to March. Along the coast, the average temperature ranges between 17 and 18.7°C annually, with July being the warmest month (Torina & Khoury, 2006). Sicily's weather is characterized by a hot and dry Summer season, and a mild and rainy Winter season (Bonaccorso et al., 2015). The meteorological data are provided by the Agrometeorological Information Service of Sicily (SIAS,

http://www.sias.regione.sicilia.it/), having 46 meteorological stations distributed all over the region. Specifically, for each meteorological station, minimum, maximum, and mean temperature (°C), solar radiation (MJ/m²), wind speed (m/s), and relative humidity (%) are collected from 01/01/2002 to 31/03/2022. Table 5.1 summarizes the main characteristics for each station, namely name, ID, elevation, and the coordinates of their location.

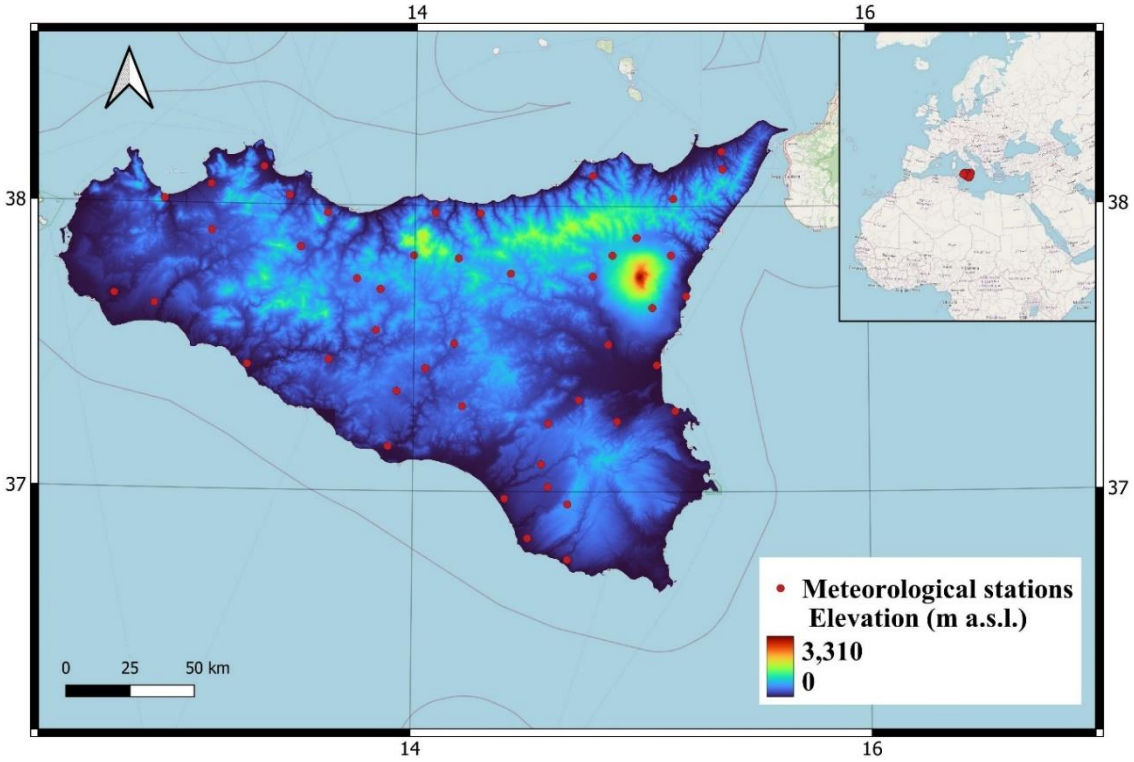

Figure 5. 1 Study area with location of meteorological stations of the SIAS network.

Table 5. 1 Main characteristics of the SIAS network meteorological stations.

Code	Name	Elevation [*m a.s.l.*]	Annual average PET [*mm*]
203	Aragona	305	1091.19
209	Licata	80	1368.18
212	Ribera	30	1119.13
214	Caltanissetta	350	1175.23
215	Delia	360	1138.6
218	Mazzarino	480	1107.06
219	Mussomeli	650	1189.08
224	Bronte	430	1040.83
227	Caltagirone	480	1101.61
228	Catania	10	1200.8
229	Riposto	50	1079.57
230	Linguaglossa	590	1049.76
231	Maletto	1040	1032.93
232	Mazzarrone	300	1177.1
233	Mineo	200	1084.08
234	Paternò	100	1156.05
235	Pedara	810	1015.08
237	Randazzo	680	1128.66
238	Enna	350	1176.78
241	Nicosia	700	1024.62
249	S. Pier Niceto	460	1103.05
254	Naso	480	948.26
256	Novara di Sicilia	750	1045.11
258	Pettineo	210	1160.26
261	Torregrotta	60	1098.13
262	Alia	560	1163.41
264	Camporeale	460	1090.79
265	Castelbuono	430	1158.36
269	Gangi	830	1105.08
273	Mezzojuso	390	1084.26
274	Misilmeri	160	1070.78
276	Palermo	50	1087.91
277	Partinico	120	1055.93
279	Polizzi Generosa	650	1106.09
222	Sclafani Bagni	497	1066.29
281	Termini Imerese	350	1086.66
282	Acate	60	1100.15
283	Comiso	220	1099.55
286	Ragusa	650	1163.68
287	Santa Croce Camerina	55	1144.41
288	Scicli	30	1188.86
289	Augusta	60	1074.76
291	Francofonte	100	1220.19
301	Castellammare del Golfo	90	1049.9
302	Castelvetrano	120	1159.07
305	Mazara del Vallo	30	1157.54

5.3 Methodology

The Penman Monteith method is used in the present study to calculate PET. This method is the most comprehensive and international standard for PET estimation, and it is also approved by Food and Agriculture Organization (FAO), and the American Society of Civil Engineers (ACSE) (Lang et al., 2017; Ndulue & Ranjan, 2021; Peng et al., 2017; Shi et al., 2008; Tellen, 2017; Utset et al., 2004).
The FAO Penman-Monteith equation has been derived by integrating the original Penman-Monteith equation with the equations of the aerodynamic and canopy resistance, yielding the following equation (Eq.5.1):

$$PET = \frac{0.408\Delta(R_n - G) + \gamma \frac{C_n}{T + 273} U_2 (e_s - e_a)}{\Delta + \gamma(1 + C_d\, U_2)} \qquad 5.1$$

where: *PET* is potential evapotranspiration [mm day^{-1}], R_n is the net radiation at the crop surface [MJ m^{-2} day^{-1}], *G* represents the soil heat flux density [MJ m^{-2} day^{-1}], *T* is the air temperature at 2 *m* height [°C], U_2 represents the wind speed at 2 *m* height [m s^{-1}], e_s is the saturation vapour pressure [kPa], e_a is the actual vapour pressure [kPa], and ($e_s - e_a$) represents the saturation vapour pressure deficit [kPa], Δ is the slope vapour pressure curve [kPa °C^{-1}], and g indicates the psychrometric constant [kPa °C^{-1}]. C_n is the ratio of the slope of the saturation vapor pressure curve to the psychrometric constant at a given temperature. It represents the energy available to drive the process of evapotranspiration. C_d is the ratio of the aerodynamic resistance to the surface resistance. It represents the resistance that water vapor encounters in the atmosphere as it moves from the leaf surface into the air. In this study we assume C_n and C_d equal to 900 and 0.34, which are the values for a grass reference crop.

Sen's slope estimator

The Sen's slope estimator is a non-parametric method used for estimating the slope of a linear relationship between two variables (Darshana et al., 2013; Kamal & Pachauri, 2019; Panda & Sahu, 2019; Peng et al., 2017; Shan et al., 2015). It is particularly useful when the data exhibits high variability, non-normal distribution, or outliers. The Sen's slope estimator is based on calculating the median of the slopes between all possible pairs of data points. This approach makes it robust to outliers and resistant to extreme values. The method is easy to apply and can be used for small or large datasets. In this study, we used 0.05 significance level, i.e., when $|Z| > 1.96$ (eq. 5.6) the null hypothesis is rejected, and the trend is significant at 5%. If a trend is mentioned in the data series, its amount can be evaluated by the

slope of the trend (noted β). In general, this method used to estimate the slope of the trend (Eymen & Köylü, 2019; Hu et al., 2019; Hwang et al., 2020; Li et al., 2018; Patle et al., 2020; Zongxing et al., 2014). Hence, the magnitudes of the trends in *ETo* were studied using Sen's slope estimator.

$$\beta = Median\left(\frac{X_i - X_j}{i - j}\right) \; for \; all \; i > j \qquad 5.2$$

where X_i and X_j are the data values at times *i* and *j*, respectively. β> 0 denotes an increasing trend.

Mann-Kendall test

It is common practice to use the Mann-Kendall (MK) test to identify statistically significant trends in various analyses of hydro-climatological time series (Alemu et al., 2015; Aschale et al., 2023; Dong et al., 2020; He et al., 2013; Hui-mean & Yusof, 2018; Nam et al., 2015; Peng et al., 2017) . It is a rank-based non-parametric method, which has been widely used for detecting trends in hydrometeorological time series. The MK test's key advantage is that it is not sensitive to extreme values and does not require that the data follow any statistical distribution (Diop et al., 2016; Ndiaye et al., 2020; Shadmani et al., 2012). The test is based on two hypotheses: the alternative hypothesis (H_1), which shows the existence of a trend and rejects the null hypothesis (H_0), which assumes that the test is stationary and thus there is no trend. Mann-Kendall's statistical *S* is given by the following formula:

$$S = \sum_{k=1}^{n-1} \sum_{j=k+1}^{n} Sgn(X_j - X_k) \qquad 5.3$$

where X_k is the value of the variable at time *k* and X_j is the value of the variable *j*, *n* is the length of the series and sign () is a function which is calculated as follows:

$$Sgn(X_j - X_k) = \begin{cases} 1 \; if \; (X_j - X_k) > 0 \\ 0 \; if \; (X_j - X_k) = 0 \\ -1 \; if \; (X_j - X_k) < 0 \end{cases} \qquad 5.4$$

It has been documented that, when *n >=10*, the statistic *S* is approximately normally distributed with the mean *E(S)=0*, and its variance is:

$$Var\ (s) = \frac{n(n\ -\ 1)(2n\ +\ 5) - \sum_{i=1}^{m} t_i(\ t_i - 1)(2t_i + 5)}{18} \qquad 5.5$$

where *n* is the number of data points, *m* is the number of tied groups (a tied group is a set of sample data having the same value), and t_i is the number of data points in the ith group.

The standardized test statistic *Z* is computed as follows:

$$Z = \begin{cases} \frac{S-1}{\sqrt{Var(s)}}, if\ S > 0 \\ 0, if\ S = 0 \\ \frac{S+1}{\sqrt{Var(s)}}, if\ S < 0 \end{cases} \quad 5.6$$

The null hypothesis H_0, meaning that no significant trend is present, is accepted if the test statistic *Z* is not statistically significant, i.e. *-Zα/2<Z<Zα/2*, where *Zα/2* is the standard normal deviate. To overcome the limitation of the MK test related to the autocorrelation of the original data the Trend-free prewhitening (TFPW) method was applied. This method introduced and enabled removing serial dependence is one of the main problems in testing and interpreting time series data (Ahmad et al., 2015; Wu et al., 2021; Zhang et al., 2020b).
The Trend-free prewhitening includes the following steps:

i. all of the PET time series data was first tested for the presence of autocorrelation coefficient (r) at a 5% significance level, using a two-tailed test.

$$r = \frac{\sum_{t=1}^{n-1}(X_t - \bar{X}_t)(X_{t+1} - \bar{X}_{t+1})}{\sqrt{\sum_{t-1}^{n-1}(X_t - \bar{X}_t)^2}\sqrt{\sum_{t-1}^{n-1}(X_{t+1} - \bar{X}_{t+1})^2}} \quad 5.7$$

ii. the autocorrelation coefficient value of r was tested against the null hypothesis at a 95% confidence interval, using a two-tailed test

$$r\ (95\%) = \frac{-1 + 1.96\sqrt{(n-2)}}{n-1} \quad 5.8$$

iii. removing any trend items from the time series variables to form a sequence without trend items

$$Y_t = X_t - \beta_t \quad 5.9$$

iv. adding the trend term β_t to obtain a new sequence without an autocorrelation effect

$$Y_t = Y_t - rY_{t-1} + \beta_t \qquad 5.10$$

where X_t is the value at time *t*, *n* is the length of the data, and $\bar{X}_t$ is the mean value. The original MK test is applied to Y_t to assess the significance of the trend.

5.4 Results

Annual PET trends have been observed only in 5 locations out of 46. Figure 5.2 shows the PET timeseries for these five locations.

Table 5.2, shows that 83% of the meteorological stations recorded a trend in at least one month or season. Changes of PET trend in the last 21 years, i.e., of the 46 analysed meteorological stations, 38 of them resulted in PET trend, at different temporal scales, while only 8 of them have not resulted in trend. Specifically, the latter are mostly located close to northern and southern coastlines of the island.

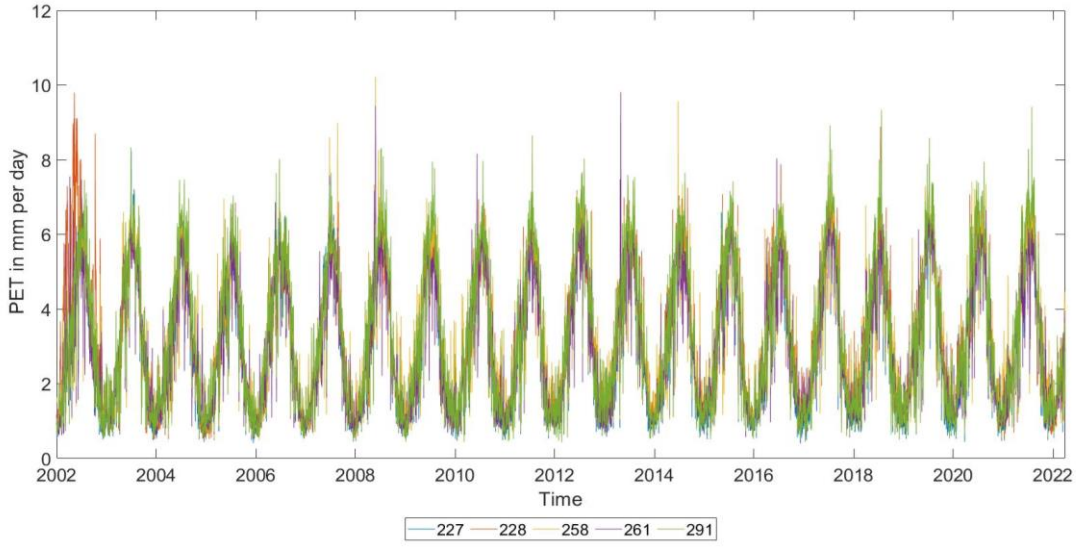

Figure 5. 2: Time series for five meteorological stations confirmed an annual trend.

Table 5.2, instead, summarizes Z values of the PET trend for each meteorological station and at different temporal scale.

Table 5. 2: *Z* value of the PET trend for each meteorological station at different temporal scale. Yellow shaded represents the *Z* value decreasing PET trend, while the reddish shaded are the Z value increasing PET trend.

Code	Name	Jan	Feb	Mar	Apr	May	Jun	Jul	Aug	Sep	Oct	Nov	Dec	Win	Spr	Sum	Aut	Ann
203	Aragona	0.68	1.07	-0.2	0.81	-0.4	0	0.68	1.14	1.65	0.55	-0.9	1.01	3.28	0	0.68	1.07	0.94
209	Licata	2.76	1.46	1.27	1.14	0.75	0.29	2.89	3.15	0.49	0.16	0.81	0.84	3.41	0.98	0.81	-0.29	-0.1
212	Ribera	1.27	1.59	0.55	0.94	0.49	2.5	2.82	3.41	2.82	1.72	-1	0.03	1.85	0.88	1.82	0.7	0.81
214	Caltanissetta	1.27	1.85	0.81	1.59	0.68	0.03	0.94	0.94	1.33	0.68	-0.6	0.23	0.49	1.26	0.94	0.84	0.62
215	Delia	-0.8	0.55	0.03	0.81	-0.8	-0.5	0.16	1.14	0.91	-0.1	-0.9	0.03	1.05	0.03	0.55	0.1	0.62
218	Mazzarino	2.11	1.78	1.14	1.52	0.62	1.01	1.68	1.65	3.34	1.36	1.52	1.4	0.81	1.59	2.1	2.89	1.85
219	Mussomeli	1.72	1.59	0.94	1.65	0.42	1.14	1.14	2.11	1.91	0.49	-1	3.08	1.01	1.14	1.46	0.94	1.91
224	Bronte	2.24	1.69	0.42	2.14	0.88	1.46	1.91	2.08	0.55	1.59	-0.2	1.47	1.27	1.52	2.21	-0.36	0.75
227	Caltagirone	1.52	2.17	0.55	1.65	1.62	0.62	1.72	1.52	1.72	0.36	0.62	2.56	3.28	1.33	1.14	1.14	2.11
228	Catania	-0.4	2.69	1.72	1.72	1.33	1.33	0.62	1.14	0.75	1.07	1.27	1.61	0.94	1.65	1.91	1.98	2.82
229	Riposto	1.27	1.98	0.81	0.42	0.49	0.35	1.52	1.85	1.27	0.49	1.59	0.49	0.36	0.68	1.27	0.84	0.75
230	Linguaglossa	1.14	-0	-0.9	0.16	-2.6	-1.5	-0.4	-0.2	0.1	-0.4	-0.2	3.02	1.85	-2.04	-1.4	-0.62	-1.52
231	Maletto	0.55	0.68	-0.8	-0.5	-1.7	-2	-2.4	-1	-0.3	-1.5	-0.3	0	1.01	-1.2	-2.43	-0.77	-0.42
232	Mazzarrone	1.91	1.27	1.07	0.81	0.42	1.12	0.03	2.17	1.75	1.2	1.07	1.59	2.63	0.55	1.19	0.36	0.42
233	Mineo	0.81	1.07	1.46	0.36	2.11	2.43	2.95	2.24	2.69	1.33	0.49	2.17	2.1	0.81	3.41	0.81	1.52
234	Paternò	1.07	1.2	0.68	0.88	0.42	0.29	-1.1	1.14	2.11	0.88	2.63	0.88	0.55	1.14	1.12	1.98	1.4
235	Pedara	0	-0	-0.2	-0.2	-1.5	-1.4	-0.7	-0	-0.4	-2	-1	0.29	1.85	-1.07	-1.65	-2.37	-1.33
237	Randazzo	1.2	0.81	-0.4	-0.6	-1.1	-1.1	-0.4	-0.4	0.36	-1	-1.3	0	1.52	-1.01	-0.62	-1.01	-1.07
238	Enna	0.03	1.68	1.27	1.61	1.01	1.33	1.01	2.24	1.68	1.78	0.68	0.62	0.68	0.94	2.3	0.55	0.88
241	Nicosia	1.17	1.85	0.49	2.04	1.07	1.01	1.65	1.33	2.11	0.29	0.58	0.16	0.36	1.72	1.52	1.27	1.01
249	S. Pier Niceto	-0.4	-0.2	-0.3	1.07	-0.8	-1.1	-0.5	0.68	1.27	-0.8	-1.7	-1.46	-1.2	-0.55	-0.29	-0.62	-0.68
254	Naso	0	0.36	-1.2	0.88	-1.3	-2.2	-0.8	0.36	-0.3	-0.6	-1.3	-0.49	-0.55	-1.01	-1.07	-1.27	-1.4
256	Novara di Sicilia	1.27	1.46	0.23	1.01	-1.1	0.23	1.01	1.59	1.59	-0.7	0.49	0.91	1.27	0.32	1.07	0.23	1.33
258	Pettineo	3.21	2.37	1.2	0.23	0.1	1.07	2.04	2.04	1.65	0.55	0.88	1.59	3.02	1.46	1.98	1.33	3.02
261	Torregrotta	0.62	0.81	1.52	1.3	-0.3	0.42	2.11	2.43	3.08	0.75	0.62	0.75	0.81	1.01	2.37	1.98	3.08
262	Alia	1.17	1.65	1.07	2.04	0.68	0.23	1.01	0.81	0.68	-0.9	-2.6	0.62	1.98	1.14	1.46	-0.81	1.2
264	Camporeale	2.47	1.07	-0.6	0.49	-0.6	-0.8	0.55	1.2	2.11	0.81	-0.8	2.3	1.61	-0.58	0.49	1.43	0.94
265	Castelbuono	2.24	0.62	-1.1	0.49	-0.7	-0	1.01	0.75	-0.2	-1.2	-1.1	-0.75	0.88	-0.42	0.75	-1.46	0.03
269	Gangi	1.27	1.72	0.42	1.78	0.62	0.23	1.52	2.08	2.11	-0	-0.2	-1.4	1.12	0.68	1.4	-0.16	1.59
273	Mezzojuso	-0.8	-0.1	-1.4	-0	-0.6	-1.3	0.55	0.55	-0.2	-1.5	-1.3	-2.11	-1.91	-1.07	-0.62	-2.11	-1.56
274	Misilmeri	1.33	1.78	0.23	1.52	0.03	0.68	2.3	2.04	1.27	0.42	-1	0.16	1.07	1.01	1.98	0.16	1.85
276	Palermo	3.19	3.02	1.27	0.42	1.27	0.49	1.91	2.43	0.68	0.49	1.07	0.1	0.36	2.37	2.11	0.29	0.88
277	Partinico	3.47	2.24	0.94	1.59	0.62	1.14	1.82	2.76	2.63	1.07	1.33	1.98	0.81	1.07	2.63	2.5	1.72
279	Polizzi Generosa	0.75	0.88	-0.1	1.52	-0	0.75	1.65	1.46	1.14	-0.3	-1.5	-0.16	0.63	0.49	1.33	-0.36	0.75
222	Sclafani Bagni	1.26	2.17	1.01	0.55	1.14	1.27	0.49	2.5	1.47	1.2	0.49	0.62	0.81	1.59	2.43	0.42	1.2
281	Termini Imerese	0.42	1.04	-0.1	0.68	0.16	1.01	2.82	1.78	0.49	-0.8	-1.9	-0.94	0	0.29	2.24	-0.88	0.62
282	Acate	-1.3	-0.7	-0.9	-0.5	-1.5	-0	0.81	1.14	0.75	-2	-1.6	-1.82	-1.65	-1.59	0.36	-1.59	-1.72
283	Comiso	1.65	1.04	-0	0.62	0.94	1.59	3.15	1.98	0.81	0.75	-0.4	1.59	1.65	0.68	2.82	0.03	1.59
286	Ragusa	0.42	0.45	-0.2	0.68	0.55	0.03	0.68	1.2	0.81	-0.9	-1.4	-0.1	1.14	0.03	0.88	-0.16	0.1
287	Santa Croce Camerina	-2.4	-1	-0.9	-0.2	-0.2	1.52	1.85	2.11	0.29	-1.5	-2.1	-2.5	-2.3	-0.88	1.52	-1.2	-1.01
288	Scicli	0.36	-0.2	-0.6	0.16	-0.2	-0.2	0.13	0.29	-0.4	-1.3	-1.5	-0.55	-0.71	-0.23	0.16	-0.94	-0.81
289	Augusta	0.81	0.23	0.55	1.07	-0.2	0.23	0.55	1.4	2.5	-0.6	-0.6	1.12	0.42	0.94	0.36	0.58	0.94
291	Francofonte	1.65	1.59	1.14	1.65	1.4	1.33	0.75	1.78	2.04	0.29	1.52	2.3	2.69	1.91	2.24	1.78	3.08
301	Castellammare del Golfo	1.01	0.55	-1.4	-0.6	-0.2	0.49	1.91	1.07	0.75	-0.2	-2	-1.07	0.1	-0.88	1.27	-0.65	-0.16
302	Castelvetrano	2.69	1.52	0.68	0.42	0.62	0.16	2.24	2.5	2.17	1.33	0.42	1.33	0.16	0.49	1.85	-0.49	0.29
305	Mazara del Vallo	0.68	1.2	1.14	0.94	0.36	1.91	0.81	2.76	1.46	1.91	0.62	1.91	0.36	1.27	1.27	1.07	1.4

Temporal trend of the PET

Looking at the different analysed temporal scales, no increasing trend was observed in March and October. Specifically, in October exclusively decreasing trends were detected in correspondence of two meteorological stations, while in March, any trend was detected, neither positive nor negative, for all meteorological stations. If increasing trend of PET is considered, at August, and September monthly temporal scale, as well as at Summer seasonal temporal scale was recorded the highest number of involved meteorological stations, namely 15 on average for each of these

temporal scales. On the contrary, the decreasing trend of PET mostly revealed at November, June, October, December, monthly temporal scale and Autumn annual temporal scale for each of which the number of the concerned meteorological stations ranges between 2 and 3. Figure 5.3 shows a quantitative overview related to the number of the meteorological stations interested or not in any trend. As can be seen, for each analysed temporal scale, if mean values are considered with respect to the whole of 46 meteorological stations: *i*) about 39 stations have not highlighted trend, with a peak at March monthly scale with all 46 meteorological stations involved; *ii*) about 6 stations recorded an increasing trend of PET, with a peak at August monthly scale having 18 stations involved; *iii*) only 1 meteorological station recorded a decreasing trend, with a peak equal to 3 at November monthly scale.

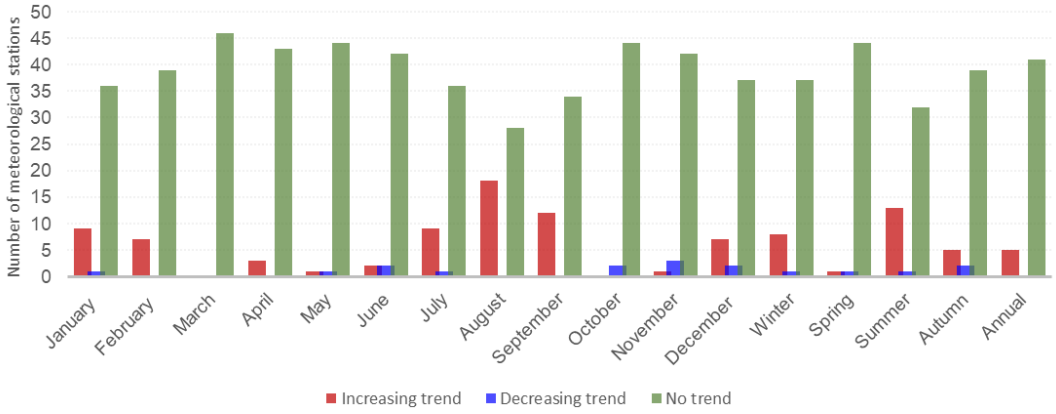

Figure 5. 3 Summary of the trend of PET in different temporal scale

Sen's slope (the PET trend magintiude)

The magnitude of PET trend in all 46 meteorological stations was also investigated.The results show that there was different magnitude of the PET trend in different meteorolgical stations. On one side, the highest increasing of PET trend is recorded at the annual temporal scale for three stations located just up the northern and eastern sicilian coastline, namely the stations 228, 258 and 261 with 10.68mm, 5.15mm and 4.96 mm per year, respectively. On the other side, the highest decreasing of PET trend is recorded for the meteorological station 231, situated on the western side of Mt. Etna, at both Summer seasonal monthly temporal scale (3.28mm) and at July monthly temporal scale (1.82 mm). Additionally, the Spring seasonal trend of station 230, another meteorological stations located at foot of Mt. Etna, showed the third highest decreasing trend with 1.67 mm in the last 21 years (Table 5.3).

Table 5. 3: The Sen's Slope result in mm.

Code	Name	Jan	Feb	Mar	Apr	May	Jun	Jul	Aug	Sep	Oct	Nov	Dec	Win	Spr	Sum	Aut	Ann
203	Aragona													0.63				
209	Licata	0.64						1.35	1.59					2.07				
212	Ribera						0.53	1.01	1.19	0.61								
214	Caltanissetta																	
215	Delia																	
218	Mazzarino	0.36								0.8						2.47	1.44	
219	Mussomeli								1.33				0.57					
224	Bronte	0.34			0.7				0.87							1.89		
227	Caltagirone		0.37										0.26	0.85				3.36
228	Catania		0.8														2.11	10.68
229	Riposto		0.54															
230	Linguaglossa					-1.37							0.63		-1.67			
231	Maletto						-1.24	-1.82								-3.28		
232	Mazzarrone								0.74					1.19				
233	Mineo					0.88	0.86	1.33	1.12	0.84			0.24	0.51		3.13		
234	Paternò									0.73		0.39					1.45	
235	Pedara										-0.62						-1.11	
237	Randazzo																	
238	Enna								1.58							3.42		
241	Nicosia				0.84					0.74								
249	S. Pier Niceto																	
254	Naso						-0.62											
256	Novara di Sicilia																	
258	Pettineo	0.72	0.62					0.67	1.04					1.75		2.14		5.15
261	Torregrotta							0.6	1.02	0.82						1.79	1.01	4.96
262	Alia				0.98							-0.5		1.01				
264	Camporeale	0.28								0.61			0.43					
265	Castelbuono	0.48																
269	Gangi								1.73	0.88								
273	Mezzojuso												-0.47				-1.51	
274	Misilmeri							0.66	0.78							1.53		
276	Palermo	0.61	0.79						0.8						1.41	1.69		
277	Partinico	0.56	0.68						1.27	0.82			0.44			2.77	1.73	
279	Polizzi Generosa																	
222	Sclafani Bagni		0.6						1.43							2.46		
281	Termini Imerese							0.75								2.19		
282	Acate										-0.49							
283	Comiso							0.96	1.24							2.53		
286	Ragusa																	
287	Santa Croce Camerina	-0.41							0.77			-0.37	-0.39	-0.83				
288	Scicli																	
289	Augusta									0.45								
291	Francofonte									0.82			0.48	1.6		2.78		6.45
301	Castellammare del Golfo											-0.3						
302	Castelvetrano	0.48						0.67	1.04	0.62								
305	Mazara del Vallo								1.33									
Max		0.72	0.8		0.98	0.88	0.86	1.35	1.73	0.88	-0.49	0.39	0.63	2.07	1.41	3.42	2.11	10.68
Min		-0.41	0.37		0.7	-1.37	-1.24	-1.82	0.74	0.45	-0.62	-0.5	-0.47	-0.83	-1.67	-3.28	-1.51	3.36
Average		0.36	0.62		0.84	-0.25	-0.14	0.47	1.17	0.72	-0.56	-0.15	0.21	0.91	-0.13	1.73	0.64	6.38

Spatial distribution of the PET trend

In order to further provide a detailed framework, a spatial distribution analysis on PET trends was also carried out. Therefore, monthly, seasonal, and annual trends of PET in Sicily, over the last 21 years, were represented using GIS application, and then reported in Figure 5.4.

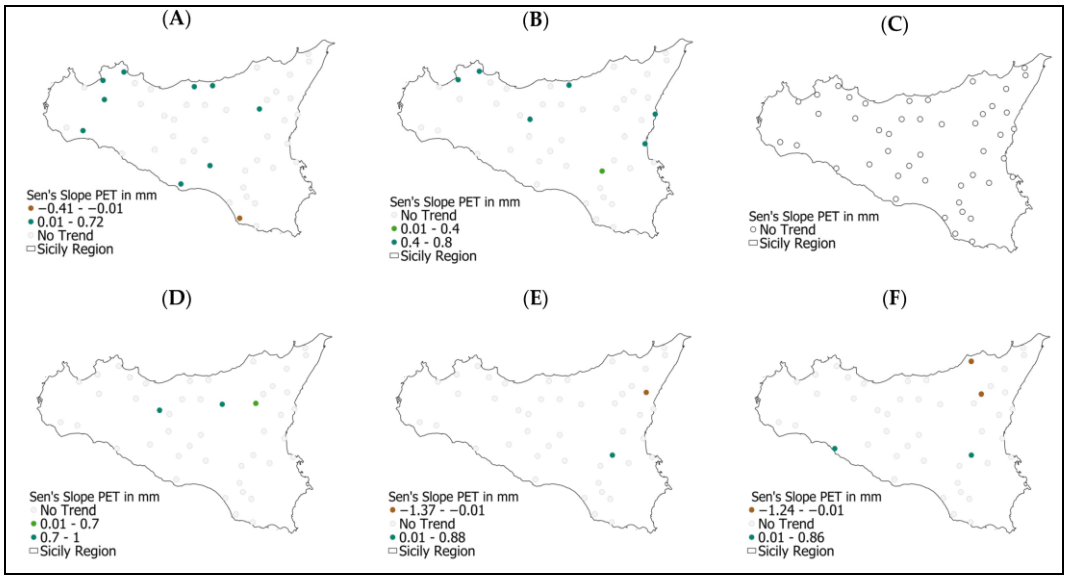
(A)
Sen's Slope PET in mm
−0.41 - −0.01
0.01 - 0.72
No Trend
Sicily Region
(B)
Sen's Slope PET in mm
No Trend
0.01 - 0.4
0.4 - 0.8
Sicily Region
(C)
Sen's Slope PET in mm
No Trend
Sicily Region
(D)
Sen's Slope PET in mm
No Trend
0.01 - 0.7
0.7 - 1
Sicily Region
(E)
Sen's Slope PET in mm
−1.37 - −0.01
No Trend
0.01 - 0.88
Sicily Region
(F)
Sen's Slope PET in mm
−1.24 - −0.01
No Trend
0.01 - 0.86
Sicily Region

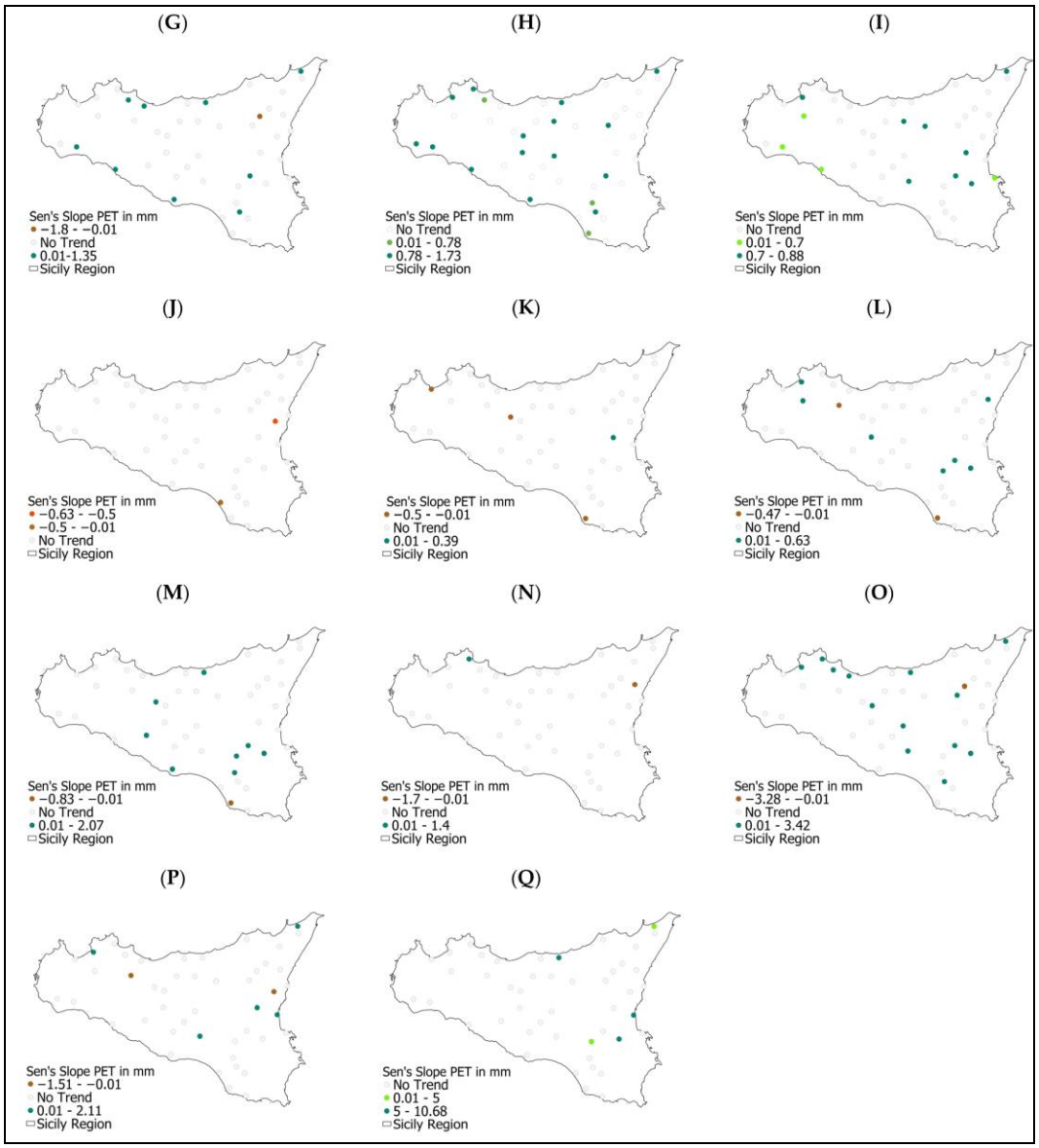

Figure 5. 4 Map of the spatial distribution of the PET trend over the Sicily in January (A), February (B), March (C), April (D), May (E), June (F), July (G), August (H), September (I), October (J), November (K), December (L), Winter (M), Spring (N), Summer (O), Autumn (P) and Annual (Q)

Monthly Spatial Trend

Overall, the spatial distribution of PET trends, either positive or negative, does not highlight a specific tendency. Looking at the distributions from January to June monthly temporal scale, indeed, increasing trends of PET are prevalent, and involve maximum nine meteorological stations distributed fairly evenly within the island (January), and minimum one meteorological station (May). Furthermore, it should

be noted that at March monthly scale there is no trend, as previously noted. Going more into the details, *i*) at January monthly scale nine stations are interested by an increasing of PET trend (Figure 5.4A) ranging between 0.72 mm and 0.28 mm, and only one station in the southern island shows a decreasing trend equal to 0.41 mm; *ii*) at February monthly scale (Figure 5.4B) only increasing trends of PET are observed in correspondence of seven meteorological stations distributed in the northern and eastern side of Sicily; *iii*) at April monthly scale (Figure 5.4D) just three meteorological station are characterized by PET trend, namely an increasing trend ranging from 0.7 mm to 0.98 mm; *iv*) on May monthly scale (Figure 5.4E) only one station presents an increasing trend (0.88 mm), and only another one presents aa decreasing trend (1.37 mm), both station placed in the eastern side of Sicily; *v*) at June monthly scale (Figure 5.4F) four meteorological stations present PET trend, specifically two of them in the east-northern a decreasing trend (1.24 mm and 0.62 mm), while the other two in the centre of the island present an increasing trend (0.53 mm and 0.86 mm).

If the spatial trends' distribution is analysed at July, August, and September monthly scale, a general rise of the meteorological stations having PET trends may be observed. More specifically, with the exception of station 231 characterized by the second highest decreasing trend at the July monthly scale (Figure 5.4G), all of the remaining present increasing PET trends ranging from 0.6 mm and 1.73 mm, and are distributed within the surroundings of the coastlines, for the most. Particular attention should be paid to the August monthly scale, at which increasing PET trends are detected in in 18 meteorological stations (39%) distributed all over the region.

Finally, moving from October to December monthly scale, a general decrease in the meteorological stations presenting PET trends can be observed. Specifically, *i*) at October monthly scale (Figure 5.4J) only two meteorological stations located in the eastern and southern side of Sicily, respectively, detected trends which are both decreasing (0.62 mm and 0.49 mm); *ii*) at November monthly scale (Figure 5.4K), of the four meteorological stations involved in trends, three of them, distributed from the north-western to the southern island, present decreasing trend (0.5 mm, 0.37 mm, 0.3 mm), while only one station on the eastern side is characterized by an increasing PET trend (0.93 mm); *iii*) at December monthly scale (Figure 5.4L), seven meteorological stations, scattered through the island, detected increasing trends of PET ranging from 0.24 mm to 0.57 mm, while two other stations on the north-western and southern island detected decreasing trends of PET with 0.47 and 0.39 mm.

The stacked bar chart reported in Figure 5.5 summarizes, for each meteorological station and for each monthly scale, the magnitude of the detected PET trends. As can be seen, station 233 which is located on the south-eastern side of Sicily,

recorded the highest number of PET trends (i.e., all increasing trends ranging from 2.11 mm and 2.95 mm) at the monthly scale, namely from June to September, and December.

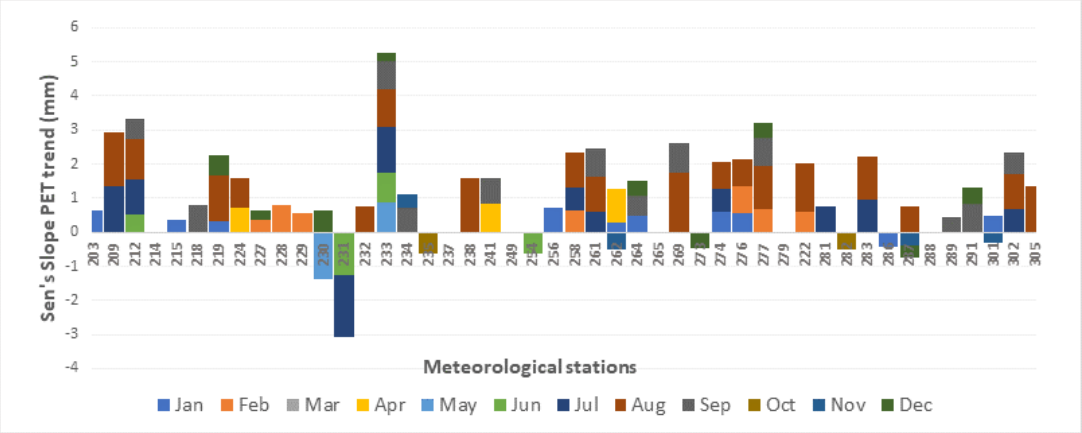

Figure 5. 5 The monthly trend Sen's slope magnitude of PET in mm in all analysed meteorological stations

Seasonal and Annual Spatial Trend

As previously mentioned, the spatial distribution analysis of PET trends was also carried out at the seasonal scale (Figure 5.4M-P), and at the annual scale (Figure 5.4Q). Results highlighted that at Summer seasonal scale, among 14 meteorological stations involved in increasing PET trends ranging from 1.53 mm to 3.42 mm, only station 231 detected a decreasing trend with the highest recorded value equal to 3.28 mm. On the contrary, at Spring seasonal scale only two meteorological stations in the northern of the region highlighted PET trends, namely an increasing (1.41 mm) one, and a decreasing one (1.67 mm). Regarding instead, the Winter and Autumn seasonal scales, nine and seven meteorological stations, respectively, detected PET trends with no a specific spatial distribution within the island.

Lastly, in the annual scale is analysed, only five meteorological stations, located from the north-eastern side of Sicily to the east-coast, are characterized by increasing trends of PET, ranging from 3.36 mm (station 227) to 10.68 mm (station 228), that represents the highest trend in the region in the last 21 years. The stacked bar chart reported in Figure 5.6 summarizes, for each meteorological station and for each seasonal and annual scale, the magnitude of the detected PET trends.

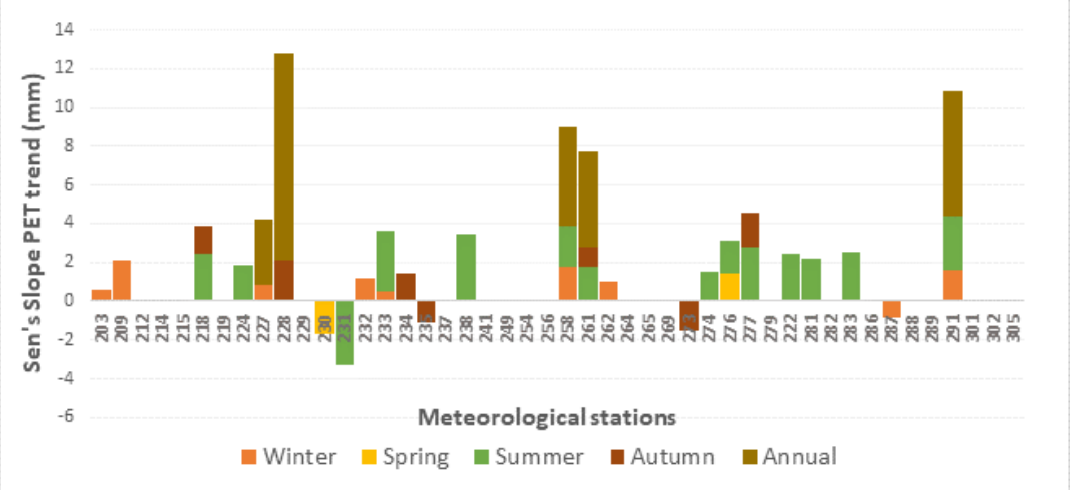

Figure 5. 6: The seasonal and annual trend Sen's slope magnitude of PET in mm in different meteorological stations

5.5 Discussion

The temporal trend of PET

As revealed by literature, the analysis of PET trends was carried out for other several regions belonging and distributed throughout Italy. Therefore, the results of our study were compared with those obtained for other regions inside out Italy. In norther Italy, for instance, it was observed an increasing of PET in the upper part of the Adda river catchment in the Central Italian Alps (Crespi et al., 2021; Ranzi et al., 2021); heading centre Italy, an increasing trend of reference evapotranspiration from 1951 to 2008 (Vergni & Todisco, 2011) was also detected, with specific reference to Spoleto meteorological station, that showed an increasing annual trend of PET through the Hargreaves and Samini estimation model (Todisco & Vergni, 2008), and the historical meteorological station of University of Bologna that highlighted an increase at all seasonal mean PET (for the 1972–2007 period), with an increase of 13 mm in Winter, 39 mm in Spring, 60 mm in Summer and 14 mm in Autumn (Vergni & Todisco, 2011). Coming to the South Italy, increasing of PET with related to increasing of temperature (Liuzzo et al., 2016) were observed. In more detail, the Apulia region is characterized by an annual PET trend equal to 18.6 mm was (Elferchichi et al., 2017), and particularly for the Apulian Tavoliere an increasing trend of evapotranspiration in 8mm per decade in 1957-2008 is recorded.

Beyond Italy, different parts of the world showed increasing trend of the annual PET trend. The IPPC 6th technical report, indeed, showed that there is an increase in evapotranspiration due to growing atmospheric water demand will decrease soil moisture over the Mediterranean region (Arias et al., 2021). In mor detail, the Mediterranean and the Iberian regions showed increasing trends of

evapotranspiration from 1971-2015 (Páscoa et al., 2021). This is also confirmed by to the recourse of different satellite sources trough which it was possible to detect increasing evapotranspiration trends in several Mediterranean regions, including the Sicily from 2009-2018 (Li et al., 2021). Moving forward, in Spain from 1922-2020, the evapotranspiration trend showed increasing trend and resulted for worsening the growth of crop water requirements (Li et al., 2021), as well as in the semi-arid part of Spain which presented an annual increasing trend from (1970–2000) and confirmed the future projection also will be increased (Ruiz-AÍvarez et al., 2021). Surprisingly, a monthly study revealed that June, the month with the biggest relative changes, is primarily responsible for guiding Summer trends and Spring trends, respectively (Tomas-Burguera et al., 2021). This study's findings are likewise in line with ours, according to which the majority of meteorological stations saw an upward trend over the Spring and Summer seasons (Figure 5.3). Moving out onto a broader view, increase in annual (0.009–0.026 mm/year) and seasonal (0.014–0.027 mm/year during southwest monsoon and 0.015–0.074 during northeast monsoon) ETo in peninsular Malaysia (Hadi et al., 2020) was observed, as well as in the most part of the Wei River basin (WRB) (Zuo et al., 2012), north-eastern China, in the southern coastal region, and the north-western corner of China (Yang et al., 2021), in 90% of Moldova from 1981–2012 (Piticar et al., 2016), in South Korea (Hwang et al., 2020), and in the centre and south part of Mongolia (Yu et al., 2016).

Concluding, if the evapotranspiration paradox is taken into account (Hadi et al., 2020; Liuzzo et al., 2016; Shan et al., 2015; Vicente-Serrano et al., 2014; Zhao et al., 2018), our study on Sicily island shows that it was observed at monthly Winter, Spring, Summer, and Autumn seasonal trend on our study (Table 5.2). Similarly, in the Calabria region, an analysis carried out using the Hargreaves and Samani estimation model for PET showed a decreasing trend in different Winter, Spring, Summer, and Autumn seasons and dry and wet seasons (Capra et al., 2013). In south-eastern Umbria, Central Italy in two areas asymmetric warming results in a decreasing evapotranspiration level (Todisco & Vergni, 2008). Moreover, our study confirmed that there was a decreasing trend of PET in January, May, June, July, October, November, and December monthly seasons. Likewise, the Calabria meteorological station analysis showed decreasing trend in all months (Capra et al., 2013).

5.6 Conclusions

Understanding trends of evapotranspiration is crucial for water resources management, irrigation, and the implementation of climate change adaptation measures. This study aimed at analysing trends of PET in Sicily (southern Italy) over the last 21 years using the hydro-meteorological data provided by 46 meteorological stations distributed all over the region. PET has been estimated by the FAO Penman-Monteith method, and the Mann Kendall test as well as the Sen's Slope estimator were used to identify the trends over time. The results showed that there were significant monthly, seasonal, and annual trends in different stations. August is the month where the majority of temporal trends were detected (18 out of 46 stations). On the other hand, for March not trend has been detected. Regarding the seasonal temporal scale, Summer season showed the highest number of stations with significant trends (14 stations) and Winter season was the one with lowest number of significant trends (only 2 stations). For 5 locations an increasing trend has been identified at the annual time scale. August corresponds to the highest increasing PET trend with 1.73 mm per year at one meteorological station. Regarding the seasonal temporal trend, meteorological station 238 had the highest increasing trend, with 3.42 mm/year in the Summer season. Finally, the highest estimated increasing trend of annual PET is of 10.68 mm/year. Overall, the analysis showed that there is increasing trend in some parts of Sicily Island. This is key information for future agricultural irrigation practices and a call for the implementation of climate change adaptation measures. As a further development of this study, geostatistical techniques will be applied to spatialize the information derived for single locations.

Chapter 6

Modelling stormwater runoff changes induced by ground-mounted photovoltaic solar parks: a conceptualization in EPA-SWMM

Abstract

A modelling framework for the simulation of stormwater runoff in ground-mounted photovoltaic solar parks is proposed. Elements in the solar park and their mutual interactions during precipitation events are conceptualized in EPA-SWMM. We demonstrate the potential of the framework by exploring how different factors influence runoff formation. Specifically, we carry out simulations for different sizes of the installation, soil types and input hyetographs. We also show the effect of ground cover, by changing the surface roughness. Outflow discharge from the park is compared to that from a reference catchment to evaluate variations of peak flow and runoff volume. Results highlight no practical changes in runoff in the short term after installation. However, in the long term, modifications in soil cover may lead to some potential increase of runoff. For instance, increments of the peak flow from the solar park up to 21% and 35% are obtained for roughness coefficient reductions of 10% and 20%, respectively. The proposed modelling approach can be beneficial for studying hydrological impacts of solar parks and thus for planning measures for their mitigation.

Keywords: Environmental impacts; Renewable energy; Sustainable water resources management; peak flow; EPA-SWMM.

6.1 Introduction

The continuous growth of global population causes increasing concerns on food, water, and energy sectors (Sarkodie and Owusu, 2020; Makaronidou, 2020). The energy generation processes are facing major challenges such as sustainability, cost, security, and market price fluctuations (Almomani, 2020; Ebhota and Jen, 2020). In addition, the increase in environmental awareness and the application of more stringent discharge regulations has directed the scientific community to work on developing alternative, sustainable, and renewable energy sources (Ahmad et al., 2020; Tawalbeh et al., 2021; Yavari et al., 2022; Bertsiou and Baltas, 2022; Loucks, 2023).

Among all the renewable energy sources, solar photovoltaic (PV) is one of the most widespread in the world (Ravi et al., 2014; Armstrong et al., 2016; Barron-Gafford et al., 2016; Hassanpour et al., 2018). Although solar energy is universally recognised as environmentally friendly energy source, impacts on surface hydrology of large parks have not been comprehensively addressed in literature (Turney and Fthenakis, 2011; Pisinaras et al., 2014; Yavari et al., 2022). With growing concern over the impact of land use changes on stormwater runoff, the construction of large-scale solar power plants may face obstacles in the future unless appropriate quantification of this impact is addressed and proper measures are taken to mitigate potential increment of flow peak and volume discharge (Turney and Fthenakis, 2011).

Assessment of runoff generation in PV solar parks can be carried out by modelling-based approaches, that have the advantage, with respect to purely experimental studies, to allow the investigation of the influence of different hydrological conditions (Yavari et al., 2022). For instance, among the studies based on such approach, Bernard at al. (2017) set up a 1D/2D model by coupling Flo-2D and HEC-HMS to simulate stormwater runoff at three selected solar PV installations in west Texas. However, no comparison with the pre-installation scenario has been carried out thus preventing the possibility to evaluate the impacts on stormwater runoff induced by the presence of solar panels. HEC-HMS was also used to study hydrologic dynamics in a Nevada solar farm (Edalat, 2017). The simulations showed that runoff volume always increases after solar panels installation.

However, one major limitation of this study was that solar panels were represented as an impervious surface on the ground, and simulation of the infiltration process could not be permitted under the panels, as it would indeed occur at an actual site. Thus, this approach likely overestimates runoff volume. The Soil & Water Assessment Tool (SWAT) was used for assessing the impact of PV solar parks on watershed hydrology by Pisinaras et al. (2014). Solar parks installation was represented by implementing in the model soil physical properties/ground cover changes, curve number increases associated with imperviousness, and reduced solar radiation. In this case, model limitations consist in the fact that the dynamics of the runoff formation in the solar park are not explicitly taken into account. Other researchers developed a custom-built model for representing runoff in solar parks (Cook and McCuen, 2013). The results indicated that the addition of solar panels over a grassy field does not change the volume of runoff, the peak discharge, nor time to peak. More recently, Wang and Gao (2023) conducted experiments at the plot-scale to investigate impacts of PV panels on rainfall-runoff and soil erosion processes. Results showed that runoff volume, peak flow discharge rate and overland flow velocity are not remarkably impacted by the presence of PV panels. However, further investigations are needed to transfer the obtained results at the plot scale to a real scale solar park.

Analysis of the literature on the topic highlights a research gap consisting in the lack of a comprehensive tool for the assessment of the impacts of real-scale solar parks on stormwater runoff, by taking into account the hydrological processes occurring within the park and all the variables affecting the park response to precipitation events. On this study, with the aim of overcoming many of the mentioned limitations within previous studies, we propose a novel conceptualization of PV power parks response to precipitation events capitalizing on the use of the free and open-source Storm Water Management Model (SWMM) (Rossman, 2015). The conceptualization allows to take into account the complex hydrological process occurring in the solar parks during precipitation events and to assess how the process of runoff in the park is affected by the extension of the PV installation, soil properties and the characteristics of the rainfall events. Moreover, effects of long term changes in roughness surface induced by the presence of the panels can be taken into account in the analysis. We demonstrate the potentialities of the proposed approach considering a layout of the PV installation (panels size and inclination) as well as characteristics of the precipitation events that are encountered in Sicily (south Italy).

6.2 Conceptual model

6.2.1. Water paths in ground-mounted PV solar parks

Panels in ground-mounted PV solar parks are usually placed on a metal frame that is mounted on the ground to hold the panels at a fixed angle. The frame usually can hold more than one panel rows (usually from 2 to 4) in the vertical direction (Figure 6.1a). Panels on the metal frame are then arranged in rows of different length (Figure 6.1b). Panels rows are separated by corridors to allow for maintenance operations as well as the movement of vehicles.

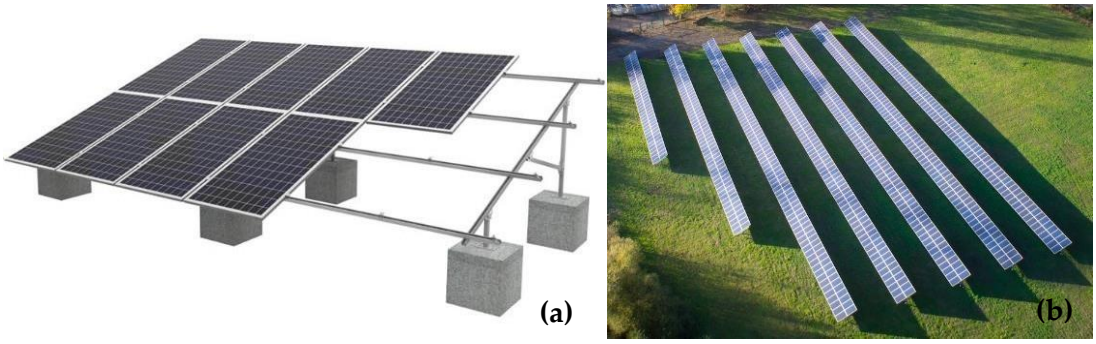

Figure 6. 1. (a) metal frame to hold panels and (b) panels arranged in rows in typical ground-mounted solar PV parks.

The presence of the panels rows in the solar park induces a redistribution of the rainfall approaching the ground as compared to the pre-installation scenario. Based on the input/output during precipitation events, three different parts of the PV installation can be distinguished: the panel area, the under-panel area and the corridor (Figure 6.2a). The water fallen on the impervious panels surface is rapidly drained towards the corridor immediately downstream the panels row. In this way, each corridor receives both direct rainfall and the runoff from the impervious surface of the panel. The under-panel area, instead, is not directly reached by the rainfall but it can receive the runoff from the upstream corridor and let the water infiltrate. Runoff from the under-panel area is collected by the corridor immediately downstream the panels row.

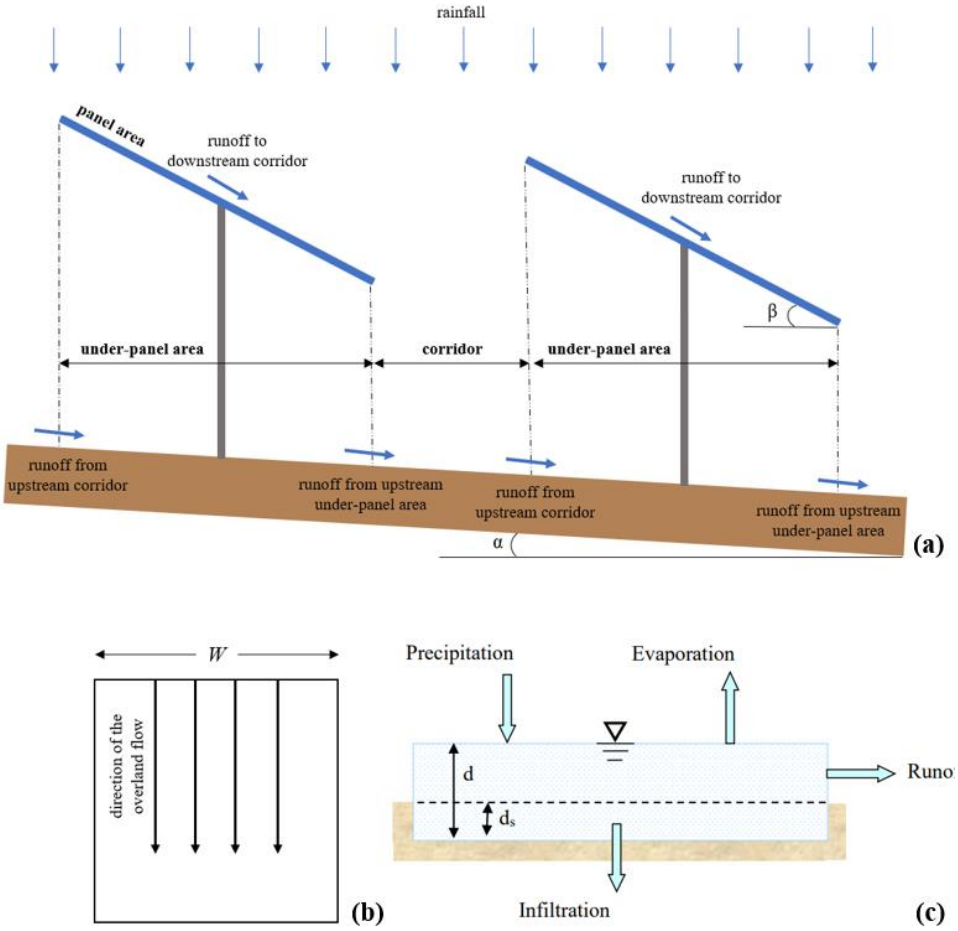

Figure 6. 2. (a) water paths in typical ground-mounted solar PV parks, (b) subcatchment conceptualization and (c) scheme of the nonlinear reservoir model in EPA-SWMM.

Water infiltration occurs both in the under-panel area and in the corridor. However, the corridor is likely to reach saturated conditions earlier as compared to the under-panel area because of the concentration of three different contributions (rainfall, runoff from panel area, runoff from the upstream under-panel area).

It is worth noting that in the adopted scheme for water paths showed in Figure 6.2a, the same flow direction is assumed for the ground and for the panels rows. Actually, direction of the PV panels is generally set with the aim to maximize the exposure of the panels to solar radiation, regardless of the ground slope direction. In case of different flow directions for the ground and for the panels rows, water paths within

the PV installation are not the same of those described in this section and have to be investigated case by case. As an example, if panels rows and are placed along the main ground flow direction, runoff from the corridors would not be routed to the under-panel areas, thus, practically, reducing the available areas for infiltration within the park.

6. 2.2. Modelling ground mounted PV solar parks with EPA-SWMM

The Storm Water Management Model (SWMM) is a free and open-source software developed by the United States Environmental Protection Agency (US-EPA). The release n. 5.1 of the software was used in this study (Rossman, 2015).

SWMM is a dynamic rainfall-runoff model used for single event or continuous simulation. The software is widely used in literature and was recently applied for estimation of runoff from urban areas also in presence of low impact development (Ferrans and Temprano, 2022; Hashemi and Mahjouri, 2022; Nazari et al., 2023; Zhuang and Lu, 2023) and for optimization problems in water distribution systems (Gullotta et al., 2021a; 2021b). The runoff component of SWMM operates on a collection of subcatchment areas that receive precipitation and generate runoff, after computation of water losses. The software conceptualizes subcatchments as rectangular surfaces with uniform slope S and width W [m] (Figure 6.2b). Overland flow is generated by modelling the subcatchment as a nonlinear reservoir (Chen and Shubinski, 1971), as sketched in Figure 6.2c.

In particular, the subcatchment experiences inflow from precipitation and losses from evaporation and infiltration. The net difference ponds on the subcatchment surface with a depth d [m] (Figure 6.2c). A part of the ponded depth, ds [m], can fill the depression storage, while the remaining part (d-ds) become runoff outflow q. From conservation of mass, the net change in depth d per unit of time t can be expressed as (Rossman, 2016):

$$\frac{\partial d}{\partial t} = i - e - f - q \qquad (1)$$

where i, e, f and q are the flow rates per unit of area [$m^3/s/m^2$] for precipitation,

evaporation, infiltration and runoff, respectively.

Flow rate is calculated by using the Manning equation for an open rectangular channel of width W, slope S and a given roughness coefficient n [s/m1/3]. Infiltration losses can be computed within the software by using different infiltration models. For the conceptualization proposed in this study, Green Ampt method is used to model infiltration in pervious subcatchments (Green and Ampt, 1911). Water losses for evaporation are not taken into account in this work since only simulations of single events have been carried out so that evaporation process can be neglected.

In order to reproduce water paths described at section 6.2.1, panel areas, under-panel areas and corridors are modelled in EPA-SWMM as rectangular subcatchments (placed in series) with different input/output settings. In particular, precipitation input is set up for subcatchments representing panel areas and corridors but not for those representing under-panel areas. Moreover, runoff from each subcatchment is discharged to downstream subcatchments according to the flow paths showed in Figure 6.2 (i.e., panel area to corridor, corridor to under-panel area and under-panel area to corridor). Runoff from the most downstream subcatchment is assumed to be the outflow from the solar park. Finally, infiltration is allowed for all the subcatchments except for those representing panel areas.

6.3. Modelling scheme

6.3.1. PV power plant hydrological characteristics

For the demonstration carried out in this study, we have considered the following characteristics of the subcatchments. Panel areas in the PV park are modelled as totally impervious subcatchments with inclination $\beta=30°$ to the horizontal (Figure 6.2a). This inclination is common for PV installations at the latitude of south Italy. A metal frame holding 2 panels in the vertical direction is supposed, with single panel having a length of 2.38 m and a width of 1.3 m, which are within typical dimensions for industrial panels used in solar parks. Panels' surface is usually made

of very smooth glass; therefore, n=0.007 is associated to subcatchments representing panel areas. Corridors and under-panel areas are modelled as totally pervious subcatchments. Length of corridors is usually optimized to minimize shadows effects between two panels rows. However, a minimum distance (range 2.5-3 m) between two panels rows has to be guaranteed to allow for the safe moving of maintenance vehicles. In the model, a length of 2.7 m is associated to the corridors, while the length of the under-panel areas can be derived projecting the length of 2 panels to the horizontal (i.e., 4.12 m). Ground slope in the solar park is set equal to 1% (Palmer et al., 2019).

Besides, a reference catchment with the same extension of the park is modelled. In order to maintain the same modelling scale and enable comparison, the reference catchment is divided in subcatchments equivalent to the corridors and the under-panel areas (same area and ground slope). In this case, all the subcatchments in the reference have the precipitation input and allow for infiltration. Moreover, each of these subcatchments discharges its runoff to the subcatchment immediately downstream. Runoff from the most downstream subcatchment is assumed to be the outflow from the reference catchment and used for comparison with runoff from the solar park. Ground cover for the reference catchment is assumed to be grass, by setting a roughness Manning coefficient n=0.15 (McCuen et al., 1996).

Since, as already stated, we are assuming that direction of flow coincides with the slope of the panels, all terms in Eq. (6.1) are linear functions of the subcatchment width W and therefore all simulations are carried out by setting W=1 m for all the subcatchments in the PV solar park and in the reference catchment. Results obtained (in terms of runoff per unit of width) can then be scaled for any size of the solar park by simply multiplying for the actual width of the installation.

Single events simulations are run in EPA-SWMM setting a time step of 1 seconds. In the following sections, variables and parameters potentially affecting the runoff from the PV solar park are discussed.

PV configurations

Simulations have been carried out considering three different configurations of the solar park. In particular, sequences of 10, 20 and 40 panels rows are modelled to represent small, medium and large PV installations, respectively. The three selected extensions (extension 1, 2 and 3 hereafter) correspond to total areas per unit of width of the installation of about 70, 135 and 270 square meters.

Soil type

To test the impacts of soil texture on runoff from solar parks, simulations have been performed for three different soil types. In particular, Green Ampt infiltration parameters for loamy sand, clay loam and silty clay soil type (soil type A, B and C hereafter) have been associated to subcatchments in the software, thus going from more pervious to less pervious soil (Rawls et al., 1983). In each simulation, the same soil type is assumed for the solar park and the reference catchment.

Fraction of soil porosity that is initially dry (i.e., initial deficit) has to be specified in the software. Initial deficit equal to zero is representative of saturated conditions. An initial deficit equal to the difference between the soil porosity (saturated soil) and the field capacity has been set up. The chosen initial condition for soil moisture is typical of soils in the winter season at the beginning of a precipitation event with a sufficient antecedent dry weather period.

Storm characteristics

Precipitation events given as input for the simulations are derived from the Depth-Duration-Frequency (DDF) curves of the rain gage of Agira in Sicily (south Italy). The values of parameters for the Depth-Duration-Frequency (DDF) curves, expressed in the power-law form $h=at^n$, from the selected rain gauge correspond to the median of 139 stations in Sicily (Failla, 2022). Here, h represents the rainfall depth; a is a constant that depends on the specific location or dataset; t represents the duration of the rainfall event; n is an exponent that also depends on the specific location or dataset. Events of 5, 20 and 50-years return period (RP) are simulated.

Parameters a of the DDF curves are equal to 34.72, 49.02 and 58.09 for RP of 5, 20 and 50 years, respectively, while corresponding exponents n are equal to 0.339, 0.354 and 0.360.

Besides magnitude, influence of duration and temporal distribution of the precipitation event is investigated. First, constant intensity rainfall events with duration of 10 minutes, 1 hour and 3 hours and rainfall intensity derived from the DDF curves are given as input to the model. Then, hyetographs of 1 and 3 hours durations derived from the Chicago method (Keifer and Chu, 1957) are considered. For the construction of the Chicago hyetographs, a time step of 10 minutes is adopted and the highest peak of precipitation height is placed almost in the middle (3rd time step for the 1-hour hyetograph and 9th time step for the 3-hour hyetograph). When deriving precipitation heights for sub-hourly durations, exponent of the DDF curve is changed in 0.5 (Engman and Hershfield, 1981).

Ground cover

Different ground covers have been assumed, related to short and long term conditions after PV installation. In the short term after installation of the PV park, no significant changes in ground cover are expected with the respect to the pre-installation scenario. In the long term, operation of the PV solar parks involves the use of maintenance vehicles that could affect the soil properties in the area between panel rows - in terms of compaction and reduced hydraulic conductivity (Pisinaras et al., 2014; Choi et al. 2020). Moreover, the area under the panel rows may experience, in time, a lower vegetation growth rate as compared to the space between rows because of the reduced amount of photosynthetic active radiation (Armstrong et al., 2016; Jahanfar et al., 2019). Hence, changes in surface roughness are taken into account here. In particular, the presence of the panels rows together with the maintenance activities of the park usually lead to a reduction of the surface roughness. Therefore, simulations have been run by assuming the same roughness coefficient of the reference catchment for corridors and under-panel areas, thus allowing evaluation of the runoff from the park in the short term after installation

(short-term condition). Secondly, progressive reduction (by 10% and 20%) of the original roughness coefficient is supposed for corridors and under-panel areas in order to evaluate the impacts on runoff of long term changes in surface roughness induced by the presence of the solar park (long-term condition).

6.4. Results and discussion

A total of 135 simulations have been run for the short-term condition by combining all the model parameters and precipitation inputs described in the methodological section.

Figures from 6.3 to 6.5 compares the outflows from the PV solar park and from the reference catchment as resulting from 9 simulations.

In order to assess the impact on runoff of the park extension, Figures 6.3a, 6.3b and 6.3c show outflows from parks of extension 1, 2 and 3, respectively, and soil type C. In the 3 simulations, the precipitation input is a Chicago hyetograph of 1 hour duration and 20-years RP.

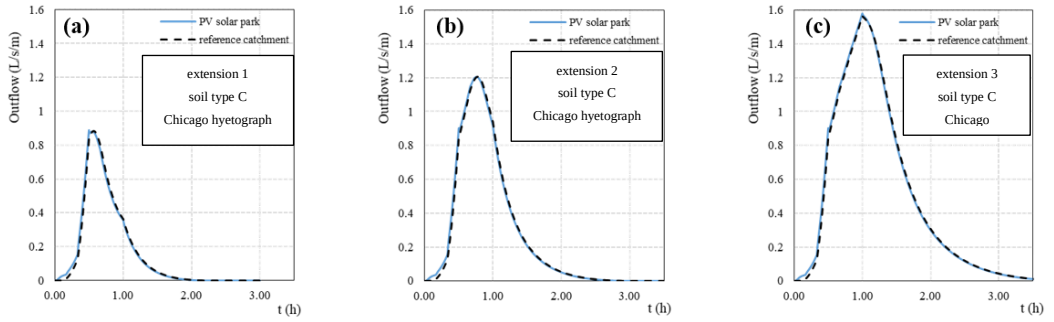

Figure 6. 3 Outflows from the PV solar park and from the reference catchment for different park extensions (short-term condition).

For fixed soil type and precipitation input, increments of the park extension result in increments of the peak flow and of the total runoff volume (Figures 6.3a, 6.3b and 6.3c). In particular, peak flow per unit of width increases by 33% each time the area of the solar park is doubled (from extension 1 to 2 and from extension 2 to 3), due to the non-linearity of the processes involved in the runoff formation. The outflow curve from the solar park follows the corresponding curve from the reference catchment both in the rising and in the recession limb of the hydrograph,

regardless of the park extension. Minimal differences between the two outflow curves can be observed at the beginning of the precipitation event (first 20 minutes), with values of the outflow from the solar park slightly higher than those from the reference catchment. Analysis of the simulations output allows to ascribe this behaviour to the most downstream part of the solar park. Indeed, the generic corridor in the solar park receives in input the direct rainfall and the runoff from the panel area. The two contributions are practically simultaneous as the time of concentration of the panel area is in the order of a few seconds. Therefore, for a given soil infiltration capacity, the corridor generates excess of runoff with the respect to the portion of the reference catchment placed at an equal distance from the outlet. This excess of runoff can be later infiltrated in downstream under-panel areas and corridors. However, the most downstream corridor delivers the runoff directly to the outlet thus anticipating the time for the beginning of the runoff as observed in Figures 6.3a, 6.3b and 6.3c.

Influence of the soil type on the runoff from the solar park is shown in Figures 6.4a, 6.4b and 6.4c, referring to simulations run for solar park of same extension (3) and precipitation input (Chicago hyetograph 3-hours duration, 50-years RP) but different soil type (A, B and C, respectively).

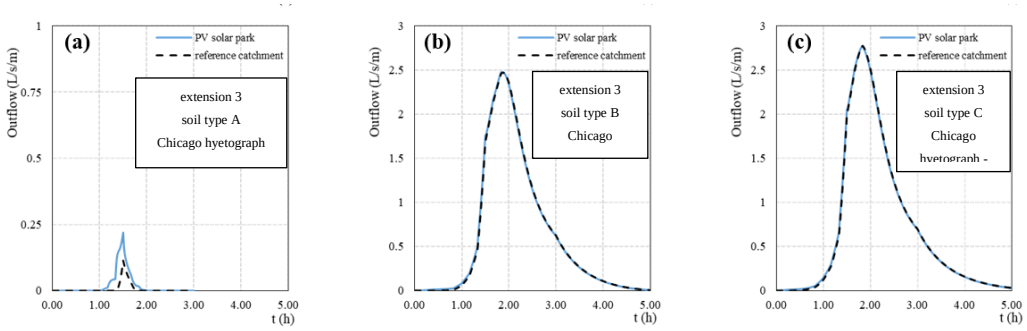

Figure 6. 4 Outflows from the PV solar park and from the reference catchment for different soil types (short-term condition).

For fixed solar park extension and precipitation input, changing from sandy to clay soils results in increased peaks flow and total runoff volumes, due to the reduction in infiltration capacity (Figures 6.4a, 6.4b and 6.4c). In particular, peaks flow from solar park results equal to 0.2, 2.5 and 2.8 L/s per unit of width for soil type A, B

and C, respectively. Peak flow and total runoff volume from the solar park are greater than the corresponding values from the reference catchment only for soil type A (Figure 6.4a). Indeed, in soil with high infiltration capacity, almost all the precipitation is infiltrated. In this case, excess of runoff from the corridor immediately upstream the outlet (with no other downstream under-panel areas and corridors available for infiltration) assumes a greater relative weight. However, the increment of peak flow and total runoff showed in Figure 6.4a is not significant in absolute terms (peak flow for unit of width less than 0.25 L/s). The same conclusion can be drawn for other simulations with soil type A in which differences in the outflows from the solar park and from the reference catchment are observed.

Finally, Figures 6.5a, 6.5b and 6.5c show outflows from solar parks of extension 2 and soil type C for constant precipitation input of durations 10 minutes, 1 hour and 3 hours, respectively, and 20-years RP.

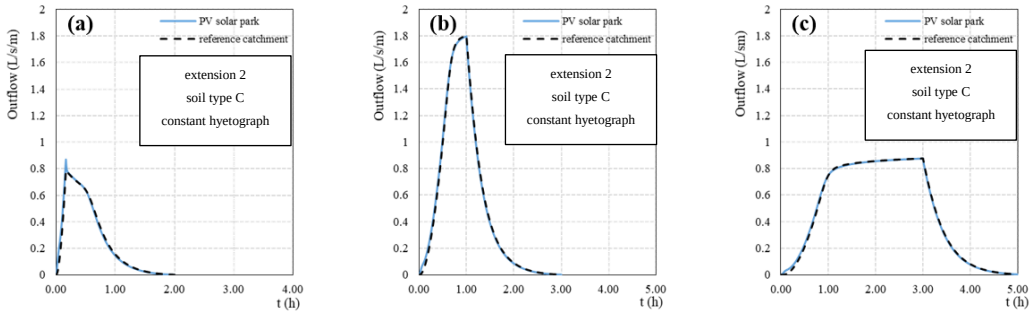

Figure 6. 5 Outflows from the PV solar park and from the reference catchment for different duration of the precipitation event (short-term condition).

For fixed solar park extension and soil type, outflow from the solar park is equal to that from the reference catchment (in terms of peak flow and total runoff volume) regardless of the duration of the precipitation event as shown in Figures 6.5a, 6.5b and 6.5c.

Temporal distribution of the rainfall does not influence the aggravation of outflow from the solar park as compared to the reference catchment. Indeed, Figures 6.3b and 6.7b report results of simulations carried out for parks of same extension and soil type, in which the 1-hour, 20-years RP precipitation event is given as input in the form of a Chicago hyetograph (Figure 6.3b) or constant rainfall (Figure 6.5b).

In both cases, outflow curves from the solar park follow the corresponding curves from the reference catchment during the whole simulation.

Finally, simulations that differ only for the RP of the precipitation event also led to outflow curves from the solar park practically equal to those from the reference catchment, regardless of the magnitude of the event.

Globally, no significant increments of the peak flow and of the total runoff volume from the solar park as compared to the reference catchment were observed in all the 135 simulations for short-term condition. This result is in line with modelling and experimental findings of previous studies (Cook and McCuen, 2013; Wang and Gao, 2023).

To evaluate the effects of possible long-term changes in land cover induced by the presence of the PV installation, a reduction of the roughness surface is supposed for subcatchments representing corridors and under-panel areas in the model. In particular, the original Manning coefficient for those subcatchments is progressively reduced by 10% and 20% (i.e., n=0.135 and n=0.12, respectively). Figure 6.6 shows comparison between outflows from the PV solar park and from the reference catchment for 3 long-term condition simulations. Model parameters and precipitation inputs of the simulations related to Figures 6.6a, 6.6b and 6.6c are the same of those discussed for Figures 6.3b, 6.4b and 6.5a, respectively.

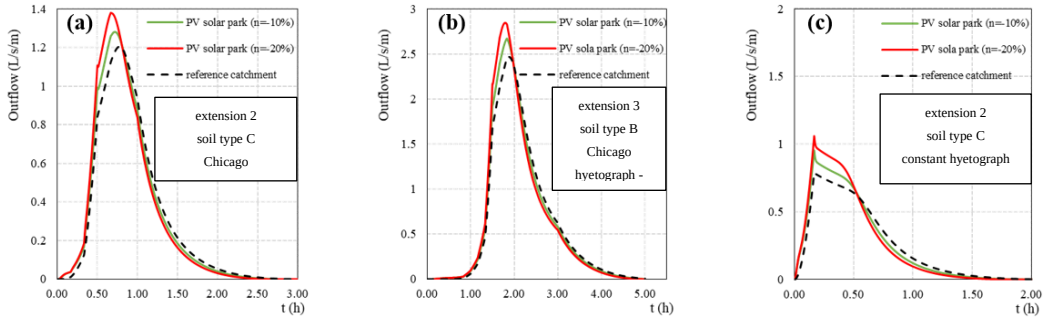

Figure 6. 6 Outflows from the PV solar park and from the reference catchment for different combinations of model parameters and precipitation inputs (long-term analysis).

In all the simulations, the reduction of the surface roughness surface in corridors and under-panel areas leads to increased peaks flow as compared to the short-term analysis. For the events analysed in Figure 6.6, a 10% reduction of the Manning

coefficient results in peak flow increases of about 6% (Figure 6.6a), 8% (Figure 6.6b) and 21% (Figure 6.6c). The percentage of peak flow increase is even greater if the Manning coefficient is reduced by 20% (15% increase for events in Figures 6.6a and 6.6b and 35% for event in Figure 6.6c).

The reduced roughness surface allows for a faster surface runoff from the upstream part of the solar park towards the outlet. Indeed, both the rising and the recession limb of the hydrograph from the solar park are anticipated with respect to those of the hydrograph from the reference catchment. Runoff velocity increases passing from a 10% to a 20% reduction of the Manning coefficient for all the events showed in Figure 6.6. Also this result is in agreement with simulation studies carried out by Cook and McCuen, 2013).

As a consequence of the increased runoff velocity, total runoff volumes from the solar park are greater than those from the reference catchment for all analysed events. Indeed, the potential of water infiltration is related to the ponding time above the subcatchment surface, which decreases as runoff velocity increases. For the events showed in Figure 6.6, runoff volumes from the solar park increase with respect to the reference catchment in the order of 1-3% for a 10% Manning coefficient reduction and in the order of 2-5% if the Manning coefficient is reduced by 20%.

6.5. Conclusion

This study applied a modelling framework for the simulation of stormwater runoff in ground-mounted photovoltaic solar parks is proposed. EPA-SWMM software is used in a novel way to model all the elements in the solar park and their mutual interactions during precipitation events.

The modelling exercise showed the potentialities of the proposed conceptualization. Specifically, by comparing outflow discharges from the park and from a reference catchment (pre-installation condition), the proposed approach was successful in simulating some of the main impacts of PV power plant realization on peak flow and total runoff volume. In particular, simulations were run considering 3 different sizes of the PV installation (small, medium, large), 3 different soil types and input

hyetographs of different return periods, shapes and durations. A first set of simulations have been run by assuming the same roughness surface for the solar park and the reference catchment (short-term condition). Then, the impacts of the presence of the panels rows (as well as of the maintenance activities) on the roughness surface have been considered. The proposed conceptualization allows to successfully simulate the spatial redistribution of the rainfall and infiltration fluxes due to the presence of the panel rows. The modelling exercise shows that when the surface roughness of the solar park is decreased, peak flow increases in the order of 6-35% as compared to the pre-installation scenario. Increased values (1-5%) of the total runoff volume are obtained as well.

The proposed modelling framework may be useful for operators in the field of photovoltaic for the evaluations of the outflow discharge from the solar park for different configurations of the installation, soil type and ground cover. The use of a free and open-source software adds value to the research and could represent a boost for the development and the improvement of the modelling framework as well as for a simple and wide diffusion of the results. Future availability of experimental data on runoff from solar park would help increasing the reliability of the obtained results; further investigations will also attempt to extend model applications at the watershed scale.

Future steps of the work may include the evaluation of other impacts on the ground cover induced by presence of the PV installation as well as the investigation of the solar park behaviour in long period simulations. Finally, other layouts of the PV installation should be considered in future works, especially those implying a reduction of the available area for infiltration within the park.

Chapter 7

Conclusions

This chapter presents the main findings of the study and suggests future work based on the results. The conclusions address the main objectives of the study and discuss the results in relation to the methods and analysis.

7.1 Main conclusions

The study confirmed that evapotranspiration trends showed an increasing and decreasing trend in monthly, seasonal, and annual trends for the last 20 years in Sicily. Specifically, in Piazza Armerina, Sicily, the reference evapotranspiration showed only a monthly decreasing trend, and different climatological variables also exhibited decreasing/increasing trends on a monthly and seasonal temporal scale for the last 17 years. This supports that the results of this thesis and other studies indicate climate change in Sicily. It necessitates climate change mitigation measures such as transitioning to solar energy to halt the emission of greenhouse gas to the atmosphere. However, this solar energy transition needs proper design, taking into account the potential impacts on local-scale hydrology, such as evapotranspiration and runoff. This study's results showed that the Priestley and Taylor (PT) and Hargreaves and Samani (HS) evapotranspiration estimation methods are best suited for monitoring the impacts of solar parks on evapotranspiration in Sicily. Moreover, there is no significant impact of solar parks on runoff in the Sicilian climate. Still, attention is needed regarding ground cover to minimize the potential increase in peak flow and volume of runoff.

The study figured out the following finding in this thesis:

- The Priestley and Taylor (PT) and Hargreaves and Samani (HS) evapotranspiration estimation methods were the first and second best-performing methods, which enable monitoring the potential impact of solar parks on evapotranspiration in Sicily.
- The trend of reference evapotranspiration (ETo) and climatological

elements in Piazza Armerina, Sicily, over a 17-year period analyze; specifically the ETo exhibited a downward trend of 0.790 mm per year in November, while no significant trend was observed in other months or on seasonal and annual time scales. Solar radiation (in November and Autumn) and rainfall (in Autumn) demonstrated a downward trend. On the other hand, the remaining meteorological variables (minimum temperature, maximum temperature, mean temperature, wind speed, and relative humidity) exhibited an upward trend both at monthly and seasonal scales in the study area. Among the variables, specific humidity and wind speed had the highest (44.59%) and lowest (0.9%) contribution rate to ETo trends in the study area, respectively.

- From 46 meteorological stations over the Sicily, 5 meteorological stations showed a significantly increasing trend of potential evapotranspiration (PET). However, there are many locations where the monthly trend is statistically significant. The number of locations where monthly trend is significant is maximum for August, where 18 out of these 46 stations have an increasing trend. In contrast in March there are no locations with significant trends.
- There were no practical changes in runoff in the short term after the installation of ground-mounted photovoltaic solar parks. However, in the long term, modifications in soil cover may lead to a potential increase in runoff.
- Moreover, in relation to the delay in installing instruments for monitoring the impact of PV, we were unable to support our study with long-term experiments. Perhaps future research will be more informative if they can conduct long-term experimental research.

7.2 Future research works

Beyond this thesis working, it still needs detailed investigation for further clarification and understanding. The following are the main themes that should be investigated in detail and require further clarification for better understanding in future works:

The study evaluated the evapotranspiration estimation method performance using the FO PM method. However, the FAO PM method has limitations in different climate systems. Thus, observation data (lysimeter) instruments will be more suitable for evaluating the performance of the evapotranspiration methods. Moreover, lysimeters will be more suitable for measuring evapotranspiration under the PV.

To understand the spatiotemporal trend of ETo and PET more precisely, it would be better to use long-term meteorological data. This could be more valuable and effective for climate change mitigation measures in Sicily and the Mediterranean climate.

When modeling the runoff induced by ground-mounted photovoltaic panels, it would be more precise to apply experiments instead of EPA SWMM simulations. Moreover, it still needs to simulate the impact of ground-mounted PV on runoff in relation to different land use and land cover scenarios and different climate systems. The PV's impacts on the local climate also need to be addressed using experimental analysis.

References

Abu-Taleb, A. A., Alawneh, A. J., & Smadi, M. M. (2007). Statistical analysis of recent changes in relative humidity in Jordan. *American Journal of Environmental Sciences*, *3*(2), 75–77. https://doi.org/10.3844/ajessp.2007.75.77

Ahmad, I., Tang, D., Wang, T., Wang, M., & Wagan, B. (2015). Precipitation trends over time using Mann-Kendall and spearman's Rho tests in swat river basin, Pakistan. *Advances in Meteorology*, *2015*. https://doi.org/10.1155/2015/431860

Ahmad, L., Khordehgah, N., Malinauskaite, J., & Jouhara, H. (2020). Recent advances and applications of solar photovoltaics and thermal technologies. *Energy*, 207. https://doi.org/10.1016/j.energy.2020.118254.

Aieb, A., Kadri, I., Lefsih, K., & Madani, K. (2022). Spatiotemporal trend analysis of runoff and actual evapotranspiration in Northern Algeria between 1901 and 2020. *Modeling Earth Systems and Environment*, *8*(4), 5251–5267. https://doi.org/10.1007/s40808-022-01453-z

Al-Sudani, H. I. Z. (2019). Derivation mathematical equations for future calculation of potential evapotranspiration in Iraq, a review of application of Thornthwaite evapotranspiration. Iraqi Journal of Science, 60(5), 1037-1048. https://doi.org/10.24996/ijs.2019.60.5.13

Alemu, H., Kaptué, A. T., Senay, G. B., Wimberly, M. C., & Henebry, G. M. (2015). Evapotranspiration in the Nile Basin: Identifying dynamics and drivers, 2002-2011. *Water (Switzerland)*, *7*(9), 4914–4931. https://doi.org/10.3390/w7094914

Alexandris, S., Stricevic, R., & Petkovic, S. (2008). Comparative analysis of reference evapotranspiration from the surface of rainfed grass in central Serbia, calculated by six empirical methods against the Penman-Monteith formula. *European Water*, 21(22), 17-28.

Allen, R. G., Pereira, L. S., Raes, D., & Smith, M. (1998). Crop evapotranspiration-

Guidelines for computing crop water requirements-FAO Irrigation and drainage paper 56. *FAO*, Rome, 300(9), D05109.

Almomani, F. (2020). Prediction of biogas production from chemically treated co-digested agricultural waste using artificial neural network. *Fuel*, 280, 118573. https://doi.org/10.1016/j.fuel.2020.118573.

Almorox, J., Senatore, A., Quej, V. H., & Mendicino, G. (2018). Worldwide assessment of the Penman–Monteith temperature approach for the estimation of monthly reference evapotranspiration. T*heoretical and applied climatology*, 131, 693-703. https://doi.org/10.1007/s00704-016-1996-2

Anapalli, S. S., Fisher, D. K., Reddy, K. N., Wagle, P., Gowda, P. H., & Sui, R. (2018). Quantifying soybean evapotranspiration using an eddy covariance approach. *Agricultural Water Management*, *209*(July), 228–239. https://doi.org/10.1016/j.agwat.2018.07.023

Antonopoulos, V. Z., & Antonopoulos, A. V. (2018). Evaluation of different methods to estimate monthly reference evapotranspiration in a Mediterranean area. *Water Utility Journal*, *18*(2002), 61–77.

Arias, P.A., N. Bellouin, E. Coppola, R.G. Jones, G. Krinner, J. Marotzke, V. Naik, M.D. Palmer, G.-K. Plattner, J. Rogelj, M. Rojas, J. Sillmann, T. Storelvmo, P.W. Thorne, B. Trewin, K. Achuta Rao, B. Adhikary, and K. Z. (2019). Foreword Technical and Preface. In *Climate Change and Land: an IPCC special report on climate change, desertification, land degradation, sustainable land management, food security, and greenhouse gas fluxes in terrestrial ecosystems*.IPCC.

Armstrong, A., Ostle, N.J. & Whitaker, J. (2016). Solar Park Microclimate and Vegetation Management Effects on Grassland Carbon Cycling. *Environmental Research Letters*, 11(7), 12. https://doi.org/10.1088/1748-9326/11/7/074016.

Aschale, T. M., Peres, D. J., Gullotta, A., Sciuto, G., & Cancelliere, A. (2023). Trend Analysis and Identification of the Meteorological Factors Influencing Reference Evapotranspiration. *Water*, *15*(3), 470. https://doi.org/10.3390/w15030470

Aschale, T. M., Sciuto, G., Peres, D. J., Gullotta, A., & Cancelliere, A. (2022). Evaluation of reference evapotranspiration estimation methods for the assessment of hydrological impacts of photovoltaic power plants in Mediterranean climates. *Water, 14(14),* 2268. https://doi.org/10.3390/w14142268.

Barnard, T., Agnaou, M. & Barbis, J. (2017). Two dimensional modeling to simulate stormwater flows at photovoltaic solar energy sites. *Journal of Water Management Modeling 2*5:C428. https://doi.org/10.14796/JWMM.C428

Barron-Gafford, G.A., Minor, R.L., Allen, N.A., Cronin, A.D., Brooks, A.E. & Pavao-Zuckerman, M.A. (2016). The Photovoltaic Heat Island Effect: Larger Solar Power Plants Increase Local Temperatures. *Scientific Reports,* 6, 35070. https://doi.org/10.1038/srep35070

Bian, Y., Dai, H., Zhang, Q., Yang, L., & Du, W. (2020). Spatial distribution of potential evapotranspiration trends in the Inner Mongolia Autonomous Region (1971–2016). *Theoretical and Applied Climatology*, *140*(3–4), 1161–1169. https://doi.org/10.1007/s00704-020-03154-y

Blain, G. C. (2014). Removing the influence of the serial correlation on the Mann-Kendall test. *Revista Brasileira de Meteorologia*, 29, 161-170. https://doi.org/10.1590/S0102-77862014000200002

Bonaccorso, B., Cancelliere, A., & Rossi, G. (2015). Probabilistic forecasting of drought class transitions in Sicily (Italy) using Standardized Precipitation Index and North Atlantic Oscillation Index. *Journal of Hydrology*, *526*, 136–150. https://doi.org/10.1016/j.jhydrol.2015.01.070

Borzì, I., Bonaccorso, B., & Aronica, G. T. (2020). The role of dem resolution and evapotranspiration assessment in modeling groundwater resources estimation: A case study in sicily. *Water (Switzerland)*, *12*(11), 1–15. https://doi.org/10.3390/w12112980

Bouklikha, A., Habi, M., Elouissi, A., & Hamoudi, S. (2021). Annual, seasonal and monthly rainfall trend analysis in the Tafna watershed, Algeria. *Applied Water Science,* 11, 1-21. https://doi.org/10.1007/s13201-021-01404-6

Brunetti, M., Buffoni, L., Maugeri, M., & Nanni, T. (2000). Trends in minimum and maximum daily temperatures in Italy from 1865 to 1996. *Theoretical and Applied Climatology*, *66*(1–2), 49–60. https://doi.org/10.1007/s007040070032

Buhairi, M. H. Al. (2010). Analysis of Monthly, Seasonal and Annual Air Temperature Variability and Trends in Taiz City - Republic of Yemen. *Journal of Environmental Protection*, *01*(04), 401–409. https://doi.org/10.4236/jep.2010.14046

Čadro, S., Uzunović, M., Žurovec, J., & Žurovec, O. (2017). Validation and calibration of various reference evapotranspiration alternative methods under the climate conditions of Bosnia and Herzegovina. *International Soil and Water Conservation Research*, *5*(4), 309–324. https://doi.org/10.1016/j.iswcr.2017.07.002

Caloiero, T., Coscarelli, R., & Ferrari, E. (2020). Assessment of seasonal and annual rainfall trend in Calabria (southern Italy) with the ITA method. *Journal of Hydroinformatics*, *22*(4), 738–748. https://doi.org/10.2166/hydro.2019.138

Caloiero, T., Coscarelli, R., Ferrari, E., & Sirangelo, B. (2017). Trend analysis of monthly mean values and extreme indices of daily temperature in a region of southern Italy. *International Journal of Climatology*, *37*(February), 284–297. https://doi.org/10.1002/joc.5003

Caloiero, Tommaso, & Guagliardi, I. (2021). Climate change assessment: seasonal and annual temperature analysis trends in the Sardinia region (Italy). *Arabian Journal of Geosciences*, *14*(20). https://doi.org/10.1007/s12517-021-08527-9

Chaouche, K., Neppel, L., Dieulin, C., Pujol, N., Ladouche, B., Martin, E., Salas, D., & Caballero, Y. (2010). Analyses of precipitation, temperature and evapotranspiration in a French Mediterranean region in the context of climate change. In *Comptes Rendus - Geoscience* (Vol. 342, Issue 3, pp. 234–243). https://doi.org/10.1016/j.crte.2010.02.001

Che, H. Z., Shi, G. Y., Zhang, X. Y., Arimoto, R., Zhao, J. Q., Xu, L., Wang, B., & Chen, Z. H. (2005). Analysis of 40 years of solar radiation data from China, 1961-2000. *Geophysical Research Letters*, *32*(6), 1–5.

https://doi.org/10.1029/2004GL022322

Chen, C.W. & Shubinski, R.P. (1971). Computer simulation of urban storm water runoff. *Journal of the Hydraulics Division*, 97(2): 289–301. https://doi.org/10.1061/JYCEAJ.0002871.

Chen, D., Gao, G., Xu, C. Y., Guo, J., & Ren, G. (2005). Comparison of the Thornthwaite method and pan data with the standard Penman-Monteith estimates of reference evapotranspiration in China. *Climate Research, 28*(2), 123–132. https://doi.org/10.3354/cr028123

Choi, C.S., Cagle, A.E., Macknick, J., Bloom, D.E., Caplan, J.S. & Ravi, S. (2020). Effects of Revegetation on Soil Physical and Chemical Properties in Solar Photovoltaic Infrastructure. *Frontiers in Environmental. Science*, 8:140. https://doi.org/10.3389/fenvs.2020.00140.

Choudhary, D. (2018). *Methods of Evapotranspiration Methods of Evapotranspiration. March*. https://doi.org/10.13140/RG.2.2.14533.76007

Chu, R., Li, M., Islam, A. R. M. T., Fei, D., & Shen, S. (2019). Attribution analysis of actual and potential evapotranspiration changes based on the complementary relationship theory in the Huai River basin of eastern China. *International Journal of Climatology*, *39*(10), 4072–4090. https://doi.org/10.1002/joc.6060

Consoli, S., Russo, A., & Snyder, R. (2006). Estimating evapotranspiration of orange orchards using surface renewal and remote sensing techniques. *AIP Conference Proceedings*, *852*(September), 185–192. https://doi.org/10.1063/1.2349343

Cook, L. M. & McCuen, R. H. (2013). Hydrologic Response of Solar Farms. *Journal of Hydrologic Engineering*, 18(5): 536-541. https://doi.org/10.1061/(ASCE)HE.1943-5584.0000530.

Crespi, A., Brunetti, M., Ranzi, R., Tomirotti, M., & Maugeri, M. (2021). A multi-century meteo-hydrological analysis for the Adda river basin (Central Alps). Part I: Gridded monthly precipitation (1800–2016) records. *International Journal of Climatology*, *41*(1), 162–180. https://doi.org/10.1002/joc.6614

Darshana, Pandey, A., & Pandey, R. P. (2013). Analysing trends in reference evapotranspiration and weather variables in the Tons River Basin in Central India. *Stochastic Environmental Research and Risk Assessment*, *27*(6), 1407–1421. https://doi.org/10.1007/s00477-012-0677-7

de Melo, G. L., & Fernandes, A. L. . (2012). Evaluation of empirical methods to estimate reference evapotranspiration in uberaba, state of minas gerais, brazil giovani l. de melo 1 , andré l. t. fernandes 2. *Eng.Agric.Jaboticabal*, *32*(9), 875–888. https://doi.org/10.1590/S0100-69162012000500007.

Dezsi, Ş., Mîndrescu, M., Petrea, D., Rai, P. K., Hamann, A., & Nistor, M. M. (2018). High-resolution projections of evapotranspiration and water availability for Europe under climate change. *International Journal of Climatology*, 38(10), 3832-3841.. https://doi.org/10.1002/joc.5537

Dickinson, R. E. (1984). Modeling evapotranspiration for three-dimensional global climate models. *Climate Processes and Climate Sensitivity*, *29*, 58–72. https://doi.org/10.1029/gm029p0058

Ding, Y., & Peng, S. (2021). Spatiotemporal change and attribution of potential evapotranspiration over China from 1901 to 2100. *Theoretical and Applied Climatology*, *145*(1–2), 79–94. https://doi.org/10.1007/s00704-021-03625-w

Diop, L., Bodian, A., & Diallo, D. (2016). Spatiotemporal Trend Analysis of the Mean Annual Rainfall in Senegal. *European Scientific Journal, ESJ*, *12*(12), 231. https://doi.org/10.19044/esj.2016.v12n12p231

Dong, Q., Wang, W., Shao, Q., Xing, W., Ding, Y., & Fu, J. (2020). The response of reference evapotranspiration to climate change in Xinjiang, China: Historical changes, driving forces, and future projections. *International Journal of Climatology*, 40(1), 235-254. https://doi.org/10.1002/joc.6206

Ebhota, W.S. & Jen, T.-C. (2020). Fossil fuels environmental challenges and the role of solar photovoltaic technology advances in fast tracking hybrid renewable energy system. *International Journal of Precision Engineering and Manufacturing,* 7 (1), 97–117. https://doi.org/10.1007/s40684-019-00101-9.

Edalat M. M. (2017) Remote Sensing of the Environmental Impacts of Utility-Scale

Solar Energy Plants. Ph.D. dissertation, University of Nevada.

EIA 2022. Annual Energy Outlook 2022 with Projections to 2050. U.S. Energy Information Administrator.

El-Sayed, M. E. M., & Zumwalt, K. W. (1991). Comparison of two different approaches for making design sensitivity analysis an integrated part of finite element analysis. *Structural Optimization*, *3*(3), 149–156. https://doi.org/10.1007/BF01743071

Elferchichi, A., Giorgio, G. A., Lamaddalena, N., Ragosta, M., & Telesca, V. (2017). Variability of temperature and its impact on reference evapotranspiration: The test case of the Apulia Region (Southern Italy). *Sustainability (Switzerland)*, *9*(12). https://doi.org/10.3390/su9122337

Ellsäßer, F., Röll, A., Stiegler, C., Hendrayanto, & Hölscher, D. (2020). Introducing QWaterModel, a QGIS plugin for predicting evapotranspiration from land surface temperatures. *Environmental Modelling and Software*, *130*. https://doi.org/10.1016/j.envsoft.2020.104739

Engman, E.T. & Hershfield, D.M. (1981). Characterizing short duration rainfall intensities for runoff calculation. Trans. *ASAE,* (24SW): 347 352. https://doi.org/10.13031/2013.34255

Eymen, A., & Köylü, Ü. (2019). Seasonal trend analysis and ARIMA modeling of relative humidity and wind speed time series around Yamula Dam. *Meteorology and Atmospheric Physics*, *131*(3), 601–612. https://doi.org/10.1007/s00703-018-0591-8

Fan, Z. X., & Thomas, A. (2013). Spatiotemporal variability of reference evapotranspiration and its contributing climatic factors in Yunnan Province, SW China, 1961-2004. *Climatic Change*, *116*(2), 309–325. https://doi.org/10.1007/s10584-012-0479-4

Fischer, E. M., Sippel, S., & Knutti, R. (2021). Increasing probability of record-shattering climate extremes. *Nature Climate Change*, *11*(8), 689–695. https://doi.org/10.1038/s41558-021-01092-9

Ghafouri-Azar, M., Bae, D. H., & Kang, S. U. (2018). Trend analysis of long-

termreference evapotranspiration and its components over the Korean Peninsula. *Water (Switzerland)*, *10*(10). https://doi.org/10.3390/w10101373

Gharsallah, O., Facchi, A., & Gandolfi, C. (2013). Comparison of six evapotranspiration models for a surface irrigated maize agro-ecosystem in Northern Italy. *Agricultural Water Management*, *130*, 119–130. https://doi.org/10.1016/j.agwat.2013.08.009

Ginley, D. & Parilla, P. (2013). Solar Energy: A Common-Sense Vision, *Frontiers in Energy Research*, 1. https://doi.org/10.3389/fenrg.2013.00003

Glenn, E. P., Nagler, P. L., & Huete, A. R. (2010). Vegetation index methods for estimating evapotranspiration by remote sensing. *Surveys in Geophysics*, 31, 531-555. https://doi.org/10.1007/s10712-010-9102-2

Gocic, M., & Trajkovic, S. (2014). Analyse des tendances des données d'évapotranspiration de référence en climat humide. *Hydrological Sciences Journal*, *59*(1), 165–180. https://doi.org/10.1080/02626667.2013.798659

Gong, L., Xu, C. Y., Chen, D., Halldin, S., & Chen, Y. D. (2006). Sensitivity of the Penman–Monteith reference evapotranspiration to key climatic variables in the Changjiang (Yangtze River) basin. *Journal of hydrology*, 329(3-4), 620-629. https://doi.org/10.1016/j.jhydrol.2006.03.027

Green, W. H. & Ampt, G. A. (1911). Studies on soil physics, *Journal of Agricultural Science*, 4(1),1–24. https://doi.org/10.1017/S0021859600001441

Gul, S., Ren, J., Xiong, N., & Khan, M. A. (2021). Design and analysis of statistical probability distribution and nonparametric trend analysis for reference evapotranspiration. *PeerJ*, *9*, 1–29. https://doi.org/10.7717/peerj.11597

Gullotta, A., Butler, D., Campisano, A., Creaco, E., Farmani, R., & Modica, C. (2021). Optimal location of valves to improve equity in intermittent water distribution systems. Journal of Water Resources Planning and Management, 147(5), 04021016.

Gullotta, A., Campisano, A., Creaco, E., & Modica, C. (2021). A simplified methodology for optimal location and setting of valves to improve equity in

intermittent water distribution systems. Water Resources Management, 35, 4477-4494.

Gunerhan H., Hepbasli A. & Giresunlu U. (2008). Environmental impacts from the solar energy systems. *Energy Sources* A 31 131–8. https://doi.org/10.1080/15567030701512733.

Guo, Q., Liang, J., Cao, X., Zhang, Z., & Zhang, L. (2020). Spatiotemporal Evolution of Evapotranspiration in China after 1998. *Water*, 12(11), 3250. https://doi.org/10.3390/w12113250

Gupta, H. V., & Kling, H. (2011). On typical range, sensitivity, and normalization of Mean Squared Error and Nash-Sutcliffe Efficiency type metrics. *Water Resources Research*, *47*(10), 2–4. https://doi.org/10.1029/2011WR010962

Hadi, S., Khairi, A., Wahab, A., Shahid, S., & Bin, Z. (2020). Changes in reference evapotranspiration and its driving factors in peninsular Malaysia. *Atmospheric Research*, *246*(June), 105096. https://doi.org/10.1016/j.atmosres.2020.105096

Han, D., Wang, G., Liu, T., Xue, B. L., Kuczera, G., & Xu, X. (2018). Hydroclimatic response of evapotranspiration partitioning to prolonged droughts in semiarid grassland. *Journal of Hydrology*, *563*(May), 766–777. https://doi.org/10.1016/j.jhydrol.2018.06.048

Han, X., Liu, W., & Lin, W. (2015a). Spatiotemporal analysis of potential evapotranspiration in the Changwu tableland from 1957 to 2012. *Meteorological Applications*, *22*(3), 586–591. https://doi.org/10.1002/met.1490

Hashemi, F., & Habibian, M. T. (1979). Limitations of temperature-based methods in estimating crop evapotranspiration in arid-zone agricultural development projects. *Agricultural Meteorology*, *20*(3), 237–247. https://doi.org/10.1016/0002-1571(79)90025-6

Hassanpour Adeh, E., Selker, J.S. & Higgins, C.W. (2018). Remarkable Agrivoltaic Influence on Soil Moisture, Micrometeorology and Water-Use Efficiency. *PLOS ONE*, 13(11), e0203256. https://doi.org/10.1371/journal.pone.0203256.

Hatfield, J. L., Prueger, J. H., Kustas, W. P., Anderson, M. C., & Alfieri, J. G. (2016). Evapotranspiration: Evolution of methods to increase spatial and temporal resolution. *Improving Modeling Tools to Assess Climate Change Effects on Crop Response*, *7*, 159–193. https://doi.org/10.2134/advagricsystmodel7.2015.0076

He, D., Liu, Y., Pan, Z., An, P., Wang, L., Dong, Z., ... & Zhao, P. (2013). Climate change and its effect on reference crop evapotranspiration in central and western Inner Mongolia during 1961–2009. *Frontiers of Earth Science*, 7, 417-428.. https://doi.org/10.1007/s11707-013-0381-z

Hobbins, M. T. (2016). The variability of ASCE Standardized reference evapotranspiration: A rigorous, CONUS-wide decomposition and attribution. *Transactions of the ASABE*, *59*(2), 561–576.

Hoegh-Guldberg, O., Jacob, D., Bindi, M., Brown, S., Camilloni, I., Diedhiou, A., ... & Zougmoré, R. B. (2018). Impacts of 1.5 C global warming on natural and human systems. Global warming of 1.5° C. *IPCC*. https://doi.org/10.13031/trans.59.10975

Hu, M., Sayama, T., Try, S., Takara, K., & Tanaka, K. (2019). Trend analysis of hydroclimatic variables in the Kamo River Basin, Japan. *Water (Switzerland)*, *11*(9). https://doi.org/10.3390/w11091782

Huang, H., Han, Y., Cao, M., Song, J., Xiao, H., & Cheng, W. (2015). Spatiotemporal Characteristics of Evapotranspiration Paradox and Impact Factors in China in the Period of 1960-2013. *Advances in Meteorology*, *2015*. https://doi.org/10.1155/2015/519207

Hui-Mean, F., Yusop, Z., & Yusof, F. (2018). Drought analysis and water resource availability using standardised precipitation evapotranspiration index. *Atmospheric Research*, 201, 102-115. https://doi.org/10.1016/j.atmosres.2017.10.014

Hwang, J. H., Azam, M., Jin, M. S., Kang, Y. H., Lee, J. E., Latif, M., Ahmed, R., Umar, M., & Hashmi, M. Z. (2020). Spatiotemporal trends in reference evapotranspiration over South Korea. *Paddy and Water Environment*, *18*(1),

235–259. https://doi.org/10.1007/s10333-019-00777-4

IPCC2013. (2013). CLIMATE CHANGE 2013 Climate Change 2013. In *Researchgate.Net*. https://www.researchgate.net/profile/Abha_Chhabra2/publication/271702872_Carbon_and_Other_Biogeochemical_Cycles/links/54cf9ce80cf24601c094a45e/Carbon-and-Other-Biogeochemical-Cycles.pdf

Irmak, S., Payero, J. O., Martin, D. L., Irmak, A., & Howell, T. A. (2006). Sensitivity Analyses and Sensitivity Coefficients of Standardized Daily ASCE-Penman-Monteith Equation. *Journal of Irrigation and Drainage Engineering*, *132*(6), 564–578. https://doi.org/10.1061/(asce)0733-9437(2006)132:6(564)

Jain, S. K., & Kumar, V. (2012). Trend analysis of rainfall and temperature data for India. *Current Science*, *102*(1), 37–49. https://www.jstor.org/stable/24080385.

Jain, S. K., & Sudheer, K. P. (2008). Fitting of Hydrologic Models: A Close Look at the Nash–Sutcliffe Index. *Journal of Hydrologic Engineering*, *13*(10), 981–986. https://doi.org/10.1061/(asce)1084-0699(2008)13:10(981)

Jerin, J. N., Islam, H. M. T., Islam, A. R. M. T., Shahid, S., Hu, Z., Badhan, M. A., Chu, R., & Elbeltagi, A. (2021). Spatiotemporal trends in reference evapotranspiration and its driving factors in Bangladesh. *Theoretical and Applied Climatology*, *144*(1–2), 793–808. https://doi.org/10.1007/s00704-021-03566-4

Jiang, Y., Luo, Y., Zhao, Z., & Tao, S. (2010). Changes in wind speed over China during 1956-2004. *Theoretical and Applied Climatology*, *99*(3–4), 421–430. https://doi.org/10.1007/s00704-009-0152-7

Stöckle, C. O., Kjelgaard, J., & Bellocchi, G. (2004). Evaluation of estimated weather data for calculating Penman-Monteith reference crop evapotranspiration. *Irrigation science*, 23, 39-46. https://doi.org/10.1007/s00271-004-0091-0

Jones, P. D. (1995). Maximum and minimum temperature trends in Ireland, Italy,

Thailand, Turkey and Bangladesh. *Atmospheric Research*, *37*(1–3), 67–78. https://doi.org/10.1016/0169-8095(94)00069-P

Kamal, N., & Pachauri, S. (2019). Mann-Kendall, and Sen's Slope Estimators for Precipitation Trend Analysis in North-Eastern States of India. *International Journal of Computer Applications*, *177*(11), 7–16. https://doi.org/10.5120/ijca2019919453

Keifer, C. J.; Chu, H. H. (1957). Synthetic storm pattern for drainage design. *Journal of the Hydraulics Division*, v. 83, p. 1-25. https://doi.org/10.1061/JYCEAJ.0000104.

Kingston, D. G., Todd, M. C., Taylor, R. G., Thompson, J. R., & Arnell, N. W. (2009). Uncertainty in the estimation of potential evapotranspiration under climate change. *Geophysical Research Letters*, 36(20). https://doi.org/10.1029/2009GL040267

Klink, K. (2002). Trends and interannual variability of wind speed distributions in Minnesota. *Journal of Climate*, *15*(22), 3311–3317. https://doi.org/10.1175/1520-0442(2002)015<3311:TAIVOW>2.0.CO;2

Kousari, M. R., Ekhtesasi, M. R., Tazeh, M., Naeini, M. A. S., & Zarch, M. A. A. (2011). An investigation of the Iranian climatic changes by considering the precipitation, temperature, and relative humidity parameters. *Theoretical and Applied Climatology*, *103*(3–4), 321–335. https://doi.org/10.1007/s00704-010-0304-9

Laib, M., Golay, J., Telesca, L., & Kanevski, M. (2018). Multifractal analysis of the time series of daily means of wind speed in complex regions. *Chaos, Solitons and Fractals*, *109*, 118–127. https://doi.org/10.1016/j.chaos.2018.02.024

Lang, D., Zheng, J., Shi, J., Liao, F., Ma, X., Wang, W., Chen, X., & Zhang, M. (2017). A comparative study of potential evapotranspiration estimation by eight methods with FAO Penman–Monteith method in southwestern China. *Water (Switzerland)*, *9*(10). https://doi.org/10.3390/w9100734

Li, G., Zhang, F., Jing, Y., Liu, Y., & Sun, G. (2017). Response of

evapotranspiration to changes in land use and land cover and climate in China during 2001–2013. *Science of the Total Environment*, 596, 256-265. https://doi.org/10.1016/j.scitotenv.2017.04.080

Li, M., Chu, R., Shen, S., & Islam, A. R. M. T. (2018). Quantifying climatic impact on reference evapotranspiration trends in the Huai River Basin of Eastern China. *Water (Switzerland)*, *10*(2). https://doi.org/10.3390/w10020144

Li, X., Gemmer, M., Zhai, J., Liu, X., Su, B., & Wang, Y. (2013). Spatio-temporal variation of actual evapotranspiration in the Haihe River Basin of the past 50 years. *Quaternary International*, *304*, 133–141. https://doi.org/10.1016/j.quaint.2013.02.027

Liang, L., Li, L., Zhang, L., Li, J., & Li, B. (2008). Sensitivity of Penman-Monteith reference crop evapotranspiration in Tao' er River Basin of northeastern China. *Chinese Geographical Science*, *18*(4), 340–347. https://doi.org/10.1007/s11769-008-0340-x

Liu, Q., Yan, C., Ju, H., & Garré, S. (2018). Impact of climate change on potential evapotranspiration under a historical and future climate scenario in the Huang-Huai-Hai Plain, China. *Theoretical and Applied Climatology*, *132*(1–2), 387–401. https://doi.org/10.1007/s00704-017-2060-6

Liuzzo, L., Bono, E., Sammartano, V., & Freni, G. (2016). Analysis of spatial and temporal rainfall trends in Sicily during the 1921–2012 period. *Theoretical and Applied Climatology*, *126*(1–2), 113–129. https://doi.org/10.1007/s00704-015-1561-4

Liuzzo, L., Bono, E., Sammartano, V., & Freni, G. (2017). Long-term temperature changes in Sicily, Southern Italy. *Atmospheric Research*, *198*(August), 44–55. https://doi.org/10.1016/j.atmosres.2017.08.007

Liuzzo, L., Noto, L. V., Arnone, E., Caracciolo, D., & La Loggia, G. (2015). Modifications in Water Resources Availability Under Climate Changes: A Case Study in a Sicilian Basin. *Water Resources Management*, *29*(4), 1117–1135. https://doi.org/10.1007/s11269-014-0864-z

Liuzzo, L., Viola, F., & Noto, L. V. (2016). Wind speed and temperature trends

impacts on reference evapotranspiration in Southern Italy. *Theoretical and Applied Climatology*, *123*(1–2), 43–62. https://doi.org/10.1007/s00704-014-1342-5

Long, D., & Singh, V. P. (2012). Remote Sensing of Environment A Two-source Trapezoid Model for Evapotranspiration (TTME) from satellite imagery. *Remote Sensing of Environment*, *121*, 370–388. https://doi.org/10.1016/j.rse.2012.02.015

Luo, Y., Gao, P., & Mu, X. (2021). Influence of meteorological factors on the potential evapotranspiration in yanhe river basin, china. *Water (Switzerland)*, *13*(9), 1–13. https://doi.org/10.3390/w13091222

Maček, U., Bezak, N., & Šraj, M. (2018). Reference evapotranspiration changes in Slovenia, Europe. *Agricultural and Forest Meteorology*, *260–261*(February), 183–192. https://doi.org/10.1016/j.agrformet.2018.06.014

Makaronidou, M. (2020). Assessment on the Local Climate Effects of Solar Photovoltaic Parks. Ph.D. dissertation, Lancaster University

Maruyama, A., Ohba, K., Kurose, Y., & Miyamoto, T. (2004). Seasonal Variation in Evapotranspiration from Mat Rush Grown in Paddy Field. *Journal of Agricultural Meteorology*, *60*(1), 1–15. https://doi.org/10.2480/agrmet.60.1

McCuen, R., Johnson, P., & Ragan, R. (1996). Hydrology, FHWA-SA-96-067, Federal Highway Administration, Washington, DC.

McCuen, R. H., Knight, Z., & Cutter, A. G. (2006). Evaluation of the Nash–Sutcliffe Efficiency Index. *Journal of Hydrologic Engineering*, *11*(6), 597–602. https://doi.org/10.1061/(asce)1084-0699(2006)11:6(597)

McGechan, M. B., & Lewis, D. R. (2002). SW—soil and water: sorption of phosphorus by soil, part 1: principles, equations and models. *Biosystems Engineering*, 82(1), 1-24. https://doi.org/10.1006/bioe.2002.0054.

Merabtene, T., Siddique, M., & Shanableh, A. (2016). Assessment of Seasonal and Annual Rainfall Trends and Variability in Sharjah City, UAE. *Advances in Meteorology*, *2016*. https://doi.org/10.1155/2016/6206238

Minacapilli, M., Agnese, C., Blanda, F., Cammalleri, C., Ciraolo, G., D'Urso, G.,

Iovino, M., Pumo, D., Provenzano, G., & Rallo, G. (2009). Estimation of actual evapotranspiration of Mediterranean perennial crops by means of remote-sensing based surface energy balance models. *Hydrology and Earth System Sciences*, *13*(7), 1061–1074. https://doi.org/10.5194/hess-13-1061-2009

Minacapilli, M., Cammalleri, C., Ciraolo, G., Rallo, G., & Provenzano, G. (2016). Using scintillometry to assess reference evapotranspiration methods and their impact on the water balance of olive groves. In *Agricultural Water Management* (Vol. 170, pp. 49–60). https://doi.org/10.1016/j.agwat.2015.12.004

Minacapilli, Mario, Ciraolo, G., Cammalleri, C., & D'urso, G. (2007). Evaluating actual evapotranspiration by means of multi-platform remote sensing data: A case study in Sicily. *IAHS-AISH Publication*, *316*, 207–219.

Moeletsi, M. E., Walker, S., & Hamandawana, H. (2013). Comparison of the Hargreaves and Samani equation and the Thornthwaite equation for estimating dekadal evapotranspiration in the Free State Province, South Africa. In *Physics and Chemistry of the Earth* (Vol. 66, pp. 4–15). https://doi.org/10.1016/j.pce.2013.08.003

Mohammad, P., & Goswami, A. (2019). Temperature and precipitation trend over 139 major Indian cities: An assessment over a century. *Modeling Earth Systems and Environment*, *5*(4), 1481–1493. https://doi.org/10.1007/s40808-019-00642-7

Mollema, P., Antonellini, M., Gabbianelli, G., Laghi, M., Marconi, V., & Minchio, A. (2012). Climate and water budget change of a Mediterranean coastal watershed, Ravenna, Italy. *Environmental Earth Sciences*, *65*(1), 257–276. https://doi.org/10.1007/s12665-011-1088-7

Mondal, A., Khare, D., & Kundu, S. (2015). Spatial and temporal analysis of rainfall and temperature trend of India. *Theoretical and Applied Climatology*, *122*(1–2), 143–158. https://doi.org/10.1007/s00704-014-1283-z

Mueller, B., Seneviratne, S. I., Jimenez, C., Corti, T., Hirschi, M., Balsamo, G., ...

& Zhang, Y. (2011). Evaluation of global observations-based evapotranspiration datasets and IPCC AR4 simulations. *Geophysical Research Letters*, 38(6).https://doi.org/10.1029/2010GL046230

Nam, W., Hong, E., & Choi, J. (2015). Has climate change already affected the spatial distribution and temporal trends of reference evapotranspiration in South Korea ? *Agricultural Water Management*, *150*, 129–138. https://doi.org/10.1016/j.agwat.2014.11.019

Ndiaye, P. M., Bodian, A., Diop, L., Deme, A., Dezetter, A., Djaman, K., & Ogilvie, A. (2020). Trend and sensitivity analysis of reference evapotranspiration in the Senegal River basin using NASA meteorological data. *Water (Switzerland)*, *12*(7). https://doi.org/10.3390/w12071957

Ndulue, E., & Ranjan, R. S. (2021). Performance of the FAO Penman-Monteith equation under limiting conditions and fourteen reference evapotranspiration models in southern Manitoba. *Theoretical and Applied Climatology*, *143*(3–4), 1285–1298. https://doi.org/10.1007/s00704-020-03505-9

Negm, A., Jabro, J., & Provenzano, G. (2017). Assessing the suitability of American National Aeronautics and Space Administration (NASA) agro-climatology archive to predict daily meteorological variables and reference evapotranspiration in Sicily, Italy. *Agricultural and Forest Meteorology*, *244–245*(May), 111–121. https://doi.org/10.1016/j.agrformet.2017.05.022

Negm, A., Minacapilli, M., & Provenzano, G. (2017, April). Spatial disaggregation of POWER-NASA air temperatures and effects on grass reference evapotranspiration in Sicily, Italy. *In EGU General Assembly Conference Abstracts* (p. 13591).

Nikam, B. R., Kumar, P., Garg, V., Thakur, P. K., & Aggarwal, S. P. (2014). Comparative evaluation of different potential evapotranspiration estimation approaches. *Int. J. Res. Eng. Technol,* 3, 543-552. https://doi.org/10.15623/ijret.2014.0306102

Ochoa-Sánchez, A., Crespo, P., Carrillo-Rojas, G., Sucozhañay, A., & Célleri, R. (2019). Actual evapotranspiration in the high andean grasslands: A

comparison of measurement and estimation methods. *Frontiers in Earth Science*, *7*(March), 1–16. https://doi.org/10.3389/feart.2019.00055

Ohmura, A. (2009). Observed decadal variations in surface solar radiation and their causes. *Journal of Geophysical Research*, *114*(April), 1–9. https://doi.org/10.1029/2008jd011290

Palumbo, A. D., Vitale, D., Campi, P., & Mastrorilli, M. (2011). Time trend in reference evapotranspiration: Analysis of a long series of agrometeorological measurements in Southern Italy. *Irrigation and Drainage Systems*, *25*(4), 395–411. https://doi.org/10.1007/s10795-012-9132-7

Pandey, P. K., Dabral, P. P., & Pandey, V. (2016). Evaluation of reference evapotranspiration methods for the northeastern region of India. *International Soil and Water Conservation Research*, *4*(1), 52–63. https://doi.org/10.1016/j.iswcr.2016.02.003

Parajuli, K., Jones, S. B., Tarboton, D. G., Flerchinger, G. N., Hipps, L. E., Allen, L. N., & Seyfried, M. S. (2019). Agricultural and Forest Meteorology Estimating actual evapotranspiration from stony-soils in montane ecosystems. *Agricultural and Forest Meteorology*, *265*(November 2018), 183–194. https://doi.org/10.1016/j.agrformet.2018.11.019

Patle, G. T., Sengdo, D., & Tapak, M. (2020). Trends in major climatic parameters and sensitivity of evapotranspiration to climatic parameters in the eastern Himalayan Region of Sikkim, India. *Journal of Water and Climate Change*, *11*(2), 491–502. https://doi.org/10.2166/wcc.2019.121

Peng, L., Li, Y., & Feng, H. (2017). The best alternative for estimating reference crop evapotranspiration in different sub-regions of mainland China. *Scientific Reports*, *7*(1), 1–19. https://doi.org/10.1038/s41598-017-05660-y

Peng, S., Ding, Y., Wen, Z., Chen, Y., Cao, Y., & Ren, J. (2017). Spatiotemporal change and trend analysis of potential evapotranspiration over the Loess Plateau of China during 2011–2100. *Agricultural and Forest Meteorology*, *233*, 183–194. https://doi.org/10.1016/j.agrformet.2016.11.129

Peres, D. J., Modica, R., & Cancelliere, A. (2019). Assessing future impacts of

climate change on water supply system performance: Application to the Pozzillo Reservoir in Sicily, Italy. Water, 11(12), 2531. https://doi.org/10.3390/w11122531.

Peres, D. J., Senatore, A., Nanni, P., Cancelliere, A., Mendicino, G., & Bonaccorso, B. (2020). Evaluation of EURO-CORDEX (Coordinated Regional Climate Downscaling Experiment for the Euro-Mediterranean area) historical simulations by high-quality observational datasets in southern Italy: Insights on drought assessment. *Natural Hazards and Earth System Sciences, 20*(11), 3057–3082. https://doi.org/10.5194/nhess-20-3057-2020

Peres, D.J.; Bonaccorso, B.; Palazzolo, N.; Cancelliere, A.; Mendicino, G.; Senatore, A (2023). Projected changes of hy-drologic vari-ables and drought indices in southern Italy through an optimized Euro-CORDEX climate model ensemble weighted average. Hydrol. Sci. J. (under review).

Pisinaras, V., Yang, W., Bärring, L. & Gemitzi, A. (2014). Conceptualizing and assessing the effects of installation and operation of photovoltaic power plants on major hydrologic budget constituents. *Science of the Total Environment*, 493C, 239-250. https://doi.org/10.1016/j.scitotenv.2014.05.132.

Piticar, A., Mihăilă, D., Lazurca, L. G., Bistricean, P. I., Puţuntică, A., & Briciu, A. E. (2016). Spatiotemporal distribution of reference evapotranspiration in the Republic of Moldova. *Theoretical and Applied Climatology*, *124*(3–4), 1133–1144. https://doi.org/10.1007/s00704-015-1490-2

Provenzano, G., & Ippolito, M. (2021, April). Using the ERA5 dataset of atmospheric variables to estimate daily reference evapotranspiration in Sicily, Italy. In EGU General Assembly Conference Abstracts (pp. EGU21-4151).

Quej, V. H., Almorox, J., Arnaldo, J. A., & Moratiel, R. (2019). Evaluation of Temperature-Based Methods for the Estimation of Reference Evapotranspiration in the Yucatán Peninsula, Mexico. *Journal of Hydrologic Engineering*, *24*(2), 05018029. https://doi.org/10.1061/(asce)he.1943-5584.0001747

Ranzi, R., Michailidi, E. M., Tomirotti, M., Crespi, A., Brunetti, M., & Maugeri,

M. (2021). A multi-century meteo-hydrological analysis for the Adda river basin (Central Alps). Part II: Daily runoff (1845–2016) at different scales. *International Journal of Climatology*, *41*(1), 181–199. https://doi.org/10.1002/joc.6678

Ravi, S., Lobell, D. B. & Field, C. B. (2014). Tradeoffs and Synergies between Biofuel Production and Large Solar Infrastructure in Deserts. *Environmental Science & Technology,* 48(5), 3021-3030. https://doi.org/10.1021/es404950n.

Rawls, W.J., Brakensiek, D.L., & Miller, N.L. (1983). Green-ampt Infiltration Parameters from Soils Data. *Journal of Hydraulic Engineering,* 109, 62-70. https://doi.org/10.1061/(ASCE)0733-9429(1983)109:1(62).

Rossman, L. A. (2015). Storm Water Management Model User's Manual Version 5.1. U.S. Environmental Protection Agency.

Rossman, L. A. (2016). Storm Water Management Model Reference Manual Volume I – Hydrology. U.S. Environmental Protection Agency.

Saboohi, R., Soltani, S., & Khodagholi, M. (2012). Trend analysis of temperature parameters in Iran. *Theoretical and Applied Climatology*, *109*(3–4), 529–547. https://doi.org/10.1007/s00704-012-0590-5

Sanchez-Lorenzo, Manara, V., Beltrano, M. C., Brunetti, M., Maugeri, M., , A., Simolo, C., & Sorrenti, S. (2015). Sunshine duration variability and trends in Italy from homogenized instrumental time series (1936–2013). *Journal of Geophysical Research: Atmospheres,* 120(9), 3622-3641. https://doi.org/10.1002/2014JD022560.

Sarkodie, S.A. & Owusu, P.A. (2020). Bibliometric analysis of water–energy–food nexus: sustainability assessment of renewable energy. *Current Opinion in Environmental Science & Health,* 13, 29–34. https://doi.org/10.1016/j.coesh.2019.10.008.

Van der Schrier, G., Jones, P. D., & Briffa, K. R. (2011). The sensitivity of the PDSI to the Thornthwaite and Penman-Monteith parameterizations for potential evapotranspiration. *Journal of Geophysical Research: Atmospheres*, 116(D3).. https://doi.org/10.1029/2010JD015001

Segnalini, M., Bernabucci, U., Vitali, A., Nardone, A., & Lacetera, N. (2013). Temperature humidity index scenarios in the Mediterranean basin. *International Journal of Biometeorology*, *57*(3), 451–458. https://doi.org/10.1007/s00484-012-0571-5

Sen, P. K. (1968). Estimates of the regression coefficient based on Kendall's tau. *Journal of the American statistical association*, 63(324), 1379-1389. https://doi.org/10.1080/01621459.1968.10480934

Senatore, A., Mendicino, G., Cammalleri, C., & Ciraolo, G. (2015). Regional-Scale Modeling of Reference Evapotranspiration: Intercomparison of Two Simplified Temperature- and Radiation-Based Approaches. *Journal of Irrigation and Drainage Engineering*, *141*(12), 04015022. https://doi.org/10.1061/(asce)ir.1943-4774.0000917

Sepaskhah, A. R., & Razzaghi, F. (2009). Evaluation of the adjusted Thornthwaite and Hargreaves-Samani methods for estimation of daily evapotranspiration in a semi-arid region of Iran. *Archives of Agronomy and Soil Science*, *55*(1), 51–66. https://doi.org/10.1080/03650340802383148

Shadmani, M., Marofi, S., & Roknian, M. (2012). Trend Analysis in Reference Evapotranspiration Using Mann-Kendall and Spearman's Rho Tests in Arid Regions of Iran. *Water Resources Management*, *26*(1), 211–224. https://doi.org/10.1007/s11269-011-9913-z

Shan, N., Shi, Z., Yang, X., Gao, J., & Cai, D. (2015a). Agricultural and Forest Meteorology Spatiotemporal trends of reference evapotranspiration and its driving factors in the Beijing – Tianjin Sand Source Control Project Region , China. *Agricultural and Forest Meteorology*, *200*, 322–333. https://doi.org/10.1016/j.agrformet.2014.10.008

Shan, N., Shi, Z., Yang, X., Gao, J., & Cai, D. (2015b). Spatiotemporal trends of reference evapotranspiration and its driving factors in the Beijing-Tianjin Sand Source Control Project Region, China. *Agricultural and Forest Meteorology*, *200*, 322–333. https://doi.org/10.1016/j.agrformet.2014.10.008

Sharifi, A., & Dinpashoh, Y. (2014). Sensitivity Analysis of the Penman-Monteith

reference Crop Evapotranspiration to Climatic Variables in Iran. *Water Resources Management*, *28*(15), 5465–5476. https://doi.org/10.1007/s11269-014-0813-x

Shi, T. T., Guan, D. X., Wu, J. B., Wang, A. Z., Jin, C. J., & Han, S. J. (2008). Comparison of methods for estimating evapotranspiration rate of dry forest canopy: Eddy covariance, Bowen ratio energy balance, and Penman-Monteith equation. *Journal of Geophysical Research Atmospheres*, *113*(19), 1–15. https://doi.org/10.1029/2008JD010174

Singh, P., Kumar, V., Thomas, T., & Arora, M. (2008). Changes in rainfall and relative humidity in river basins in northwest and central India. *Hydrological Processes: An International Journal*, 22(16), 2982-2992. https://doi.org/10.1002/hyp.6871

Sonali, P., & Nagesh Kumar, D. (2016). Spatio-temporal variability of temperature and potential evapotranspiration over india. *Journal of Water and Climate Change*, *7*(4), 810–822. https://doi.org/10.2166/wcc.2016.230

Stefanidis, S., & Alexandridis, V. (2021). Precipitation and potential evapotranspiration temporal variability and their relationship in two forest ecosystems in greece. *Hydrology*, *8*(4), 1–13. https://doi.org/10.3390/hydrology8040160

Subash, N., & Sikka, A. K. (2014). Trend analysis of rainfall and temperature and its relationship over India. *Theoretical and Applied Climatology*, *117*(3–4), 449–462. https://doi.org/10.1007/s00704-013-1015-9

Subedi, A., & Chávez, J. L. (2015). Crop Evapotranspiration (ET) Estimation Models: A Review and Discussion of the Applicability and Limitations of ET Methods. *Journal of Agricultural Science*, *7*(6), 50–68. https://doi.org/10.5539/jas.v7n6p50

Tabari, H., Marofi, S., Aeini, A., Hosseinzadeh, P., & Mohammadi, K. (2011). Agricultural and Forest Meteorology Trend analysis of reference evapotranspiration in the western half of Iran. *Agricultural and Forest Meteorology*, *151*(2), 128–136.

https://doi.org/10.1016/j.agrformet.2010.09.009

Tanner, C. B. (1967). Measurement of evapotranspiration. *Irrigation of agricultural lands*, 11, 534-574. https://doi.org/10.2134/agronmonogr11.c30

Tawalbeh, M., Al-Othman, A., Kafiah, F., Abdelsalam, E., Almomani, F., & Alkasrawi, M. (2021). Environmental impacts of solar photovoltaic systems: A critical review of recent progress and future outlook. *Science of the Total Environment*, 759, 143528. https://doi.org/10.1016/j.scitotenv.2020.143528.

Tegos, A., Malamos, N., & Koutsoyiannis, D. (2015). A parsimonious regional parametric evapotranspiration model based on a simplification of the Penman – Monteith formula. *Journal Of Hydrology*, *524*, 708–717. https://doi.org/10.1016/j.jhydrol.2015.03.024

Tellen, V. A. (2017). A comparative analysis of reference evapotranspiration from the surface of rainfed grass in Yaounde, calculated by six empirical methods against the penman-monteith formula. *Earth Perspectives*, *4*(1), 17–28. https://doi.org/10.1186/s40322-017-0039-1

Tikhamarine, Y., Malik, A., Kumar, A., Souag-Gamane, D., & Kisi, O. (2019). Estimation of monthly reference evapotranspiration using novel hybrid machine learning approaches. *Hydrological Sciences Journal*, *64*(15), 1824–1842. https://doi.org/10.1080/02626667.2019.1678750

Todisco, F., & Vergni, L. (2008). Climatic changes in Central Italy and their potential effects on corn water consumption. *Agricultural and Forest Meteorology*, *148*(1), 1–11. https://doi.org/10.1016/j.agrformet.2007.08.014

Torina, A., Khoury, C., Caracappa, S., & Maroli, M. (2006). Ticks infesting livestock on farms in Western Sicily, Italy. *Experimental and Applied Acarology*, *38*(1), 75–86. https://doi.org/10.1007/s10493-005-5629-1

Turney, D. & Fthenakis, V. (2011). Environmental Impacts from the installation and operation of large-scale solar power plants, Renewable & sustainable energy reviews, 15(6), 3261-3270. https://doi.org/10.1016/j.rser.2011.04.023.

Utset, A., Farré, I., Martínez-Cob, A., & Cavero, J. (2004). Comparing Penman-Monteith and Priestley-Taylor approaches as reference-evapotranspiration

inputs for modeling maize water-use under Mediterranean conditions. *Agricultural Water Management*, *66*(3), 205–219. https://doi.org/10.1016/j.agwat.2003.12.003

Valipour, M. (2015). Retracted: Comparative Evaluation of Radiation-Based Methods for Estimation of Potential Evapotranspiration. *Journal of Hydrologic Engineering*, *20*(5), 04014068. https://doi.org/10.1061/(asce)he.1943-5584.0001066

Ventura, F., Rossi Pisa, P., & Ardizzoni, E. (2002). Temperature and precipitation trends in Bologna (Italy) from 1952 to 1999. *Atmospheric Research*, *61*(3), 203–214. https://doi.org/10.1016/S0169-8095(01)00135-1

Vergni, L., & Todisco, F. (2011). Spatio-temporal variability of precipitation, temperature and agricultural drought indices in Central Italy. *Agricultural and Forest Meteorology*, *151*(3), 301–313. https://doi.org/10.1016/j.agrformet.2010.11.005

Vicente-Serrano, S. M., Azorin-Molina, C., Sanchez-Lorenzo, A., Revuelto, J., López-Moreno, J. I., González-Hidalgo, J. C., Moran-Tejeda, E., & Espejo, F. (2014). Reference evapotranspiration variability and trends in Spain, 1961-2011. *Global and Planetary Change*, *121*, 26–40. https://doi.org/10.1016/j.gloplacha.2014.06.005

Wang, R., Li, L., Chen, L., Ning, L., Yuan, L., & Guonian, L. (2022). Respective contributions of precipitation and potential evapotranspiration to long-term changes in global drought duration and intensity. *International Journal of Climatology*, *42*(16), 10126–10137. https://doi.org/10.1002/joc.7887

Wang, Z., Xie, P., Lai, C., Chen, X., Wu, X., Zeng, Z., & Li, J. (2017). Spatiotemporal variability of reference evapotranspiration and contributing climatic factors in China during 1961–2013. *Journal of Hydrology*, *544*, 97–108. https://doi.org/10.1016/j.jhydrol.2016.11.021

Willett, K. M., Gillett, N. P., Jones, P. D., & Thorne, P. W. (2007). Attribution of observed surface humidity changes to human influence. *Nature*, *449*(7163), 710–712. https://doi.org/10.1038/nature06207

Wu, H., Xu, M., Peng, Z., & Chen, X. (2021). Temporal variations in reference evapotranspiration in the Tarim River basin, Central Asia. *PLoS ONE*, *16*(6 June), 1–17. https://doi.org/10.1371/journal.pone.0252840

Xu, Z. X., Gong, T. L., & Li, J. Y. (2008). Decadal trend of climate in the Tibetan Plateau—regional temperature and precipitation. *Hydrological Processes: An International Journal*, 22(16), 3056-3065. https://doi.org/10.1002/hyp.6892

Yang, J., Wang, W., Hua, T., & Peng, M. (2021). Spatiotemporal variation of actual evapotranspiration and its response to changes of major meteorological factors over China using multi-source data. *Journal of Water and Climate Change*, *12*(2), 325–338. https://doi.org/10.2166/wcc.2020.221

Yang, Z., Liu, Q., & Cui, B. (2011). Spatial distribution and temporal variation of reference evapotranspiration during 1961–2006 in the Yellow River Basin, China. *Hydrological Sciences Journal, 56(6),* 1015-1026. https://doi.org/10.1080/02626667.2011.590810

Yavari, R., Zaliwciw, D., Cibin, R., & McPhillips, L. (2022). Minimizing environmental impacts of solar farms: a review of current science on landscape hydrology and guidance on stormwater management. *Environmental Research: Infrastructure and Sustainability,* 2(3), 032002. https://doi.org/10.1088/2634-4505/ac76dd.

Yu, W., Wu, T., Wang, W., Li, R., Wang, T., Qin, Y., Wang, W., & Zhu, X. (2016). Spatiotemporal Changes of Reference Evapotranspiration in Mongolia during 1980-2006. *Advances in Meteorology, 2016*. https://doi.org/10.1155/2016/9586896

Zeng, J., Li, J., Lu, X., Wei, Z., Shangguan, W., Zhang, S., Dai, Y., & Zhang, S. (2022). Assessment of global meteorological, hydrological and agricultural drought under future warming based on CMIP6. *Atmospheric and Oceanic Science Letters*, *15*(1), 100143. https://doi.org/10.1016/j.aosl.2021.100143

Zhang, Feng, Geng, M., Wu, Q., & Liang, Y. (2020a). Study on the spatial-temporal variation in evapotranspiration in China from 1948 to 2018. *Scientific Reports*, *10*(1), 1–13. https://doi.org/10.1038/s41598-020-74384-3

Zhang, F., Liu, Z., Zhangzhong, L., Yu, J., Shi, K., & Yao, L. (2020). Spatiotemporal distribution characteristics of reference evapotranspiration in Shandong province from 1980 to 2019. *Water*, 12(12), 3495. https://doi.org/10.3390/w12123495

Zhang, L., Traore, S., Cui, Y., Luo, Y., Zhu, G., Liu, B., Fipps, G., Karthikeyan, R., & Singh, V. (2019). Assessment of spatiotemporal variability of reference evapotranspiration and controlling climate factors over decades in China using geospatial techniques. *Agricultural Water Management*, *213*(January 2018), 499–511. https://doi.org/10.1016/j.agwat.2018.09.037

Zhao, Y., Zou, X., Cao, L., Yao, Y., & Fu, G. (2018). Spatiotemporal variations of potential evapotranspiration and aridity index in relation to influencing factors over Southwest China during 1960–2013. *Theoretical and Applied Climatology*, *133*(3–4), 711–726. https://doi.org/10.1007/s00704-017-2216-4

Zhou, Z., Wang, L., Lin, A., Zhang, M., & Niu, Z. (2018). Innovative trend analysis of solar radiation in China during 1962–2015. *Renewable Energy*, *119*, 675–689. https://doi.org/10.1016/j.renene.2017.12.052

Zongxing, L., Qi, F., Wei, L., Tingting, W., Yan, G., Yamin, W., Aifang, C., Jianguo, L., & Li, L. (2014). Spatial and temporal trend of potential evapotranspiration and related driving forces in Southwestern China, during 1961-2009. *Quaternary International*, *336*, 127–144. https://doi.org/10.1016/j.quaint.2013.12.045

Zuo, D., Xu, Z., Yang, H., & Liu, X. (2012). Spatiotemporal variations and abrupt changes of potential evapotranspiration and its sensitivity to key meteorological variables in the Wei River basin, China. *Hydrological Processes, 26*(8), 1149–1160. https://doi.org/10.1002/hyp.8206